

NUREG/CR--3608

DE84 011863

SAND83-2549  
NUREG/CR-3608  
R4

RELAP5 ASSESSMENT: LOFT LARGE BREAK L2-5

S. L. Thompson and L. N. Kmetyk

Date Published: February 1984

**NOTICE**  
EDITIONS OF THIS REPORT ARE UNLIMITED.  
It has been reproduced from the best  
available copy to permit the broadest  
possible availability.

Sandia National Laboratories  
Albuquerque, NM 87185  
Operated by  
Sandia Corporation  
U. S. Department of Energy

Prepared for  
Reactor Systems Research Branch  
Division of Accident Evaluation  
Office of Nuclear Regulatory Research  
U. S. Nuclear Regulatory Commission  
Washington, DC 20555

Under Memorandum of Understanding DOE 40-550-75  
NRC FIN No. A-1205

**DISCLAIMER**

This report was prepared as an account of work sponsored by an agency of the United States Government. Neither the United States Government nor any agency thereof, nor any of their employees, makes any warranty, express or implied, or assumes any legal liability or responsibility for the accuracy, completeness, or usefulness of any information, apparatus, product, or process disclosed, or represents that its use would not infringe privately owned rights. Reference herein to any specific commercial product, process, or service by trade name, trademark, manufacturer, or otherwise does not necessarily constitute or imply its endorsement, recommendation, or favoring by the United States Government or any agency thereof. The views and opinions of authors expressed herein do not necessarily state or reflect those of the United States Government or any agency thereof.

*EB*  
DISTRIBUTION OF THIS DOCUMENT IS UNLIMITED

## **DISCLAIMER**

**This report was prepared as an account of work sponsored by an agency of the United States Government. Neither the United States Government nor any agency Thereof, nor any of their employees, makes any warranty, express or implied, or assumes any legal liability or responsibility for the accuracy, completeness, or usefulness of any information, apparatus, product, or process disclosed, or represents that its use would not infringe privately owned rights. Reference herein to any specific commercial product, process, or service by trade name, trademark, manufacturer, or otherwise does not necessarily constitute or imply its endorsement, recommendation, or favoring by the United States Government or any agency thereof. The views and opinions of authors expressed herein do not necessarily state or reflect those of the United States Government or any agency thereof.**

## **DISCLAIMER**

**Portions of this document may be illegible in electronic image products. Images are produced from the best available original document.**



## ABSTRACT

The RELAP5 independent assessment project at Sandia National Laboratories is part of an overall effort funded by the NRC to determine the ability of various systems codes to predict the detailed thermal/hydraulic response of LWRs during accident and off-normal conditions. The RELAP5 code is being assessed at SNLA against test data from various integral and separate effects test facilities. As part of this assessment matrix, a large break transient performed at the LOFT facility has been analyzed.

The results show that RELAP5/MOD1 correctly calculates many of the major system variables (i.e., pressure, break flows, peak clad temperature) early in a large break LOCA. The major problems encountered in the analyses were incorrect pump coastdown and loop seal clearing early in the calculation, excessive pump speedup later in the transient (probably due to too much condensation-induced pressure drop at the ECC injection point), and excess ECC bypass calculated throughout the later portions of the test; only the latter problem significantly affected the overall results. This excess ECC bypass through the downcomer and vessel-side break resulted in too-large late-time break flows and high system pressure due to prolonged choked flow conditions. It also resulted in a second core heatup being calculated after the accumulator emptied, since water was not being retained in the vessel. Analogous calculations with a split-downcomer nodalization delivered some ECC water to the lower plenum, which was then swept up the core and upper plenum and out the other (pump-side) break; thus no significant differences in long-term overall behavior were evident between the calculations.

## TABLE OF CONTENTS

	<u>Page</u>
1.0 Introduction.....	1
2.0 Nodalization.....	3
3.0 Analyses.....	13
3.1 Steady State Calculation.....	13
3.2 Preliminary Transient Calculations.....	14
3.3 Transient Calculation Using Single Downcomer.....	16
3.4 Transient Calculation Using Split Downcomer.....	19
3.5 Computational Speed.....	21
4.0 Discussion and Conclusions.....	67
5.0 References.....	69
Appendix I Facility Description.....	71
Appendix II Input Listings.....	101
Appendix III Additional Updates Used to Create Cycle 18+.....	102

## LIST OF ILLUSTRATIONS

	<u>Page</u>
2.1 LOFT Configuration for L2-5.....	6
2.2 LOFT L2-5 (Single-Downcomer) Nodalization.....	7
2.3 LOFT (Single-Downcomer) Vessel Nodalization.....	8
2.4 Single- and Split-Downcomer Nodalizations Used in L2-5 Analyses.....	9
2.5 LOFT Steam Generator Nodalization.....	10
2.6 Loss Coefficients Used in LOFT L2-5 Nodalization.....	11
3.1.1 Steam Generator Secondary Side Liquid Level for LOFT L2-5 Steady State.....	24
3.1.2 Steam Generator Secondary Side Pressure for LOFT L2-5 Steady State.....	25
3.1.3 Hot Leg Pressure for LOFT L2-5 Steady State.....	26
3.2.1 Calculated and Measured Primary System Pressures for Preliminary LOFT L2-5 Analyses.....	27
3.2.2 Calculated and Measured Pump-side (Hot Leg) Break Mass Flows for Preliminary LOFT L2-5 Analyses...	28
3.2.3 Calculated and Measured Vessel-side (Cold Leg) Break Mass Flows for Preliminary LOFT L2-5 Analyses...	29
3.2.4 Calculated Core Clad Temperatures for Preliminary LOFT L2-5 Analyses.....	30
3.2.5 Calculated and Measured Pump Speeds for Preliminary LOFT L2-5 Analyses.....	31
3.2.6 Calculated and Measured Pump Speeds for LOFT L2-5 (using One-velocity Assumption in Pump Seal Junctions).....	32
3.2.7 Calculated and Measured Intact Loop Cold Leg Mass Flows for LOFT L2-5 (using One-velocity Assumption in Pump Seal Junctions).....	33

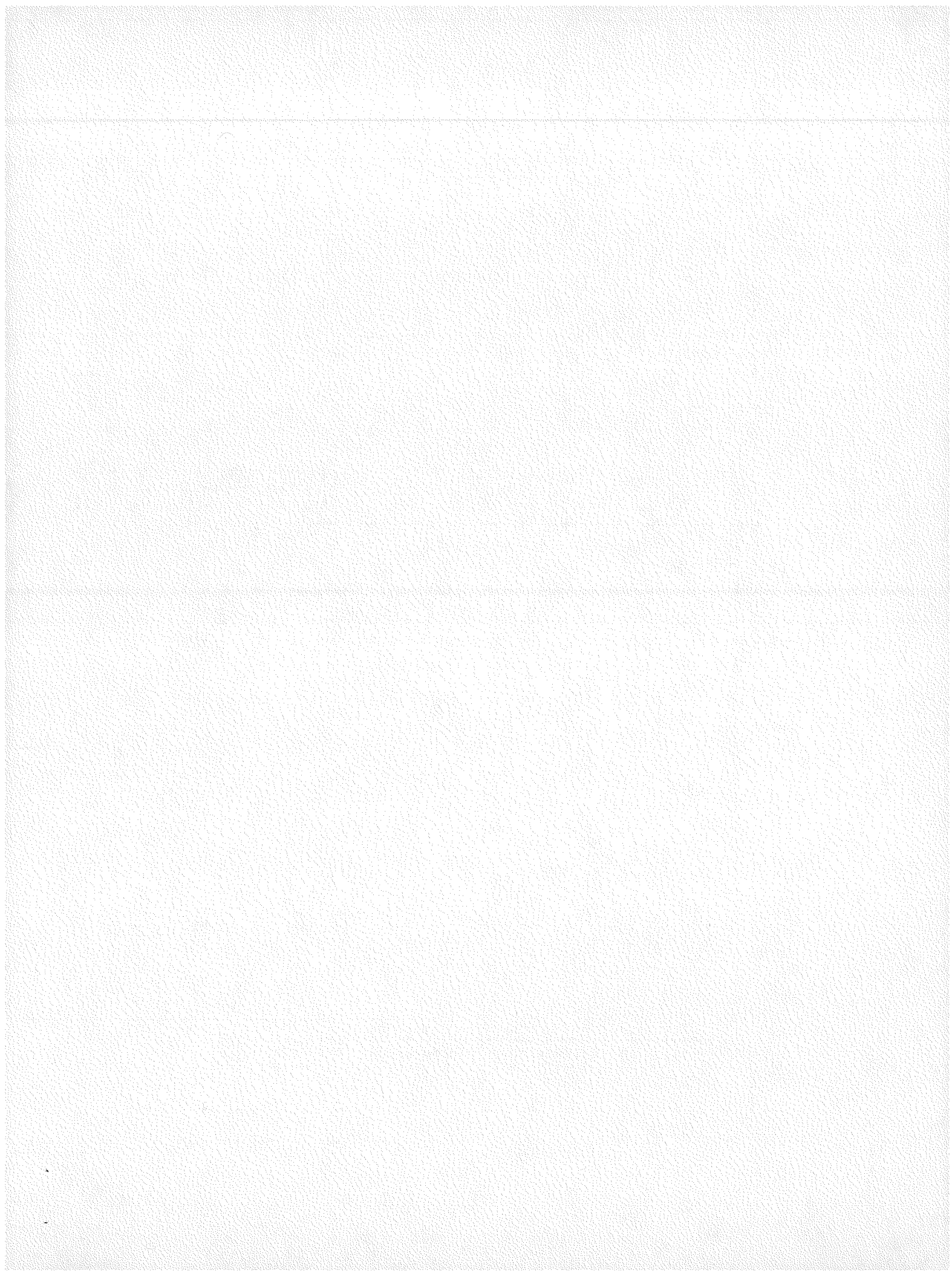
	<u>Page</u>
3.2.8 Calculated and Measured Intact Loop Hot Leg Mass Flows for LOFT L2-5 (using One-velocity Assumption in Pump Seal Junctions).....	34
3.2.9 Calculated and Measured Intact Loop Hot Leg Densities for LOFT L2-5 (using One-velocity Assumption in Pump Seal Junctions).....	35
3.2.10 Calculated and Measured Intact Loop Cold Leg Densities for LOFT L2-5 (using One-velocity Assumption in Pump Seal Junctions).....	36
3.2.11 Injection Point Nodalizations Used for ECC Injection Modelling Sensitivity Studies.....	37
3.2.12 Calculated and Measured Secondary Side Pressures for Preliminary LOFT L2-5 Analyses.....	38
3.2.13 Calculated Secondary Side Liquid Levels for Preliminary LOFT L2-5 Analyses.....	39
3.2.14 Calculated and Measured Secondary Side Pressures for LOFT L2-5 (adding Large Form Loss in Downcomer-Shroud Junction).....	40
3.2.15 Calculated Secondary Side Liquid Levels for LOFT L2-5 (adding Large Form Loss in Downcomer-Shroud Junction).....	41
3.3.1 Calculated and Measured Intact Loop Cold Leg Pressures for LOFT L2-5.....	42
3.3.2 Calculated and Measured Pump-side (Hot Leg) Break Mass Flows for LOFT L2-5.....	43
3.3.3 Calculated and Measured Vessel-side (Cold Leg) Break Mass Flows for LOFT L2-5.....	44
3.3.4 Calculated and Measured Broken Loop Cold Leg Densities for LOFT Test L2-5.....	45
3.3.5 Calculated and Measured Integrated Break Mass Flows for LOFT Test L2-5.....	46
3.3.6 Calculated Fluid Mass in Core for LOFT L2-5.....	47
3.3.7 Calculated and Measured Core Clad Temperatures at 0.21 m Core Elevation for LOFT L2-5.....	48

	<u>Page</u>
3.3.8 Calculated and Measured Core Clad Temperatures at 0.64 m Core Elevation for LOFT L2-5.....	49
3.3.9 Calculated and Measured Core Clad Temperatures at 1.06 m Core Elevation for LOFT L2-5.....	50
3.3.10 Calculated and Measured Core Clad Temperatures at 1.47 m Core Elevation for LOFT L2-5.....	51
3.3.11 Calculated and Measured Core Decay Heats for LOFT L2-5.....	52
3.3.12 Calculated and Measured Intact Loop Hot Leg Temperatures for LOFT L2-5.....	53
3.4.1 Calculated and Measured Integrated Break Flows Using Original and Split- Downcomer Nodalizations for LOFT Test L2-5.....	54
3.4.2 Calculated Primary Mass Inventories Using Original and Split- Downcomer Nodalizations for LOFT Test L2-5.....	55
3.4.3 Calculated Broken Loop Hot Leg Densities Using Original and Split- Downcomer Nodalizations for LOFT Test L2-5.....	56
3.4.4 Calculated Broken Loop Cold Leg Densities Using Original and Split- Downcomer Nodalizations for LOFT Test L2-5.....	57
3.4.5 Calculated Fluid Mass in Core Using Original and Split- Downcomer Nodalizations for LOFT Test L2-5.....	58
3.4.6 Calculated Accumulator Injection Flow Rates Using Original and Split- Downcomer Nodalizations for LOFT Test L2-5.....	59
3.4.7 Calculated Rod Clad Temperatures at 0.64 m Core Elevation Using Original and Split- Downcomer Nodalizations for LOFT Test L2-5.....	60
3.4.8 Calculated and Measured Rod Clad Temperatures at 0.64 m Core Elevation Using Split- Downcomer Nodalization for LOFT Test L2-5.....	61
3.4.9 Calculated and Measured Primary System Pressures Using Original and Split- Downcomer Nodalizations for LOFT Test L2-5.....	62

	<u>Page</u>
3.4.10 Calculated and Measured Broken Loop Hot Leg (Pump-side) Break Flows Using Split- Downcomer Nodalization for LOFT Test L2-5.....	63
3.4.11 Calculated and Measured Broken Loop Cold Leg (Vessel-side) Break Flows Using Split- Downcomer Nodalization for LOFT Test L2-5.....	64
3.5.1 CPU Time Using Original and Split- Downcomer Nodalizations for LOFT L2-5.....	65
AI.1 LOFT Configuration for L2-5.....	76
AI.2 LOFT System -- Intact Loop.....	77
AI.3 Intact Loop Piping.....	78
AI.4 Pressurizer Geometry.....	79
AI.5 Pressurizer Surge Line Routing.....	80
AI.6 Steam Generator Schematic.....	81
AI.7 LOFT System -- Broken Loop.....	82
AI.8 Broken Loop Piping.....	83
AI.9 Reactor Vessel Showing Core Bypass Paths.....	84
AI.10 Reactor Vessel Schematic with Flow Paths.....	85
AI.11 Core Bypass Details.....	86
AI.12 LOFT Core Configuration and Instrumentation.....	87

## LIST OF TABLES

	<u>Page</u>
3.1.1 L2-5 Initial Conditions.....	22
3.3.1 L2-5 Chronology with Original Model.....	23
3.4.1 L2-5 Chronology with Single- and Double-Downcomer Model.....	23
AI.1 LOFT Volume Distribution.....	88
AI.2 Intact Loop Piping Geometry.....	90
AI.3 Pressurizer Surge Line Component Identification.....	92
AI.4 Steam Generator Design Parameters.....	93
AI.5 Steam Generator Data.....	94
AI.6 Broken Loop Piping Geometry.....	95
AI.7 LOFT Reactor Vessel Volume Distribution.....	97
AI.8 Reactor Vessel Material.....	98
AI.9 Reactor Vessel Dimensional Data.....	99
AI.10 Core Bypass Channels.....	100



#### ACKNOWLEDGEMENTS

We would like to express our appreciation for the effort of other Sandia staff involved in the RELAP5 assessment project: John Orman for modifying and maintaining RELAP5 on the Sandia computer system, Katherine McFadden for graphics support and Jan Frey for final construction of the reports.

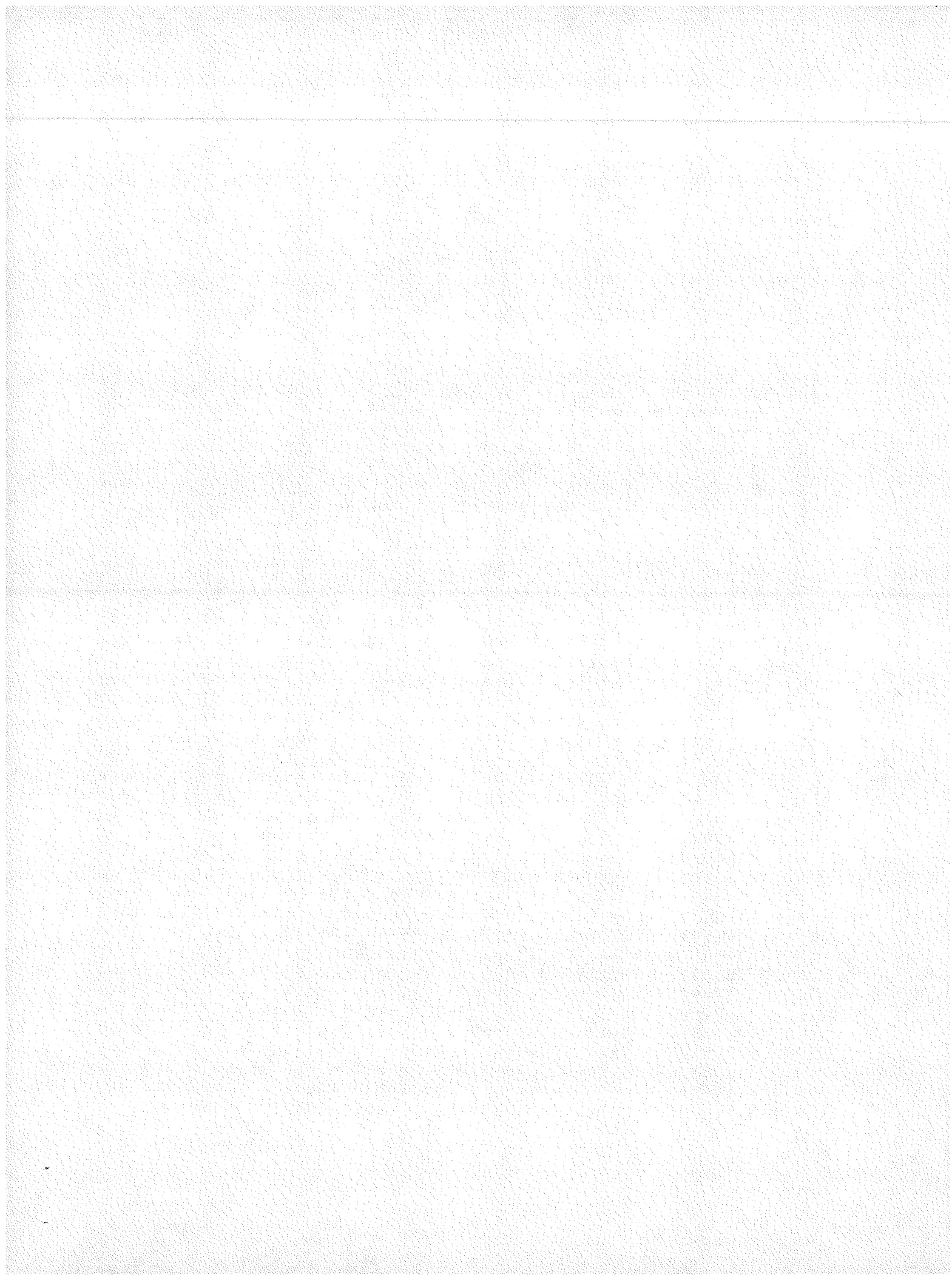


## 1.0 INTRODUCTION

The RELAP5 independent assessment project at Sandia National Laboratories in Albuquerque (SNLA) is part of an overall effort funded by the U. S. Nuclear Regulatory Commission (NRC) to determine the ability of various systems codes to predict the detailed thermal/hydraulic response of LWRs during accident and off-normal conditions. The RELAP5 code [1] is based on a nonhomogeneous and nonequilibrium one-dimensional model for two-phase systems, and has been under development at the Idaho National Engineering Laboratory (INEL) for an extended period, with the first version released in May 1979. The version first used for this assessment project was RELAP5/MOD1/CYCLE14, the latest publicly released version available at the time the project started. In June 1982, we received the formally-released updates creating cycle 18 together with some unreleased, but recommended, updates then being used at INEL. [2] These changes have been used to create and run a MOD1 version at Sandia we call cycle 18+, which was used as the assessment code for these L2-5 analyses.

The RELAP5 code is being assessed at SNLA against test data from various integral and separate effects test facilities. The assessment test matrix includes several transients performed at the Loss-of-Fluid Test (LOFT) facility [3] at INEL. One of these assigned transients was LOFT nuclear experiment L2-5, a 200% large break scenario with early pump trip. [4,5,6] This test was originally in our MOD1.5/MOD2 assessment matrix; since our version of MOD1.5 was not yet ready for production runs, we began preliminary L2-5 calculations with MOD1. The analysis was then completed with MOD1 when the NRC delayed the MOD1.5/MOD2 assessment project.

This report summarizes the RELAP5 analyses of the LOFT L2-5 transient. The RELAP5 models used for the analyses are described in Section 2, and the calculational results are presented in Section 3. The overall conclusions and their possible relevance to future RELAP5 code development are discussed in Section 4. The appendices provide a brief description of the test facility, input listings for the transient, and a list of the additional INEL updates used to create cycle 18+ from cycle 18, for reference.



## 2.0 NODALIZATION

The Loss-of-Fluid Test (LOFT) facility (shown in Figure 2.1) is located at the Idaho National Engineering Laboratory and supported by the NRC. The facility [3] is a 50 MWT pressurized water reactor (PWR) with instrumentation to measure and provide data on the thermal/hydraulic conditions during a postulated accident. The general philosophy in scaling coolant volumes and flow areas was to use the ratio of the LOFT core power (50 MWT) to a typical PWR core (3000 MWT). The experimental assembly includes five major subsystems: the reactor vessel, the intact loop (scaled to represent three operational loops), the broken loop, the blowdown suppression system and the emergency core cooling system. A more detailed description of the test facility is provided in Appendix I.

The original RELAP5 nodalization we developed for LOFT test L2-5 is shown in Figure 2.2. The intact loop is shown on the left while the broken loop is on the right; the vessel is in the middle. A complete input listing for this nodalization is given in Appendix II. The RELAP5 nodalization developed for LOFT experiment L6-7/L9-2 [7] was used as the starting point for this L2-5 nodalization; changes include removing the detailed secondary feedwater train, redefining transient trips, renoding the broken loop to include the steam generator and pump simulators and break assemblies, and adding the required ECC systems.

There are a total of 180 volumes, 194 junctions and 200 heat slabs in this nodalization. In the intact loop, 2 volumes are used for the two parallel primary coolant pumps and 30 volumes are used to model the piping. The steam generator contains a total of 31 volumes -- 10 for the primary side plena and U-tubes, 17 in the secondary side, 3 for the steam outflow and 1 for the feedwater. The pressurizer and its surge line are modelled with 21 volumes, 9 of which are in the pressurizer itself, 1 which represents the spray cooling line and 1 time-dependent volume which provides the steady state boundary condition. The broken loop contains 46 volumes, 2 of which are time-dependent volumes providing break downstream boundary conditions. The vessel itself is modelled with 45 volumes -- 9 in the main annular downcomer, 3 in the lower plenum, 4 in the core, 4 in the upper plenum, and 25 representing various secondary and bypass flow paths. The ECCS is modelled by 5 volumes, 1 for the accumulator, 2 modelling surge line piping, and one time-dependent volume each for HPIS and LPIS. Heat slabs for most of the piping and major structural mass are included, as well as for the core fuel rods and steam generator U-tubes. Most of the heat slabs contain five nodes, although the fuel rods are modelled with ten, and a few of the thick plates in the vessel have from nine to twenty nodes.

The vessel nodalization is shown in more detail in Figure 2.3. The relative elevations of the cell boundaries are given, as are either cell flow areas or volumes. Most of the vessel flow areas were taken from a careful study of the flow area data given in Table A-5 of reference [3]. We attempted to model most area changes explicitly (e.g., small flow area changes in the downcomer). However, we modelled a rapid series of area changes (such as in the lower core support structure) as a typical area with a geometrically-derived loss coefficient. The bypass controlling junctions are indicated (with the number corresponding to the bypass identifiers used in the description given in Appendix I); based on guidelines developed during this assessment project [7], these bypass paths were modelled with user-input loss coefficients at default flow areas. Besides the fuel rods themselves, heat slabs have been included for the outer vessel, the filler blocks, the core barrel, the upper and lower core support structures, and the upper closure plate. These heat slabs account for ~89,000 kg of vessel structural mass (as compared to ~93,000 kg of vessel structural mass shown in Table AI.8).

(As part of the L2-5 analyses, calculations were also done using a modified vessel nodalization with a split downcomer, in an effort to force ECC delivery to the lower plenum (as discussed below in more detail in Section 3.4). The details of this split downcomer model are shown in Figure 2.4; the downcomer piping (and, not shown, its associated heat slabs) was divided into two equal area flow paths, and limited crossflow was permitted by the two crossflow junctions (573 and 574) defined. Sensitivity studies were done in which the user-input loss coefficient at these two junctions was varied from a geometrically-based low crossflow resistance of  $K \sim 1.5$  to an artificially-increased high crossflow resistance of  $K \sim 100$ .)

The steam generator nodalization is shown in Figure 2.5, with the relative elevations of the cell boundaries. All the U-tubes are lumped into a single flow path. Besides the U-tubes themselves, heat slabs representing the tube sheet, the shroud and the external wall are included in the model. Because of the limited amount of information on the steam generator secondary side in the facility description [3], we had to estimate the secondary volume distribution, given the global secondary volumes and dimensions in Tables AI.4 and AI.5.

All area changes and elbows are carefully modelled in the loop piping. Figure 2.6 shows the loss coefficients used in the (basecase) calculations. These loss coefficients can be either user-input, as for elbow losses, or code-calculated using abrupt area change models. The user-input numbers are given first; two values are given for the forward and reverse loss coefficients respectively, if they are different. The code-calculated numbers,

which are shown in parentheses, are single-phase values (in the direction of normal steady-state flow) which may change in two-phase flow. The resulting pressure drops are in good agreement with the differential pressure measurements for steady-state conditions.

The pump homologous curves first used were those handed out at the LOFT/Semiscale modelling workshop [8]. (As discussed below in Section 3.2, we later modified some of the pump curve input.) Also taken from the data made available at that workshop were the nominal values of the various bypass flows and the estimated environmental heat loss magnitude and distribution. In our nodalization, we used average heat transfer coefficients for natural convection for the appropriate component sizes and temperatures [9], and assumed containment temperature to be 300 K. Heat transfer coefficients were approximated by linear functions of surface temperature. Three functions were used one for all of the piping, another for the vessel cylinder and a third, artificially lowered, function for the pressurizer and steam generator walls (to match the given ambient heat loss distribution [8]). These yield a steady-state heat loss of ~200 kW -- 30 kW from the steam generator secondary, 103 kW from the vessel, 29 kW and 27 kW from the intact and broken loop piping respectively, and 11 kW from the pressurizer.

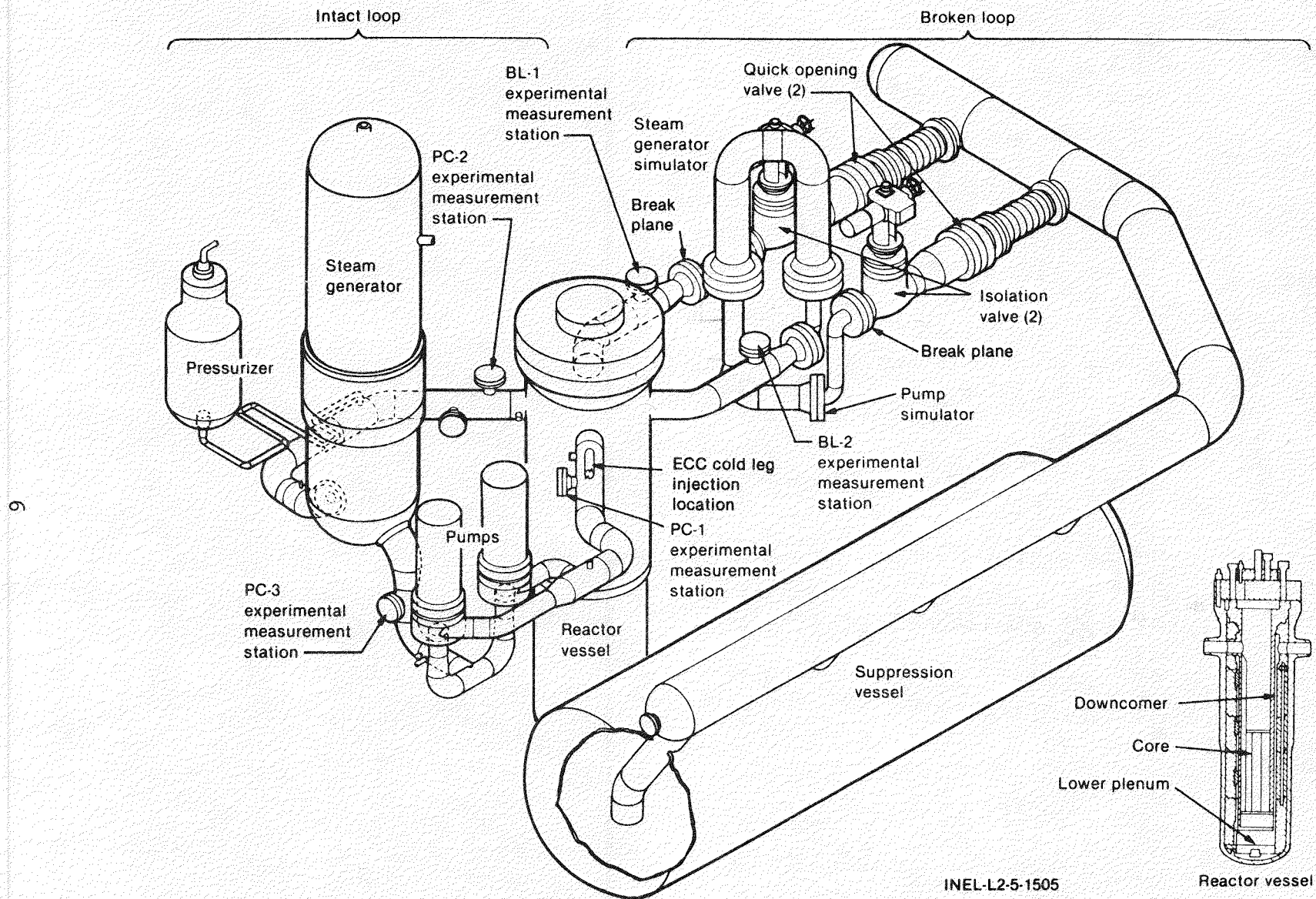


Figure 2.1 LOFT Configuration for L2-5

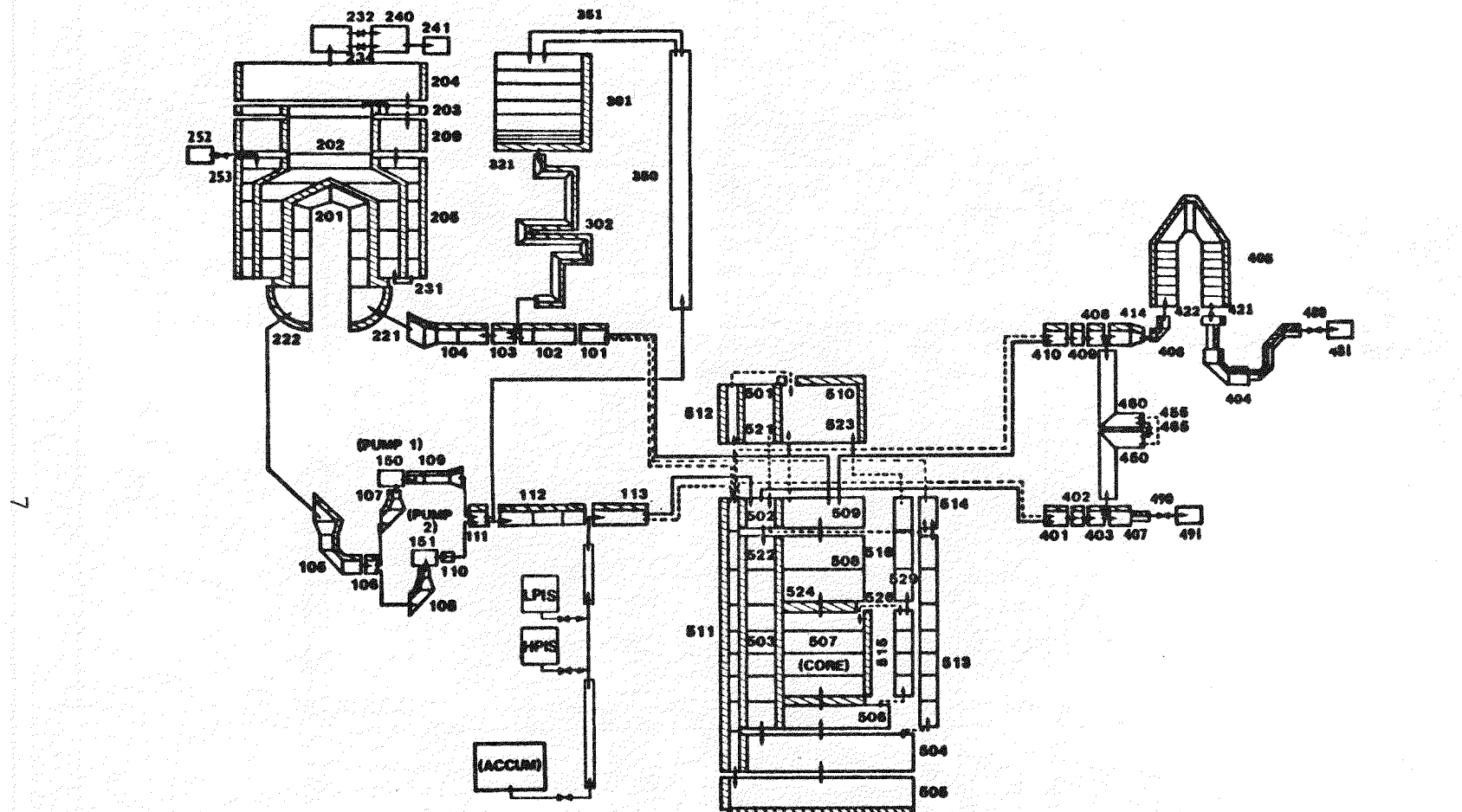


Figure 2.2 LOFT L2-5 (Single-Downcomer) Nodalization

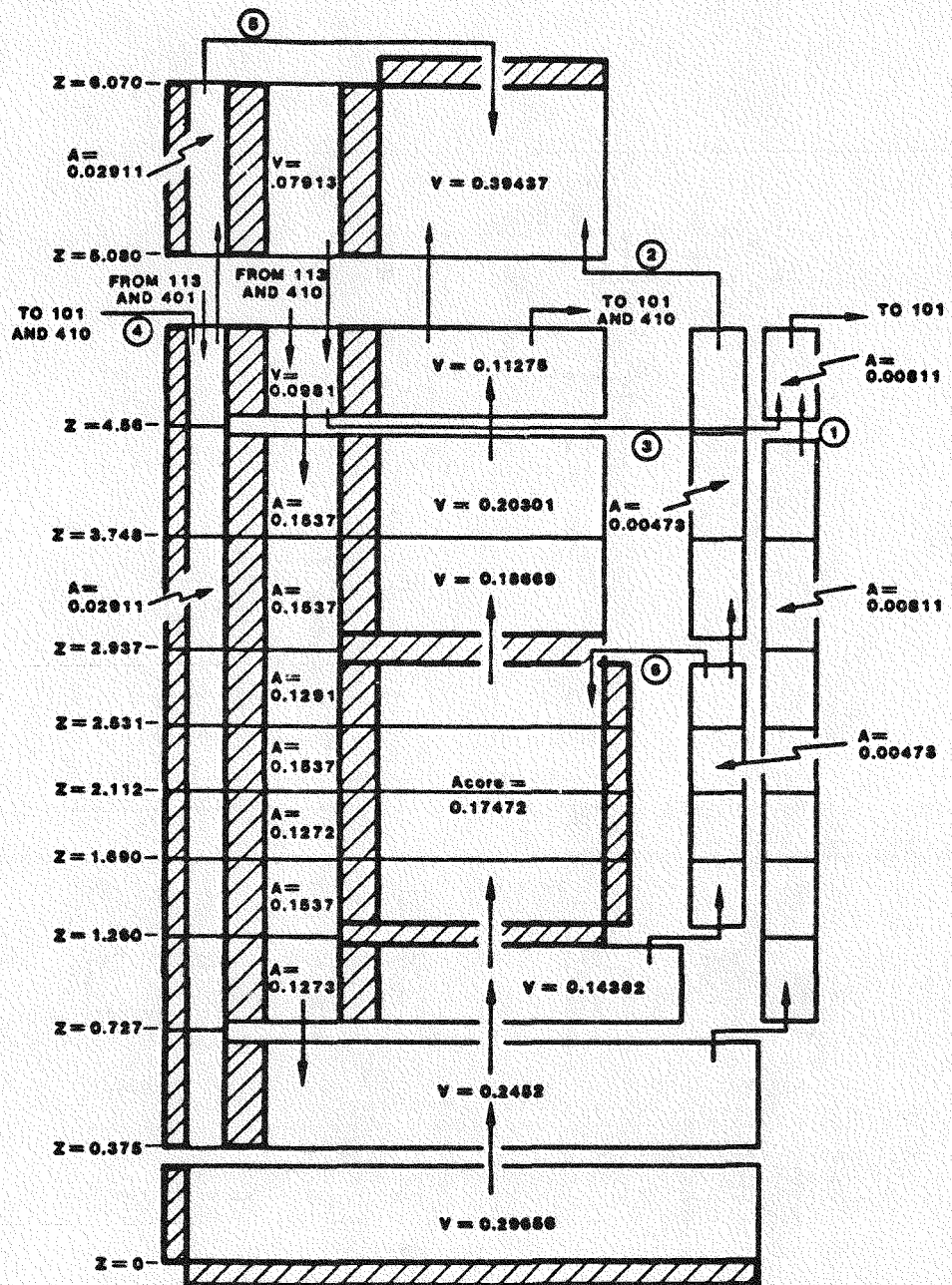


Figure 2.3 LOFT (Single-Downcomer) Vessel Nodalization

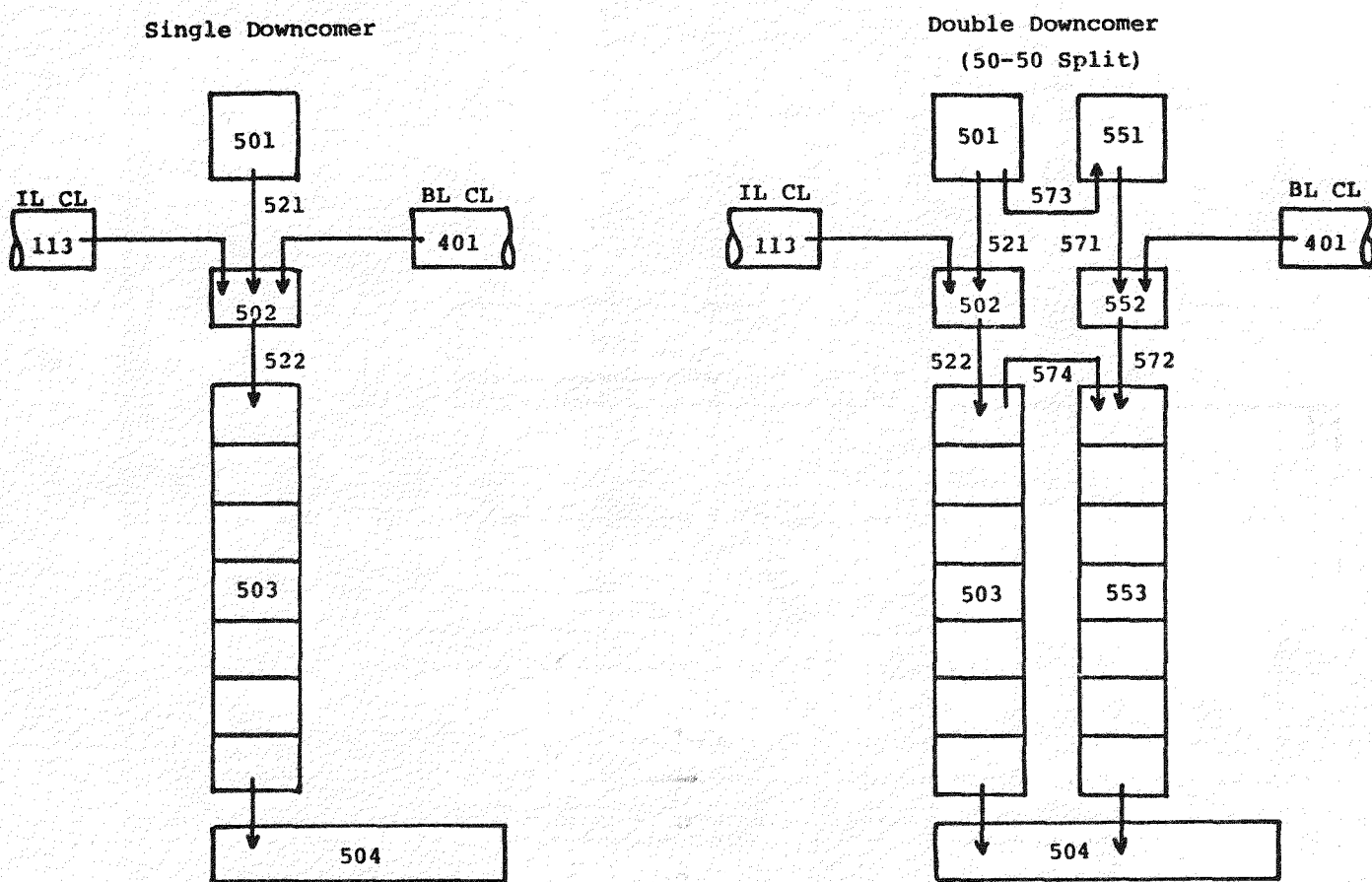


Figure 2.4 Split-Downcomer Nodalization used in L2-5 Analyses

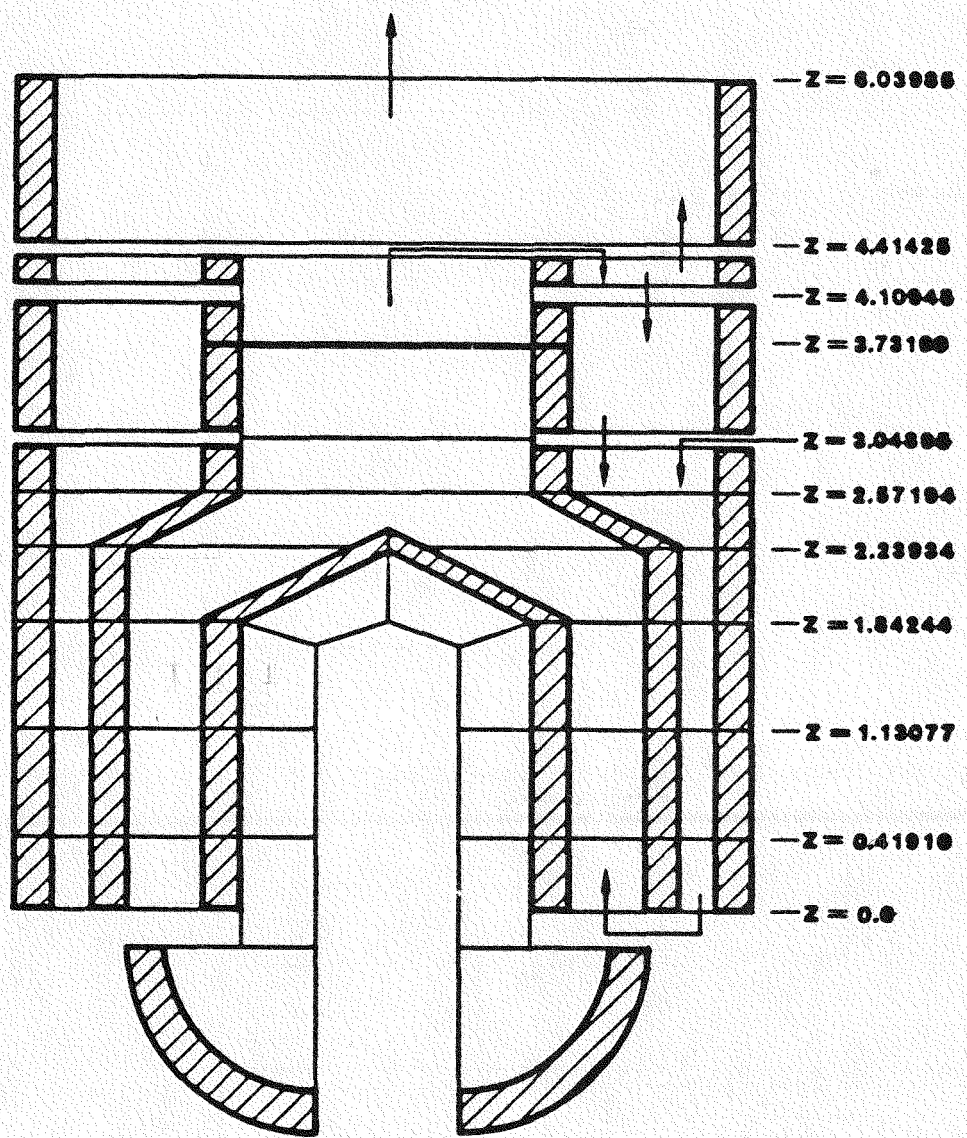


Figure 2.5 LOFT Steam Generator Nodalization

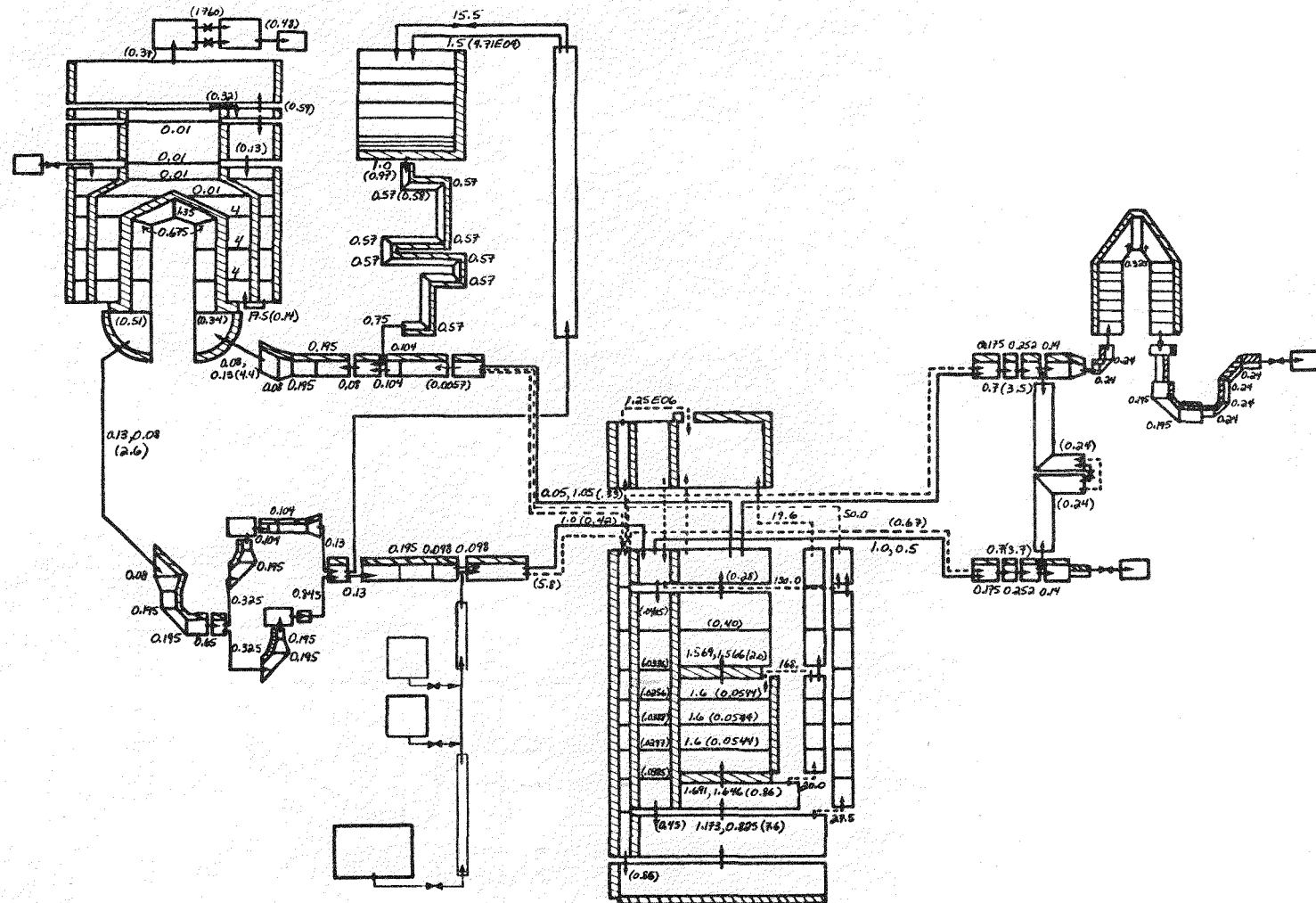
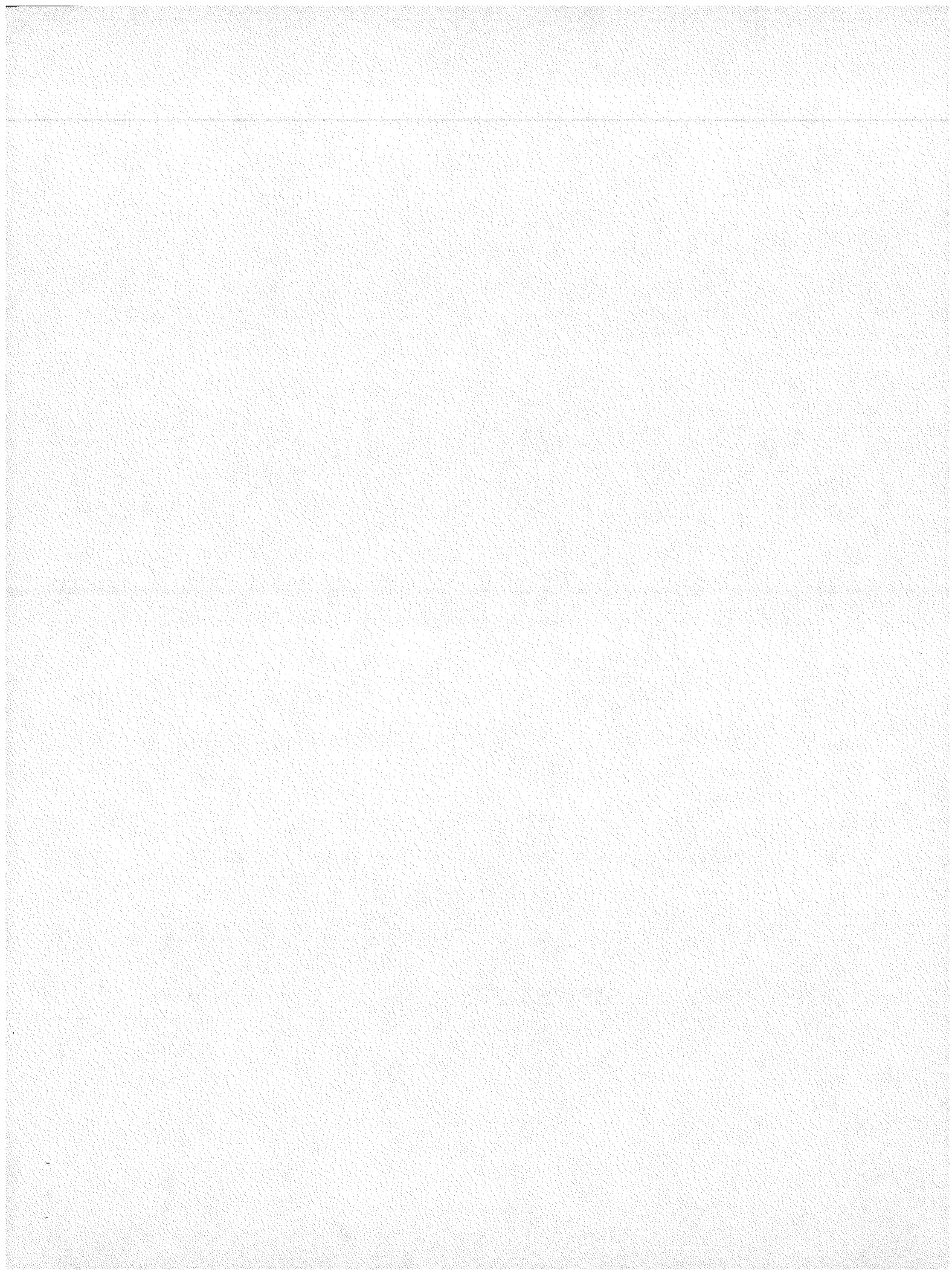


Figure 2.6 Loss Coefficients Used in LOFT L2-5 Nodalization



### 3.0 ANALYSES

LOFT experiment L2-5, successfully completed on June 16, 1982, consisted of a double-ended 200% cold leg break. The reactor scrammed on low pressure and the primary coolant pumps were manually tripped and decoupled from their flywheels within 1 second after break initiation, in an attempt to avoid early fuel rod rewet. This was generally achieved except for a rewet of the upper portion of the central fuel assembly that began at ~12 s and ended at ~23 s. Accumulator injection into the intact loop cold leg began at ~17 s; HPIS and LPIS injection were delayed until ~24 and ~37 s, respectively, to simulate the delay expected for a PWR emergency diesel to begin delivering power in response to a loss-of-offsite-power accident. The fuel rod peak clad temperature of  $1078 \pm 13$  K occurred at 28.5 s. The clad was quenched and the core recovered within 70 s of break initiation. The LPIS injection was stopped at ~107 s, after the L2-5 experiment was considered complete, and another test was begun. The blowdown suppression tank (BST) pressure was automatically controlled by the spray system throughout the test to simulate the containment backpressure expected during a PWR LOCA. [4,5,6]

#### 3.1 Steady State Calculation

Ideally, one wants to calculate all the experimental initial conditions for the primary and secondary sides simultaneously, within the given experimental uncertainties. We were readily able to achieve such an initial condition for L2-5 (shown in Table 3.1.1), starting from the L6-7/L9-2 steady state [7]; the user experience gained in that calculation and others [10,11] simplified the L2-5 initialization considerably.

A steam-filled time-dependent volume attached to the top of the pressurizer maintained the desired primary pressure without difficulty, and, as in our previous assessment calculations, using an integral controller to adjust the primary pump speed worked very well. Also as before, the steam flow valve was controlled to match the steam dome pressure using an exponential relaxation scheme. The desired secondary pressure resulted in primary side temperatures within the high side of the experimental uncertainties after defining the U-tube secondary side heated equivalent diameter to be the U-tube minimum tube-to-tube spacing; this particular value had already been determined from previous assessment calculations [7,10,11], and was not further adjusted during the L2-5 initialization.

A small increase in a Courant limit condition allowed the code-selected time step to double during the latter part ( $> 50$  s) of the steady state calculation, resulting in oscillations in both the secondary side liquid level (shown in Figure 3.1.1) and

secondary pressure (shown in Figure 3.1.2); these oscillations were then transmitted to the primary side, as shown by the hot leg pressure in Figure 3.1.3. The oscillations, however, were a relatively minor problem that could be eliminated by a user-forced reduction of the time step, as demonstrated at 190 s in the figure.

### 3.2 Preliminary Transient Calculations

The L2-5 transient was run several times. In the first transient calculations, the broken loop steam generator simulator nodalization was refined to model the multiple orifice plates explicitly; we found that this allowed better prediction of the very-early-time sequential flashing throughout the broken loop and the peak hot leg (pump-side) subcooled break flow, without any additional user-input loss coefficients being required. The primary system pressure (shown in Figure 3.2.1), and the cold leg (vessel-side) and hot leg (pump-side) break flows (shown in Figures 3.2.2 and 3.2.3) during the first ~30 seconds were all in reasonably good agreement with experimental data for these early calculations. The predicted clad temperatures (shown for our four core nodes in Figure 3.2.4) were also well-behaved, particularly during the blowdown time of ~10 s. The various studies reported in this section had very little visible effect on these major system variables.

Although the primary pressure and break flows were well-behaved, Figure 3.2.5 shows that the primary coolant pump response was not being correctly predicted after ~8 seconds: the pump data shows a plateau with the pump "free-wheeling" until established accumulator injection began forcing a slow speedup, while the calculation continues the initial rapid coastdown until the start of full accumulator injection at ~20 seconds when the pump speed rises very rapidly to ~300 rad/s. This discrepant pump response did not apparently feed back significantly to the overall calculated behavior.

The first efforts to calculate pump coastdown and subsequent speedup in better agreement with the L2-5 experimental data involved replacing parts of the pump homologous curves (the head and torque two-phase multiplier tables and first quadrant two-phase difference curves) with new pump curves developed by LOFT personnel. The new curves were based on the L3-6 (pumps-off small break test) experimental data [12]. This modification allowed the change in pump speed at ~8 seconds in L2-5 to be calculated correctly, but the revised calculation ran into trouble later when attempting to calculate the intact loop pump seal clearing at ~20-30 s; the seal cleared late and catastrophically. We have not yet found a way to calculate the "correct" intact loop pump seal behavior, but by using the

one-velocity formalism in the loop seal junctions (i.e., setting  $h=2$  in the cahs junction flag) we can force the desired behavior since the liquid present is then constrained to move with the vapor flow. These two changes yield better calculated early-time pump behavior, as shown in Figure 3.2.6, but the different pump behavior has no significant effect on the overall system behavior.

Although the pump still speeds up too much when the ECC injection begins at  $\sim 15-20$  s, it then begins a series of small oscillations from 150 rad/s to 280 rad/s qualitatively similar to those in the experimental data. The high pump speeds persist until about 70 s, and the timing provides a clue to a possible source of this problem. The period between  $\sim 20-70$  s in the calculation corresponds to the time during which the accumulator is injecting a large amount of subcooled ECC water into the intact loop cold leg, just as the somewhat shorter period of measured pump speedup of  $\sim 20-60$  s corresponds to the slightly shorter time the accumulator was actually injecting in the experiment (discussed later in more detail in Section 3.3). The most probable cause of the calculated excessive pump speedup is over-estimation of the condensation-induced pressure drop at the ECC injection point, which creates a suction effect pulling more flow through the intact loop. Too much flow is being pulled through the hot leg piping, steam generator and pump as a result.

Figures 3.2.7 and 3.2.8 show the calculated and measured intact loop cold and hot leg mass flow rates. (The instrumentation for the hot leg flow does not measure direction, but only magnitude, of flow.) While the cold leg flow rate shows relatively good agreement with data, the hot leg flow is high compared to data when the excessive pump speeds are being calculated. Comparison of measured and calculated intact loop hot leg densities shown in Figure 3.2.9 shows that the high calculated mass flow is not a result of much more liquid, and thus must be due to higher velocities. Irregardless of whether the higher mass flows are caused by too large an ECC condensation pressure drop (as suggested by the timing), or are simply due to the code calculating too high a two-phase natural circulation flow rate (as indicated by other assessment calculations [13,14]), the higher mass flow calculated accounts for the incorrect pump speedup.

Some sensitivity studies were also done in these early transient calculations on the ECC injection modelling, with part of the injection being forced to flow upstream toward the pump in an effort to calculate the slugs of water appearing upstream of the injection point in the data, shown in the intact loop density data plot in Figure 3.2.10. Calculations were done with the ECC injection junction pointing toward the vessel (the basecase, as

shown in Figures 2.2 and 3.2.11a), pointing back toward the pump (Figure 3.2.11b), and split into two junctions, one pointing upstream and the other downstream (Figure 3.2.11c). The two junction configuration required a check valve to prevent unphysical recirculation flows before ECC injection began, and then still calculated some unphysical recirculation flow patterns after ECC injection initiation. Injecting all the ECC water toward the pump eventually filled up the upstream cold leg, pump and pump suction leg. Injecting the ECC toward the vessel (in the normal manner) gave the best calculated results, although the slugs of water appearing in the data upstream of the injection point were seldom or never calculated.

Another problem encountered in these preliminary calculations was the unavoidable code failure when the accumulator emptied and was supposed to start injecting nitrogen. Discussions with the code developers revealed that this is a known (but undocumented) problem in both MOD1 and MOD1.5 which has to be modelled around; the accumulator must be valved shut when it runs out of water. (Currently the accumulator will correctly empty and inject nitrogen only if all volumes in the model are defined to be (nonstandard) equilibrium volumes. The difficulty arises from an incomplete model in the wall heat transfer package.)

Although apparently having no significant effect on the overall transient behavior being calculated, the early calculations also showed problems matching the observed (slight) secondary side depressurization. As shown in Figure 3.2.12, the analyses predicted a much greater pressure drop than measured in the latter portion of the test. The lower secondary side pressure and associated low saturation temperature affected the primary side steam generator outlet plenum temperature being calculated. The source of the greater calculated depressurization was found to be manometer-type oscillations in the (stagnant) secondary side, shown in Figure 3.2.13; every cycle, some steam was condensed, with a consequent drop in pressure. This resulted in a steady oscillation which would last throughout the L2-5 transient. An artificially large form loss ( $K = 200$ ) was added in the downcomer-shroud junction to damp these oscillations and help maintain secondary pressure after the start of the transient, as shown in Figures 3.2.14 and 3.2.15.

### 3.3 Transient Calculation Using Single Downcomer

Despite the known problems discussed in the previous section, the L2-5 transient was run to completion, i.e., until the official end of the experiment at ~100 s; Table 3.3.1 gives the measured and calculated sequence of events. (The calculations discussed in this and the next section used the revised pump curves, the one-velocity formalism in the loop seal junctions and

a large form loss coefficient in the secondary side downcomer-shroud junction to damp the secondary side oscillations. The ECC injection was pointed toward the vessel as was shown in Figure 2.2.)

The intact loop cold leg pressure for the final calculation is shown in Figure 3.3.1. Despite slightly overpredicted depressurization around 5-10 s and later-time (~30-70 s) pressure oscillations traceable to the effects of ECC injection, the overall agreement with the measured data is very good. The vessel-side (cold leg) and pump-side (hot leg) break flows are shown in Figures 3.3.2 and 3.3.3. Again, despite some discrepancies due to excessive calculated ECC bypass, the overall agreement between analysis and data is very good, using subcooled and saturated discharge coefficients of 0.85. The effect of the accumulator injection beginning at ~15 s can clearly be seen in the broken loop cold leg flow; the analysis bypasses the injected ECC water to the broken loop and out the vessel-side break. The excess ECC bypass causes the break flow to remain choked longer in the calculation, holding up the system pressure at later times.

Figure 3.3.4 shows the calculated and measured broken loop cold leg density, with the analysis showing much more water present in the broken loop cold leg throughout the period of accumulator injection (~15-70 s) than was measured, particularly at late times (~60-70 s). The broken loop cold leg does not void in either the calculation or the test until about 10 seconds after the accumulator empties; as shown in Table 3.3.1, the accumulator in the experiment ran out of water somewhat sooner (~50 s) than occurred in the analysis (~68 s), primarily because the calculated accumulator injection appears about 10% low. (No experimental accumulator flow rate is given, so the flow must be estimated from the change in accumulator liquid level.)

This excess ECC bypass is best seen by looking at the integrated break flows, shown in Figure 3.3.5. The agreement with data is excellent until accumulator injection begins, but the calculated mass lost quickly diverges from measurement thereafter. The higher calculated mass lost corresponds to bypassing most of the ECC water through the downcomer and out the broken loop cold leg (vessel-side) break throughout the period of accumulator injection. The actual behavior expected and observed consists of a relatively short period of ECC bypass followed by substantial delivery down the downcomer to the vessel lower plenum at later times. The broken loop hot leg (pump-side) break flow is also a bit high compared to data at late times, the result of any ECC liquid reaching the lower plenum being entrained and swept up the core and out that break (as will be discussed in more detail in the next section). Thus, any accumulator water reaching the lower plenum is not retained in the vessel.

Unlike the discrepant pump coastdown/speedup behavior being calculated, this excess ECC bypass and entrainment significantly affects the overall results being calculated at late times; the analysis will show no vessel and core refill and reflood, and the core will not be recovered and quenched at the end of the transient. Figure 3.3.6 shows the fluid mass in the core throughout the transient calculation. Although there is a slight increase in the amount of water in the core during the period of accumulator injection, this water is swept up the vessel and out the hot leg break very soon after the accumulator empties and, as will be seen in the rod temperature plots, the core begins heating up again at the end of the transient.

Rod clad temperatures are shown in Figures 3.3.7 through 3.3.10. The plotted experimental data in each figure includes all thermocouples closest in elevation to that particular heat slab midpoint, to give an idea of the overall core response. The considerable radial power variation in the facility, which we are not attempting to model, contributes to the different thermocouple readings throughout the core.

The early heatup is calculated well, except at the top of the core, where the initial rise is late but the first total rewet is correctly calculated. The calculated PCT of 1105 K is in good agreement with data (noting that the experimental PCT of 1077 K occurs at a core elevation not included in the plots, between our second and third core levels), but the code predicts an early blowdown PCT at ~10 s while the data shows PCT occurring at ~30 s, corresponding to the start of reflood. (The data does show an almost flat plateau in the higher-powered regions through these times.) We are, however, comparing an average calculated PCT (with no radial peaking modelled), with an absolute PCT given by a single thermocouple measurement in a facility with significant radial peaking, so that the calculated PCT is high compared to the average data. The reason for this may be found by comparing the calculated and experimental core decay heats shown (together with the calculated total power) in Figure 3.3.11, showing that cycle 18 of RELAP5/MOD1 is overpredicting the decay heat throughout most of the transient, which results in higher calculated clad temperatures. Similar behavior has been seen in other Sandia assessment calculations [15,16], with cycle 14 calculating decay heats lower than data and cycle 18 (with an update "fix" to the reactor kinetics which results in higher calculated decay heat) giving decay heats higher than experimental data.

The core response after PCT occurs consists of a gradual cooldown calculated with roughly half the thermocouples showing significantly higher temperatures while the other half show quench to the saturation temperature. Although a sharp quench

front progressing through the core is not being calculated by MOD1, the lower half of the core in particular is calculated to all be "quenched" (i.e., at saturation) by the correct time. However, due to the excess ECC bypass being calculated, the analysis incorrectly shows the core beginning to heat up again after the end of accumulator injection at ~70 s.

The clad temperature agreement is generally better in the lower half of the core and calculated rod temperatures fall progressively below data higher in the core, and at later times. This is not thought to be due to any axial power shape uncertainty since the same behavior is seen with electrically heated rods (LOBI) [17] as with nuclear fuel in LOFT. The main reason appears to be that MOD1 cannot calculate a mixture of superheated steam and entrained saturated droplets (with the heat transfer from the rods to the steam), because it vaporizes all liquid before superheating any steam. We expect such a mixture of superheated steam and entrained saturated droplets to be generated in the lower portions of the core as the ECC water comes in. Among the supporting evidence is that hot leg superheat resulting from superheated steam leaving the core is seen experimentally, but no hot leg superheat is calculated, as shown in Figure 3.3.12. (The data shows hot leg superheat from ~30 s, the start of core reflood, until ~50 s when the accumulator injection ends in the experiment; the timing apparently verifies the generation of superheated steam from the ECC water in the core.)

### 3.4 Transient Calculation Using Split Downcomer

The major problems encountered in the L2-5 transient calculations were the error in calculated pump coastdown, the failure of the loop seal to clear properly and the excess ECC bypass being calculated (with resulting errors in both break flow and late-time vessel inventory). The discrepant early-time loop seal clearing and pump response have been discussed in Section 3.2, and are not considered major problems. The excess ECC bypass and entrainment being calculated, on the other hand, which keeps the break flow choked and the system pressure up later in the transient, and results in a late-time core heatup being calculated, is much more significant.

Difficulties calculating correct ECC bypass/penetration behavior have been encountered in many other RELAP5 analyses, notably in our BCL assessment calculations [18]. These BCL results, and the reported INEL L2-5 analyses [19], led us to redo the transient calculation using a split downcomer nodalization, described earlier in Section 2. (In the crossplots given in this section, "calc 1" and "sdc" refer to the original single downcomer analyses while "calc 2" and "ddc" refer to the final double-downcomer calculations.)

The results of early double-downcomer analyses were still similar to the original single-downcomer results, because the geometrically-derived resistance in each crossflow junction was relatively low ( $K \sim 1.5$ ). The crossflow resistance was then artificially increased to more closely resemble the INEL [19] value ( $K \sim 100$ ), with considerably different results. Accumulator ECC water is now delivered to the lower plenum but, rather than remain and slowly refill the vessel, it is then pulled through the core and upper plenum and out the pump-side hot leg break; this was also what happened to the much smaller amount of ECC water reaching the lower plenum in the original single-downcomer calculation discussed above in Section 3.3.

Figure 3.4.1 shows the integrated break flows for both the single-downcomer calculation discussed in Section 3.3 and the high-crossflow-resistance split-downcomer calculation. Both lose too much mass compared to data, with the original nodalization losing somewhat more total mass (shown better by the primary mass inventories in Figure 3.4.2). However, the double-downcomer model loses more mass out the hot leg (pump-side) break and less out the cold leg (vessel-side) break than the single-downcomer model; this is also seen by comparing the broken loop hot and cold leg densities in the two calculations, as is done in Figures 3.4.3 and 3.4.4.

The relatively large amount of entrained ECC water being pulled through the core in the double-downcomer analysis, compared to that in the original single-downcomer calculation, is shown in Figure 3.4.5. (As shown in Figure 3.4.6, the accumulator injection is virtually identical in the two calculations.) The greater quantity of liquid present in the core during the period of accumulator injection (~15-65 s) results in slightly more rapid fuel rod cooling, shown for the hottest of the four core nodes in Figure 3.4.7. The comparison to rod temperature data is, however, similar to that seen in the single-downcomer analysis, because of the wide variation in the various thermocouple readings (as shown for the same node plotted against experimental data in Figures 3.3.8 and 3.4.8). The peak clad temperature in the split-downcomer calculation is a few degrees lower than that in the original single-downcomer analysis. The slightly larger late-time system inventory (Figure 3.4.2) and the relatively later voiding of the core (Figure 3.4.5) in the double-downcomer analysis results in later onset of the late-time core heatup compared to that calculated using the original single-downcomer model.

Despite the different ECC behavior being calculated in the two calculations, the overall system response is not significantly affected, as shown by the primary system pressure in Figure 3.4.9, although the double-downcomer nodalization does

yield slightly better early time agreement with data with the large crossflow resistance holding up the intact loop pressure slightly during the period ~10-20 s. And, although the integrated break flows in the two calculations are quite visibly different (Figure 3.4.1), the calculated hot (pump-side) and cold (vessel-side) break flows evince similar agreement with data as did the results of the single-downcomer calculation, as seen by comparing Figures 3.3.2 and 3.3.3 to Figures 3.4.10 and 3.4.11; the differences in calculated behavior are hard to see amid the experimental noise.

### 3.5 Computational Speed

The single-downcomer L2-5 calculation, run with RELAP5/MOD1/CYCLE18+, required 3.27 hours of CPU time on a CRAY-1S computer to run a total of 112 seconds of problem time (which includes 10 seconds of steady state for plot purposes), while the double-downcomer calculation required 4.02 hours of Cray CPU time to run 113 seconds of problem time (again with 10 seconds of steady state), as shown in Figure 3.5.1. Except for a short time in the split-downcomer analysis when the time step had to be forcibly cut in order to continue calculating (discussed below in more detail), the time step used in both calculations was dominated by Courant limits in the broken loop piping.

The ~20% difference in run time is not due to the slightly greater number of cells in the double-downcomer model, but is primarily caused by a code problem encountered at ~50 s in the latter calculation which required the user to drastically reduce the time step in order to avoid a code abort. When a plug of water temporarily blocked the broken loop hot leg flow, a low pressure region caused one of the cells in the broken loop piping to suddenly dry out and heat up sufficiently ( $T > 1500$  K) to cause a steam table failure; cutting the time step for a few seconds of problem time allowed the difficulty to be bypassed.

Table 3.1.1 L2-5 Initial Conditions

Parameter	Data	RELAP5
Core Power (MW)	36.0 $\pm$ 1.2	36.0
Pressure (MPa)	14.94 $\pm$ 0.06	14.91
IL Hot Leg Temp (K)	589.7 $\pm$ 1.6	590.2
IL Cold Leg Temp (K)	556.6 $\pm$ 4.0	557.1
Core $\Delta T$ (K)	33.1 $\pm$ 4.3	33.1
IL Mass Flow (kg/s)	192.4 $\pm$ 7.8	195.9
Pump Speed (rad/s)	131	134
Pressurizer Temp (K)	615.0 $\pm$ 0.3	614.8
Przr Steam Vol (m $^{**3}$ )	0.32 $\pm$ 0.02	0.35
Przr Liquid Vol (m $^{**3}$ )	0.61 $\pm$ 0.02	0.61
BL Hot Leg Temp (K)	561.9 $\pm$ 4.3	561.9
BL Cold Leg Temp (K)	554.3 $\pm$ 4.2	554.2
SG Sec Pressure (MPa)	5.85 $\pm$ 0.06	5.85
SG Sec Temperature (K)	547.1 $\pm$ 0.6	547.0
SG Sec Mass Flow (kg/s)	19.1 $\pm$ 0.4	19.1
Accum Liquid Vol (m $^{**3}$ )	2.92 $\pm$ 0.01	2.92
Accum Pressure (MPa)	4.29 $\pm$ 0.06	4.29

Table 3.3.1 L2-5 Chronology with Original Model

Event	Time (s)	
	Data	RELAP5
Experiment Initiated	0.0	0.0
Reactor Scrammed	0.24±0.01	0.24
Pumps Tripped	0.94±0.01	0.94
Pressurizer Empty	15.4 ±1.0	11.7
Accumulator Begins	16.8 ±0.1	15.1
HPIS Injection Begins	23.9 ±0.02	23.9
LPIS Injection Begins	37.32±0.02	37.32
Accumulator Empty	49.6 ±0.1	68.4
End of L2-5	107.1	

Table 3.4.1 L2-5 Chronology with Single- and Double-Downcomer Nodalization

Event	Time (s)		
	Data	SDC*	DDC**
Experiment Initiated	0.0	0.0	0.0
Reactor Scrammed	0.24±0.01	0.24	0.24
Pumps Tripped	0.94±0.01	0.94	0.94
Pressurizer Empty	15.4 ±1.0	11.7	11.7
Accumulator Begins	16.8 ±0.1	15.1	16.0
HPIS Injection Begins	23.9 ±0.02	23.9	23.9
LPIS Injection Begins	37.32±0.02	37.32	37.32
Accumulator Empty	49.6 ±0.1	68.4	66.5
End of L2-5	107.1		

\* SDC = Single-Downcomer Calculation

\*\* DDC = Double-Downcomer Calculation

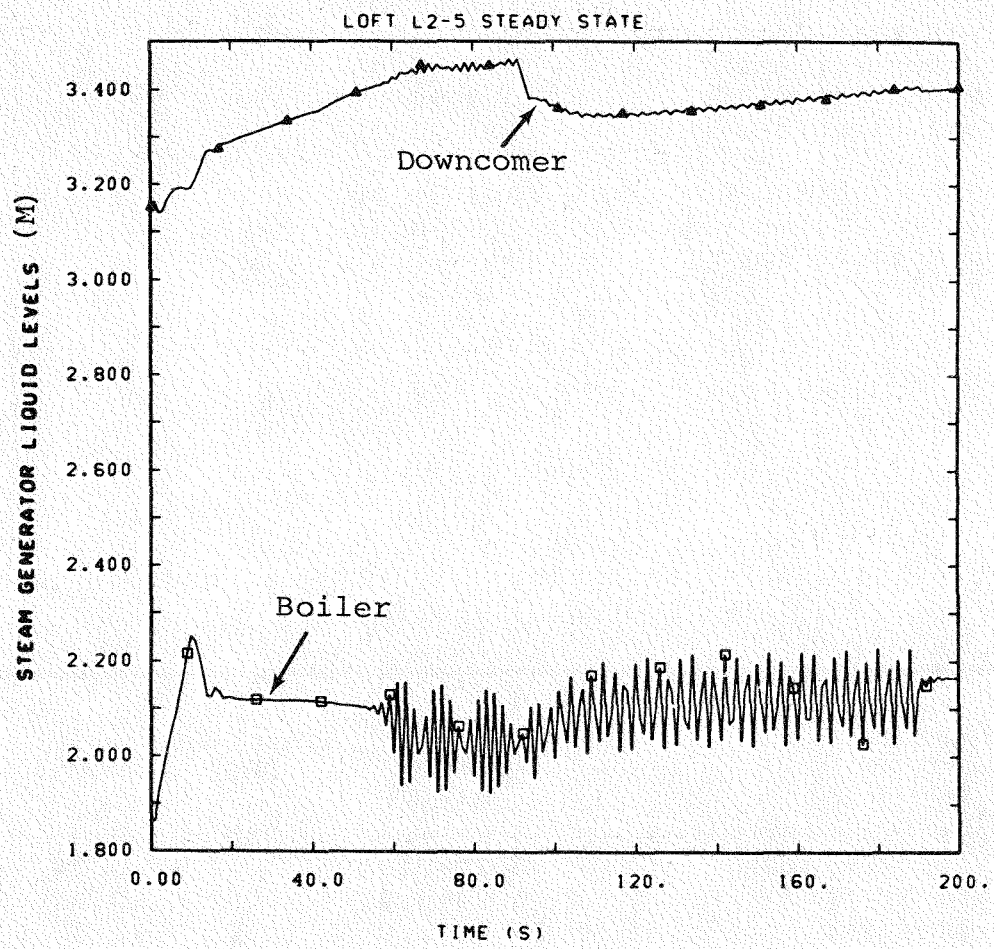


Figure 3.1.1 Steam Generator Secondary Side Liquid Level for LOFT L2-5 Steady State

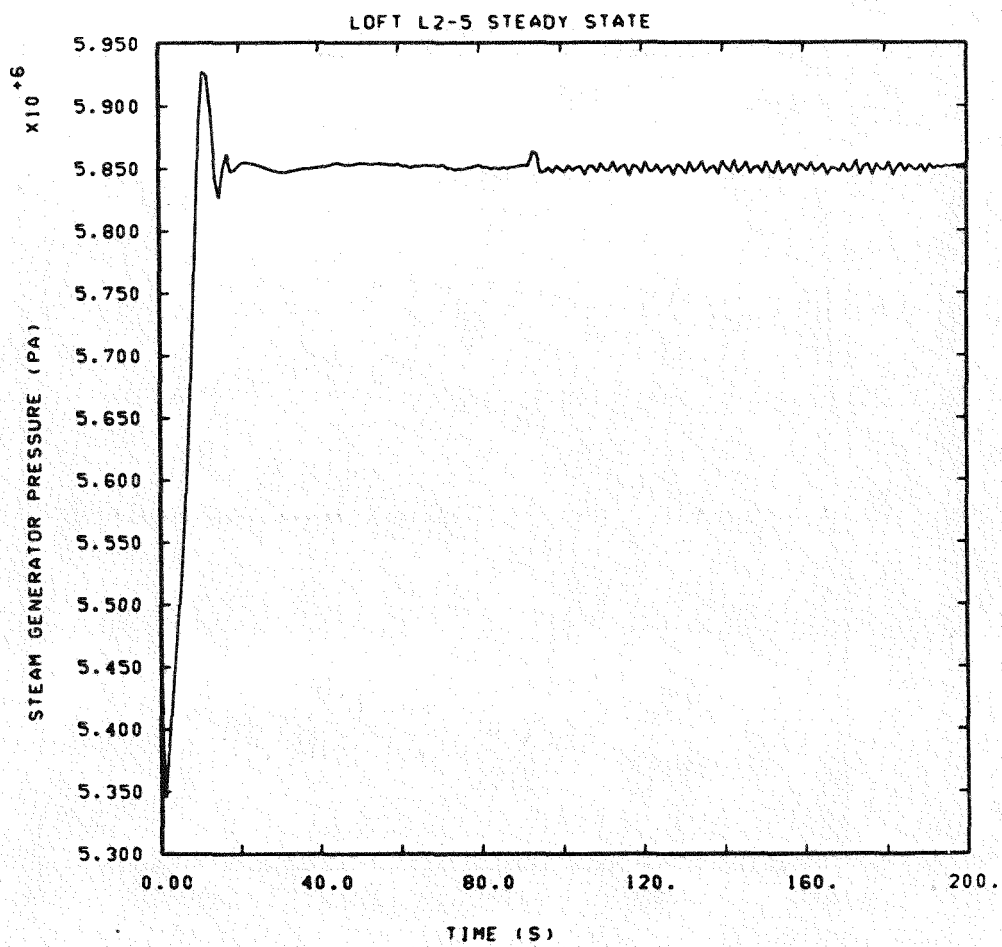


Figure 3.1.2 Steam Generator Secondary Side Pressure for LOFT L2-5 Steady State

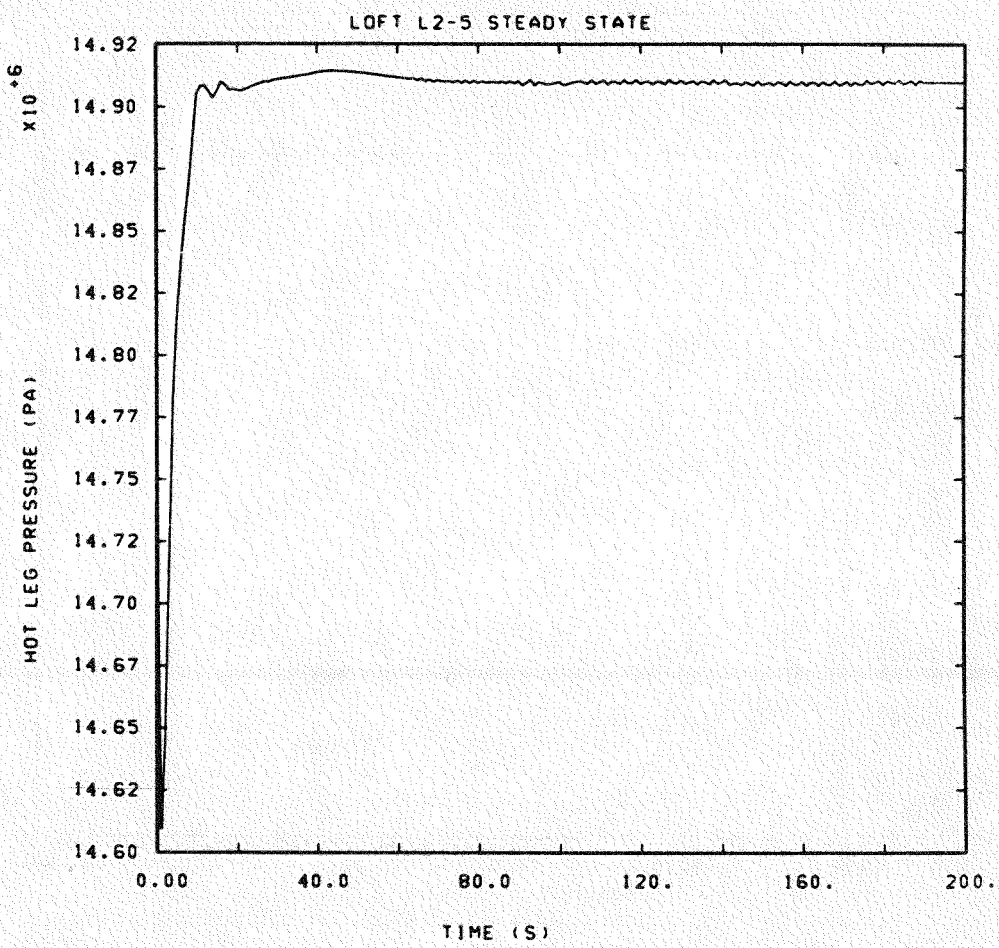


Figure 3.1.3 Hot Leg Pressure for LOFT L2-5 Steady State

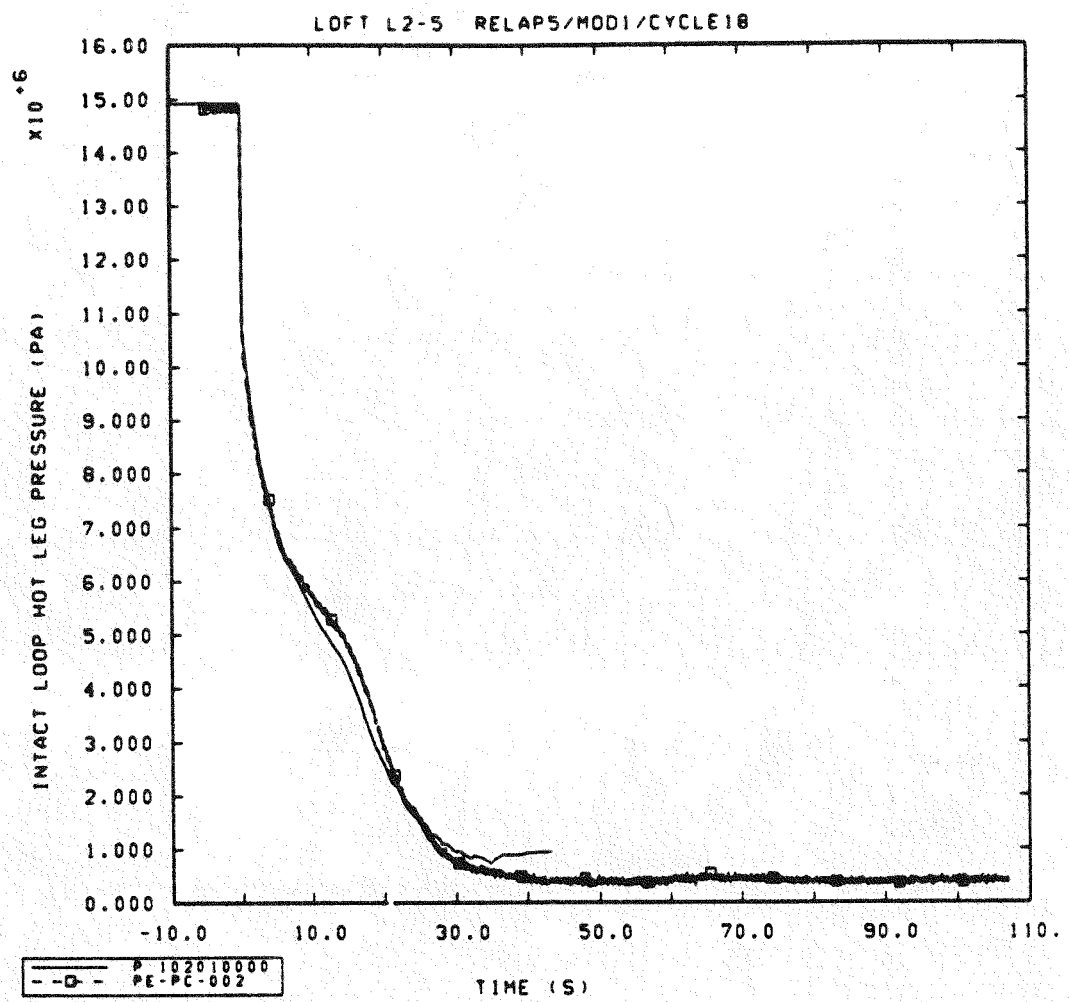


Figure 3.2.1 Calculated and Measured Primary System Pressures for Preliminary LOFT L2-5 Analyses

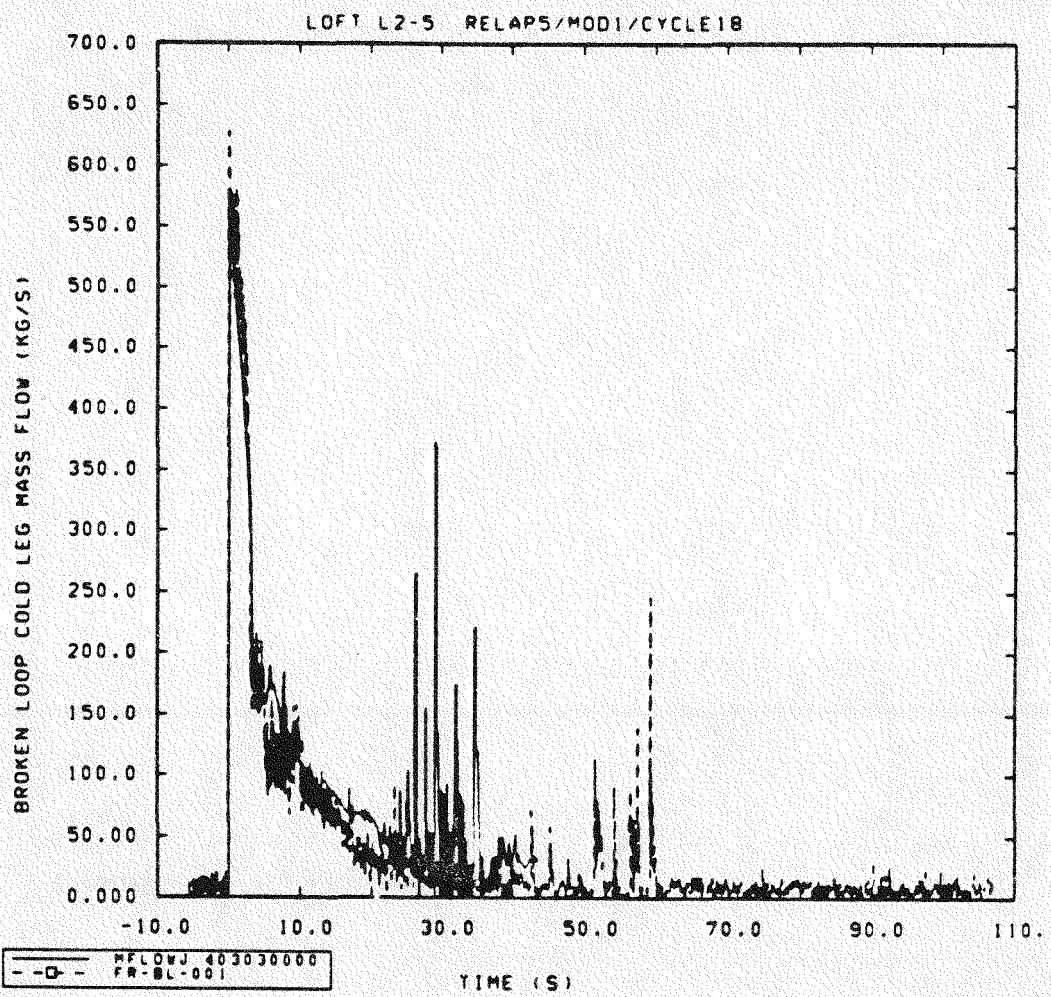


Figure 3.2.2 Calculated and Measured Pump-side (Hot Leg) Break Mass Flows for Preliminary LOFT L2-5 Analyses

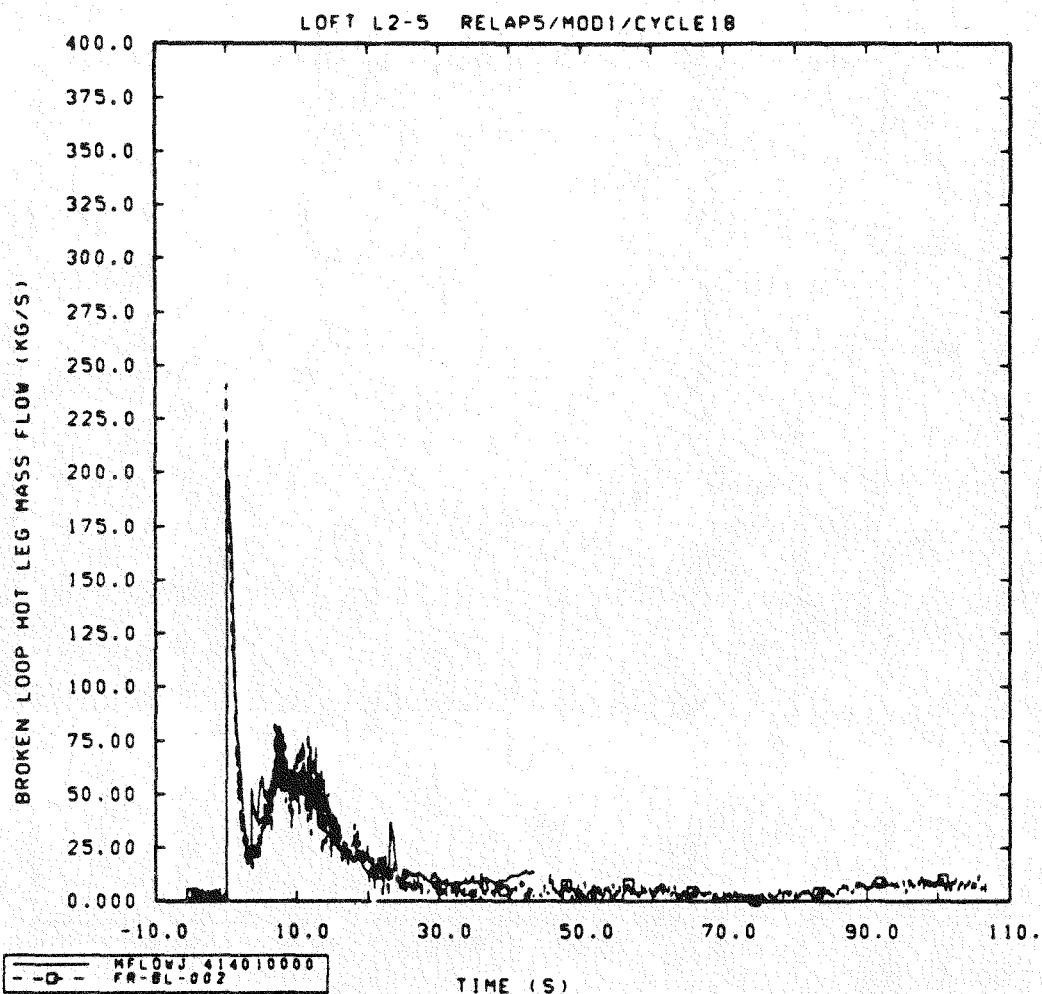


Figure 3.2.3 Calculated and Measured Vessel-side (Cold Leg) Break Mass Flows for Preliminary LOFT L2-5 Analyses

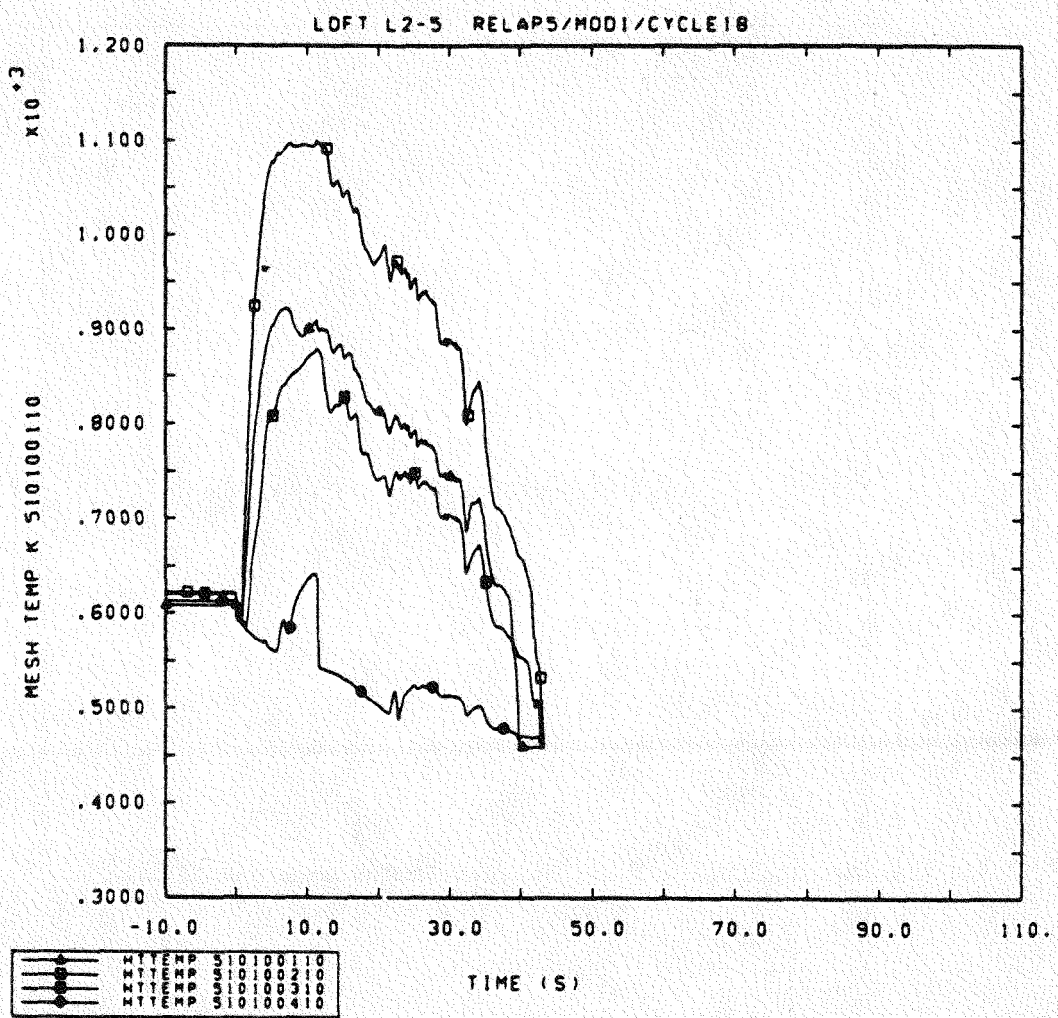


Figure 3.2.4 Calculated Core Clad Temperatures for Preliminary LOFT L2-5 Analyses

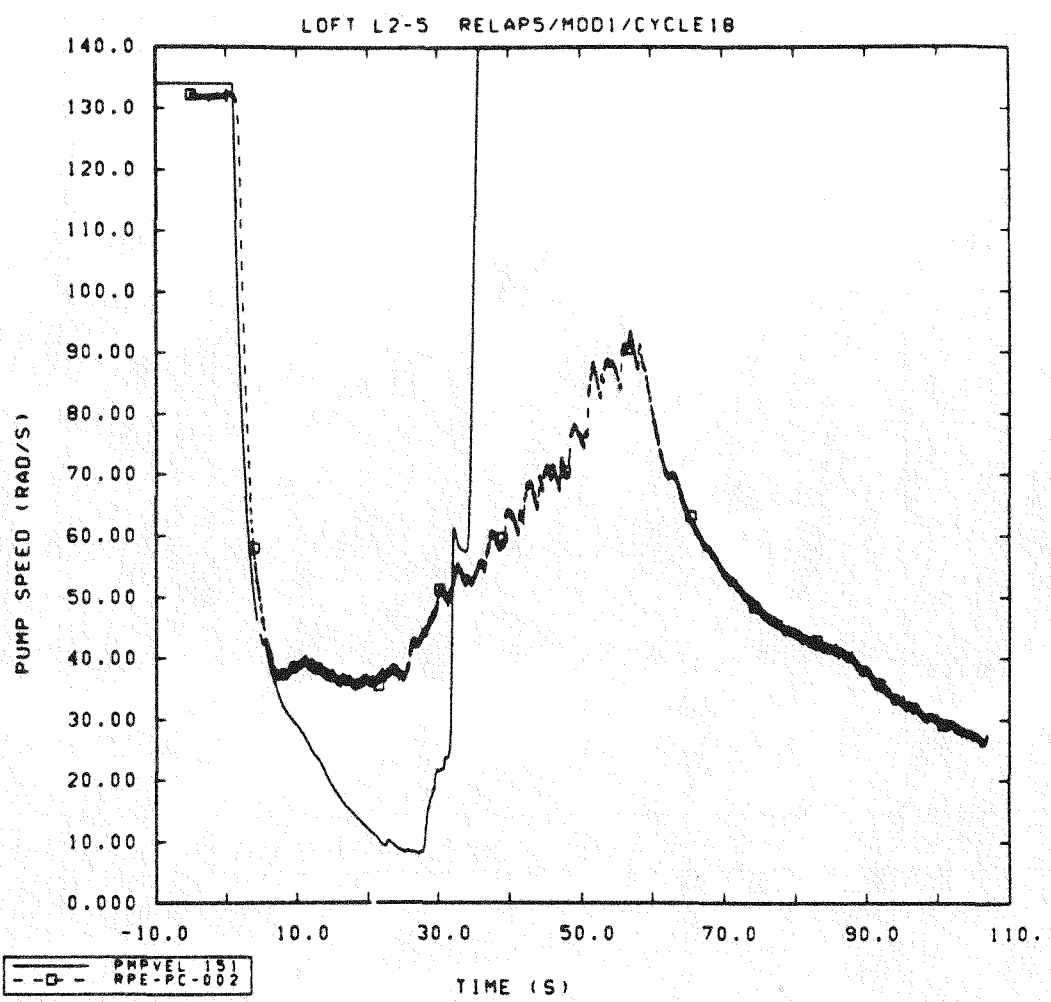


Figure 3.2.5 Calculated and Measured Pump Speeds for Preliminary LOFT L2-5 Analyses

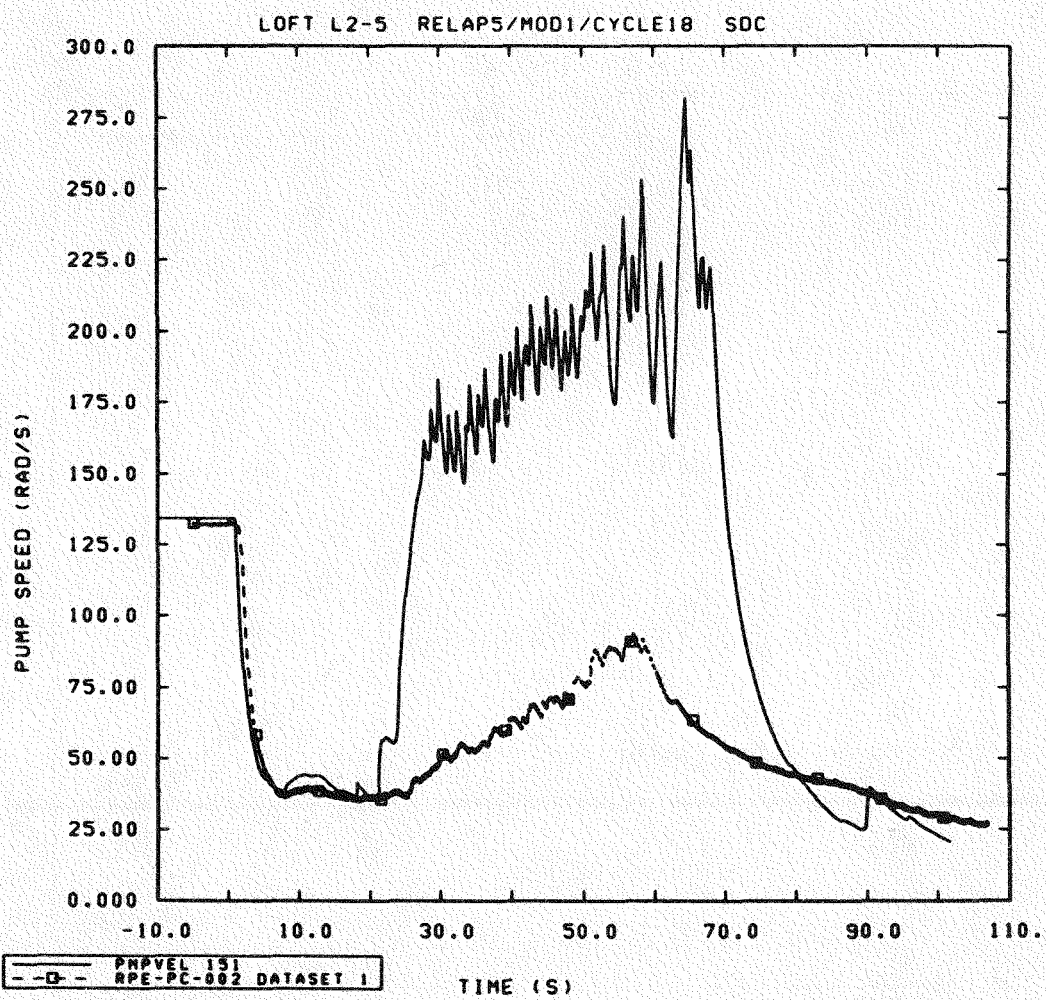


Figure 3.2.6 Calculated and Measured Pump Speeds for LOFT L2-5 (using One-Velocity Assumption in Pump Seal Junctions)

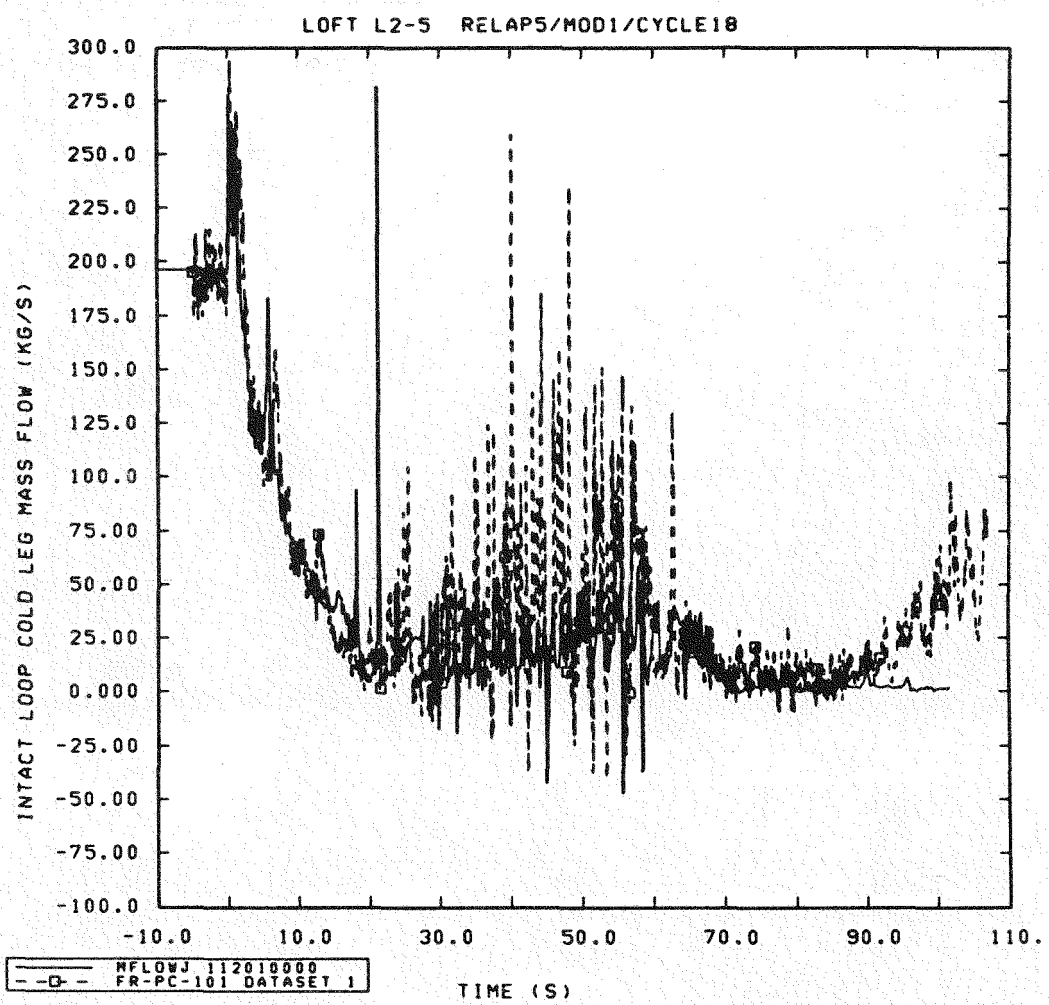


Figure 3.2.7 Calculated and Measured Intact Loop Cold Leg Mass Flows for LOFT L2-5 (using One-velocity Assumption in Pump Seal Junctions)

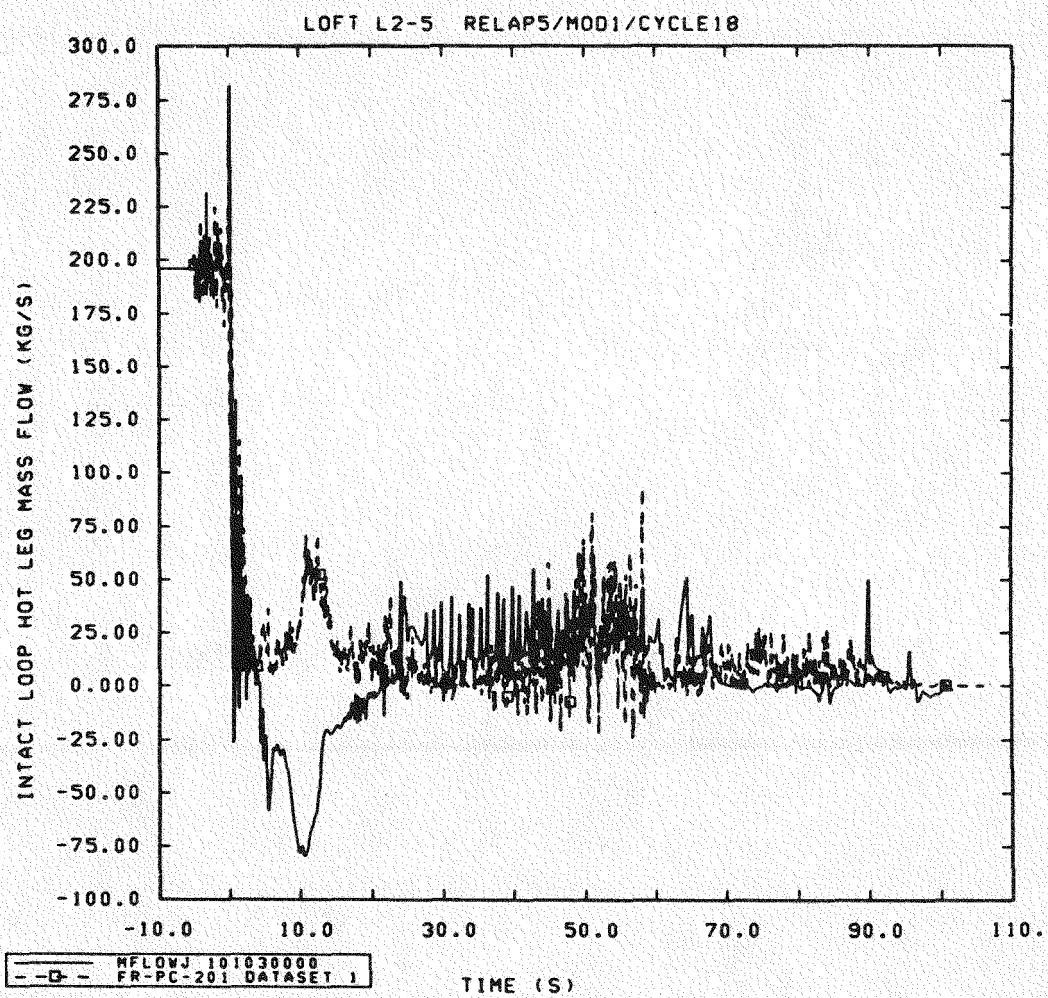


Figure 3.2.8 Calculated and Measured Intact Loop Hot Leg Mass Flows for LOFT L2-5 (using One-velocity Assumption in Pump Seal Junctions)

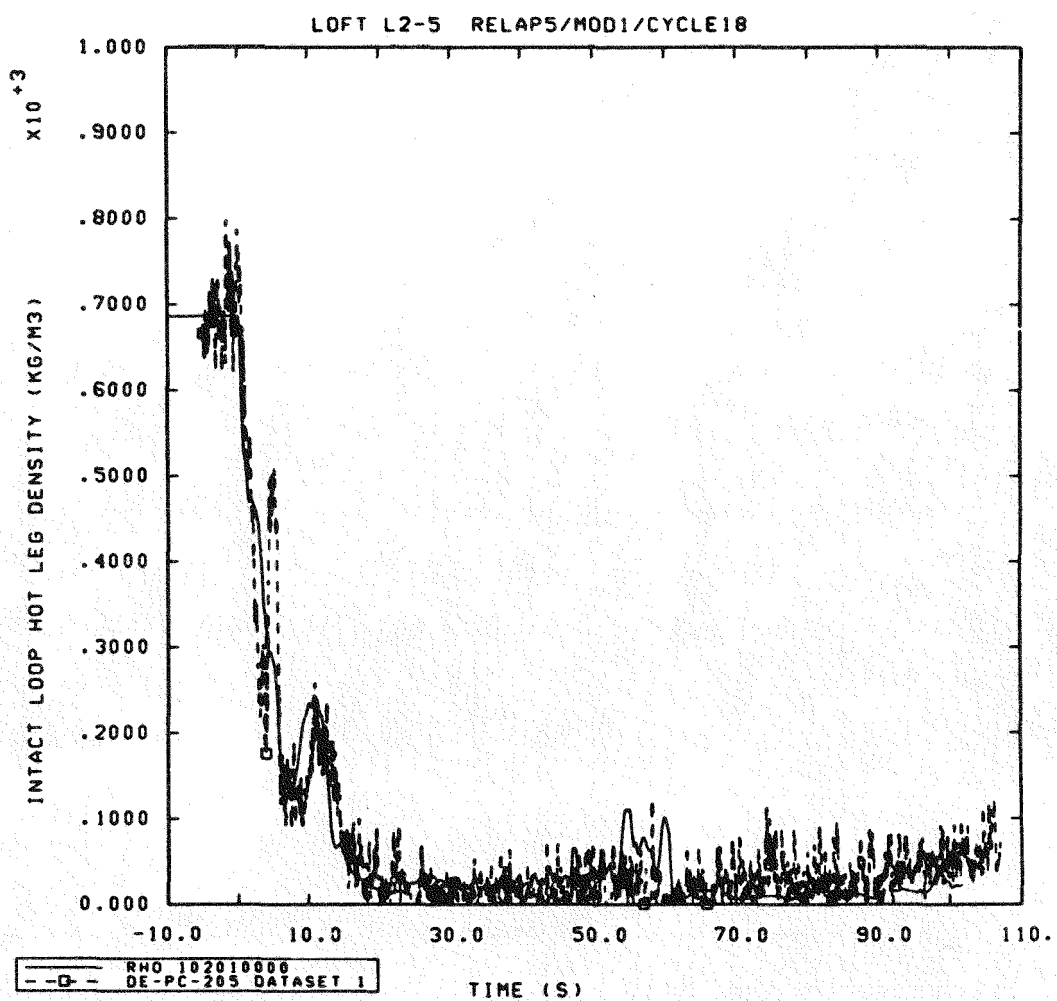


Figure 3.2.9 Calculated and Measured Intact Loop Hot Leg Densities for LOFT L2-5 (using One-velocity Assumption in Pump Seal Junctions)

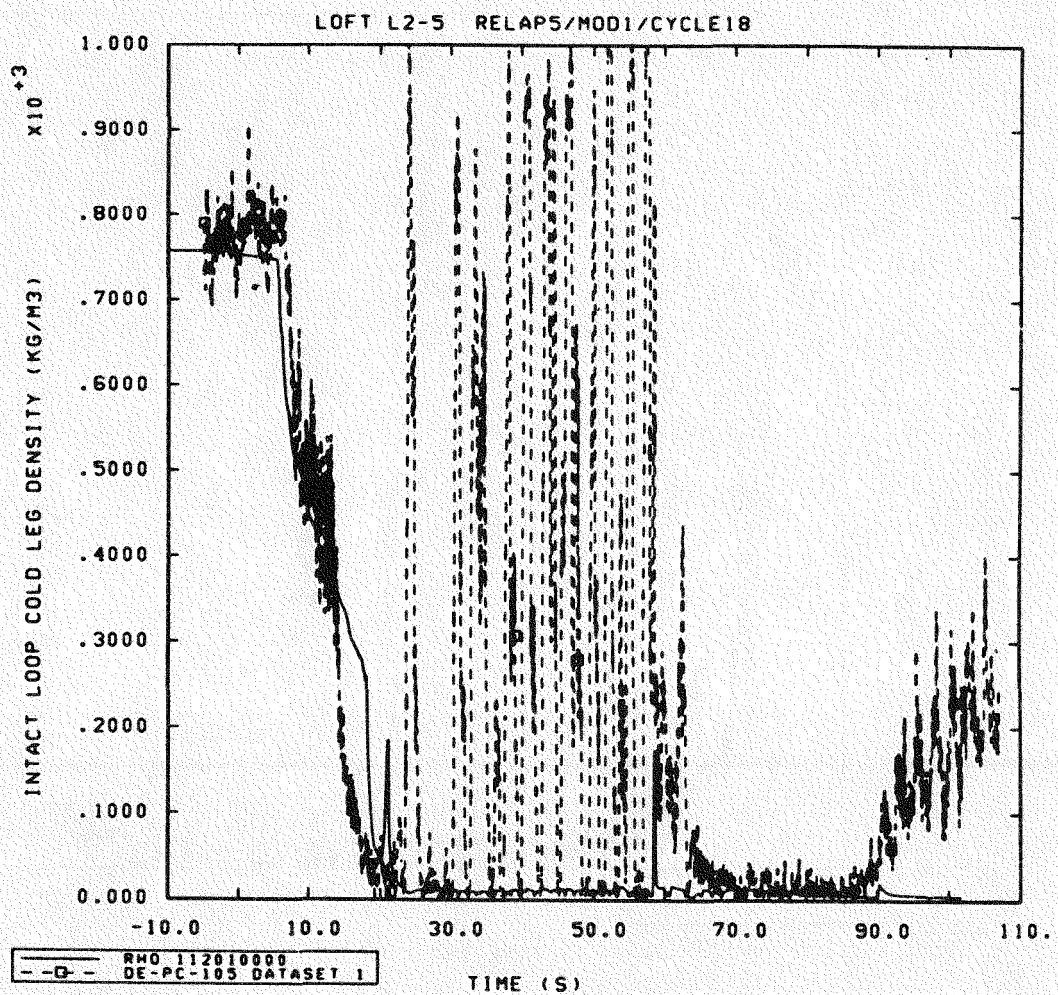


Figure 3.2.10 Calculated and Measured Intact Loop Cold Leg Densities for LOFT L2-5 (using One-velocity Assumption in Pump Seal Junctions)

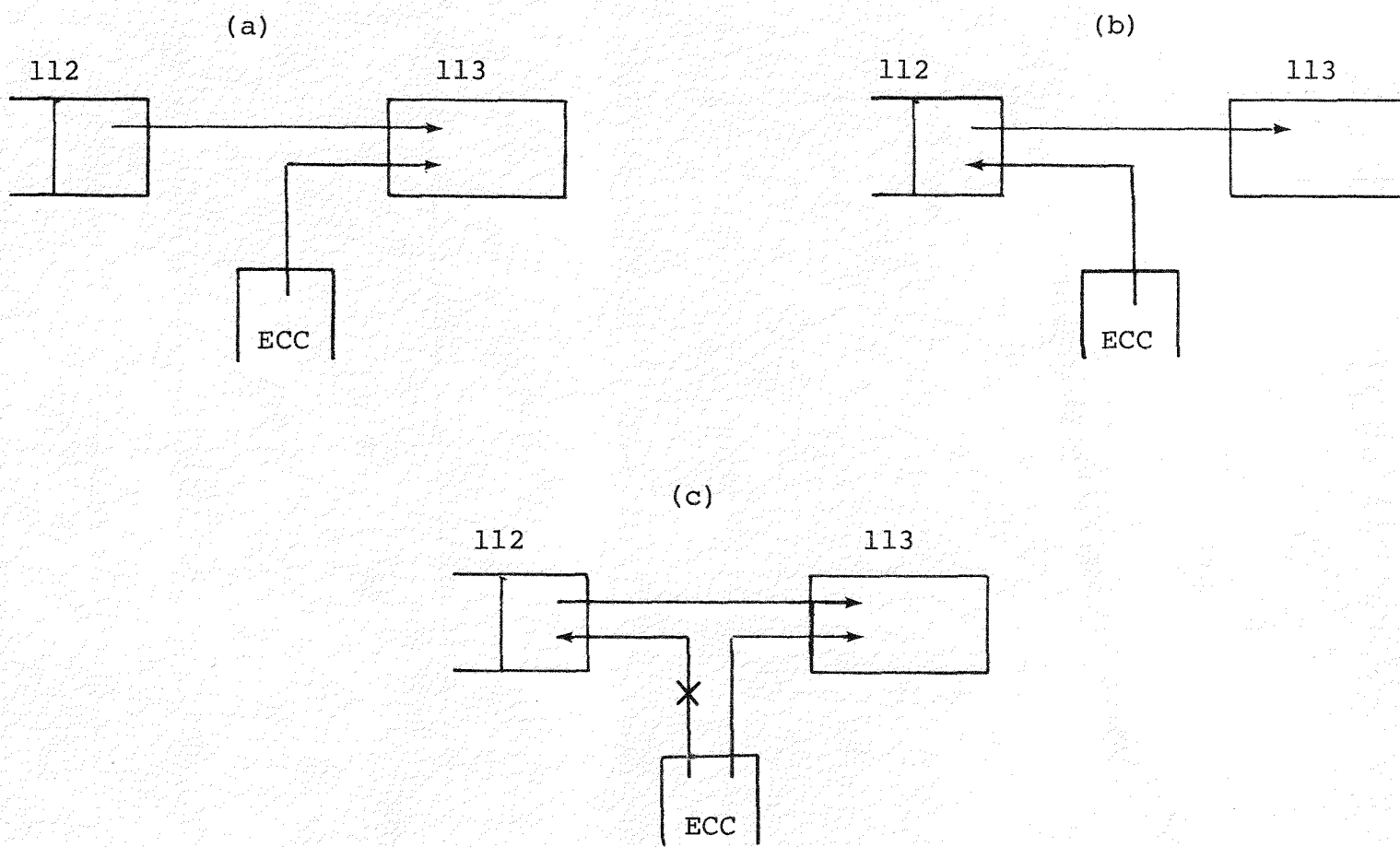


Figure 3.2.11 Injection Point Nodalizations Used for ECC Injection Modelling Sensitivity Studies

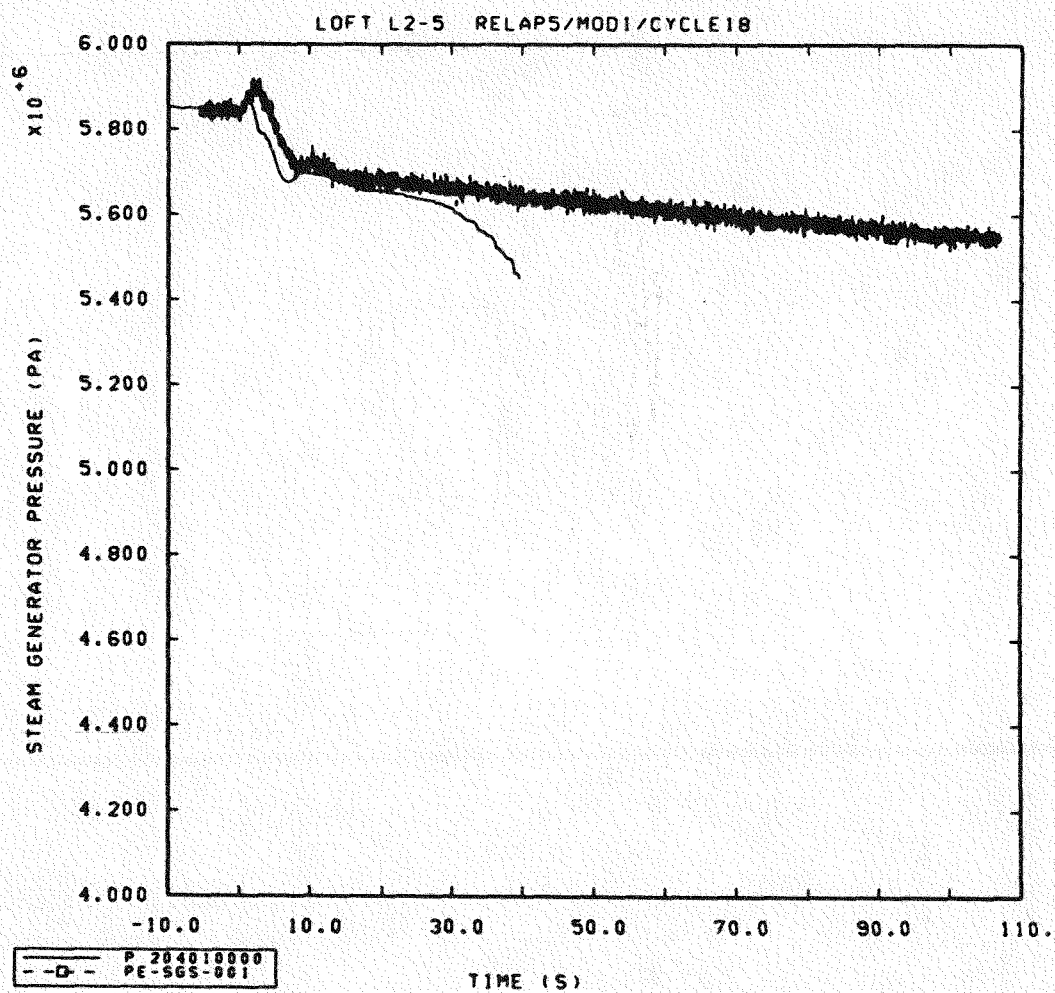


Figure 3.2.12 Calculated and Measured Secondary Side Pressures for Preliminary LOFT L2-5 Analyses

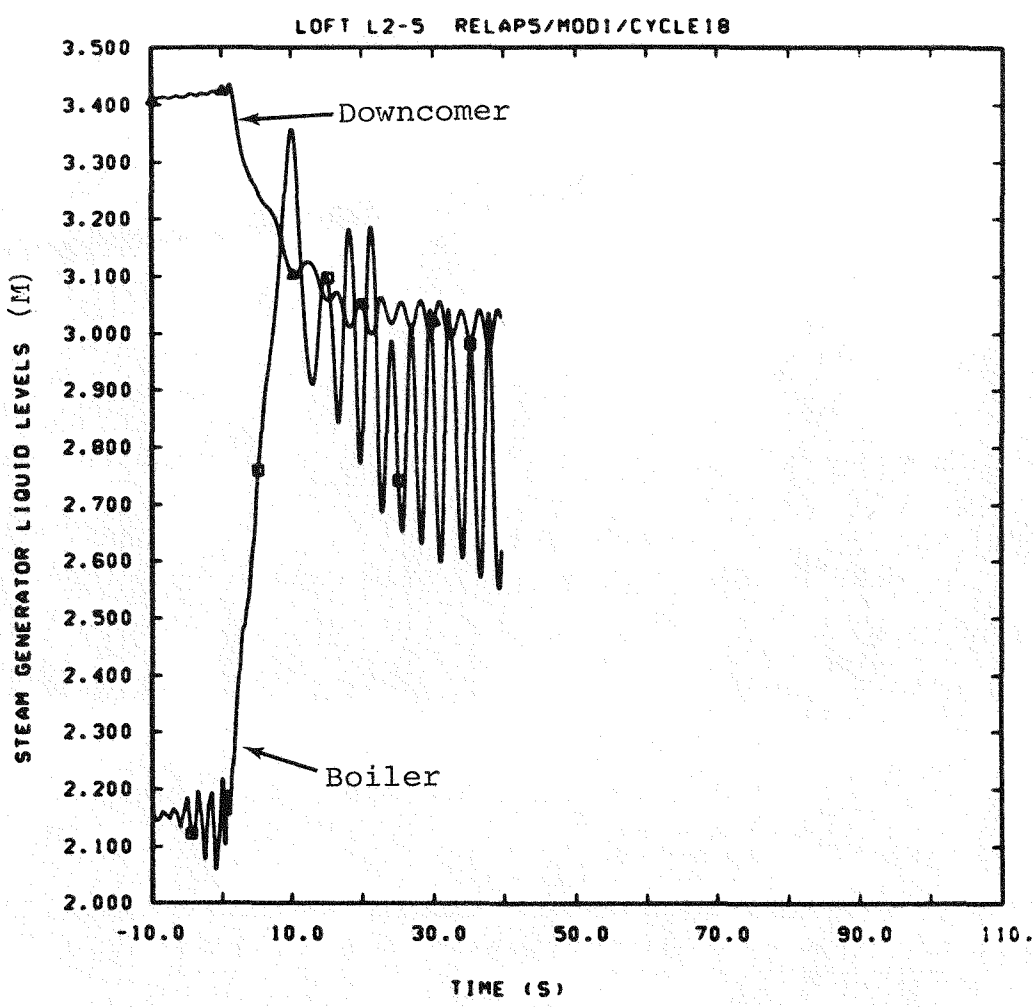


Figure 3.2.13 Calculated Secondary Side Liquid Levels for Preliminary LOFT L2-5 Analyses

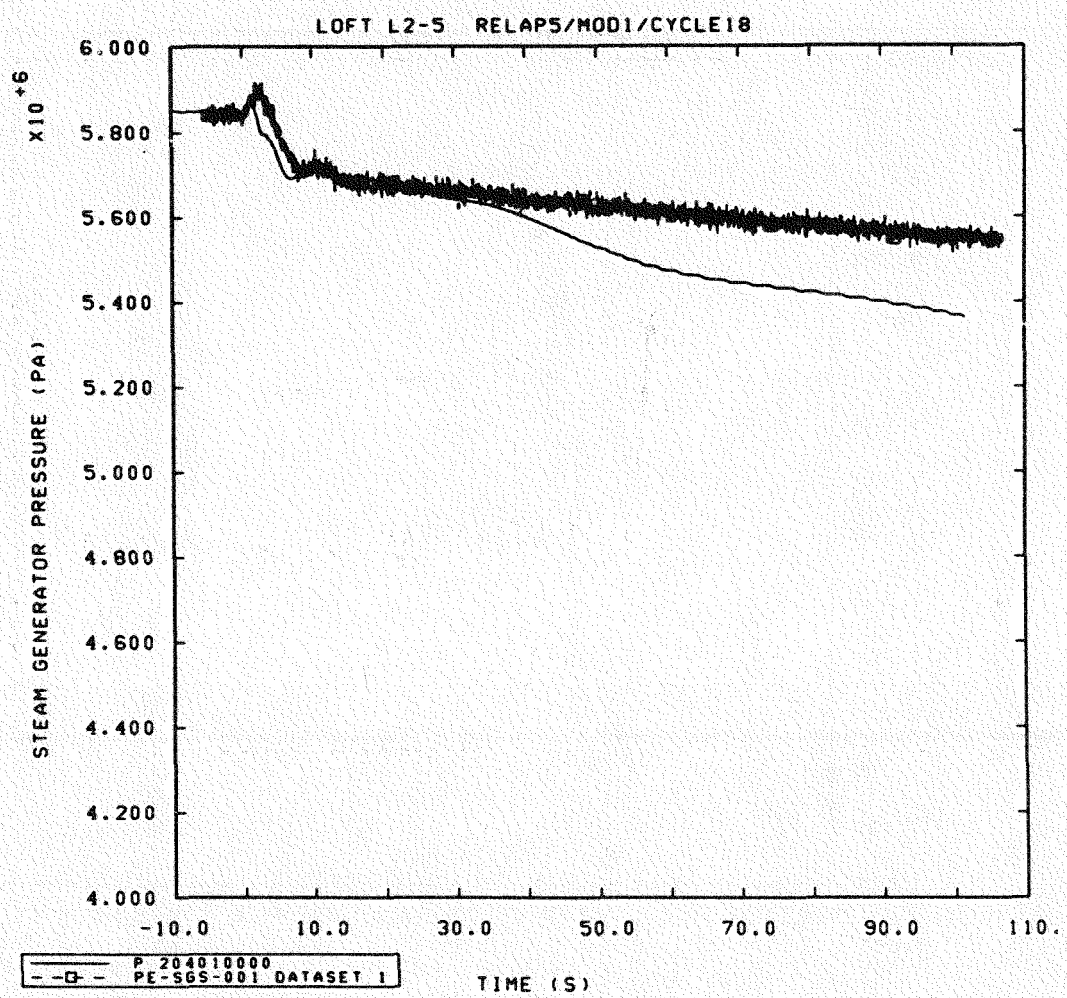


Figure 3.2.14 Calculated and Measured Secondary Side Pressures for LOFT L2-5 (adding Large Form Loss in Downcomer-Shroud Junction)

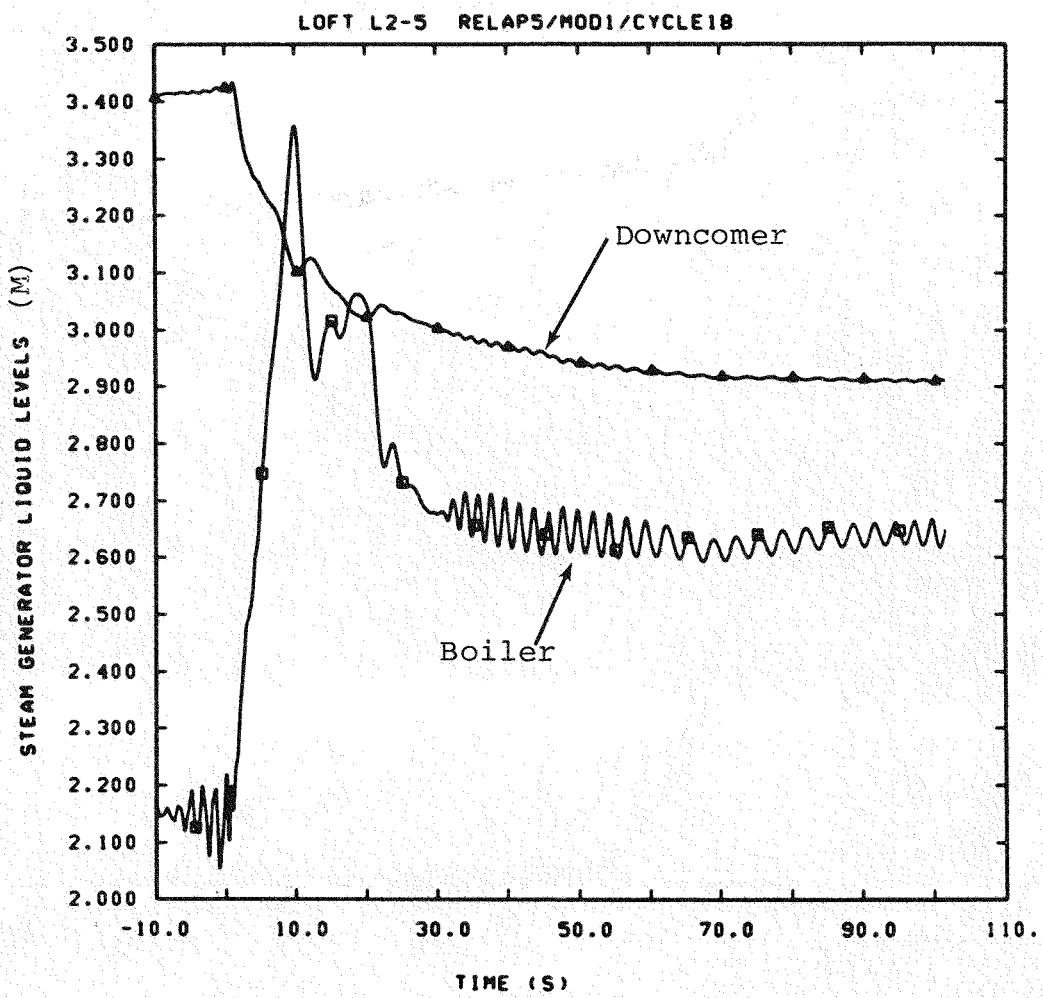


Figure 3.2.15 Calculated Secondary Side Liquid Levels for LOFT L2-5 (adding Large Form Loss in Downcomer-Shroud Junction)

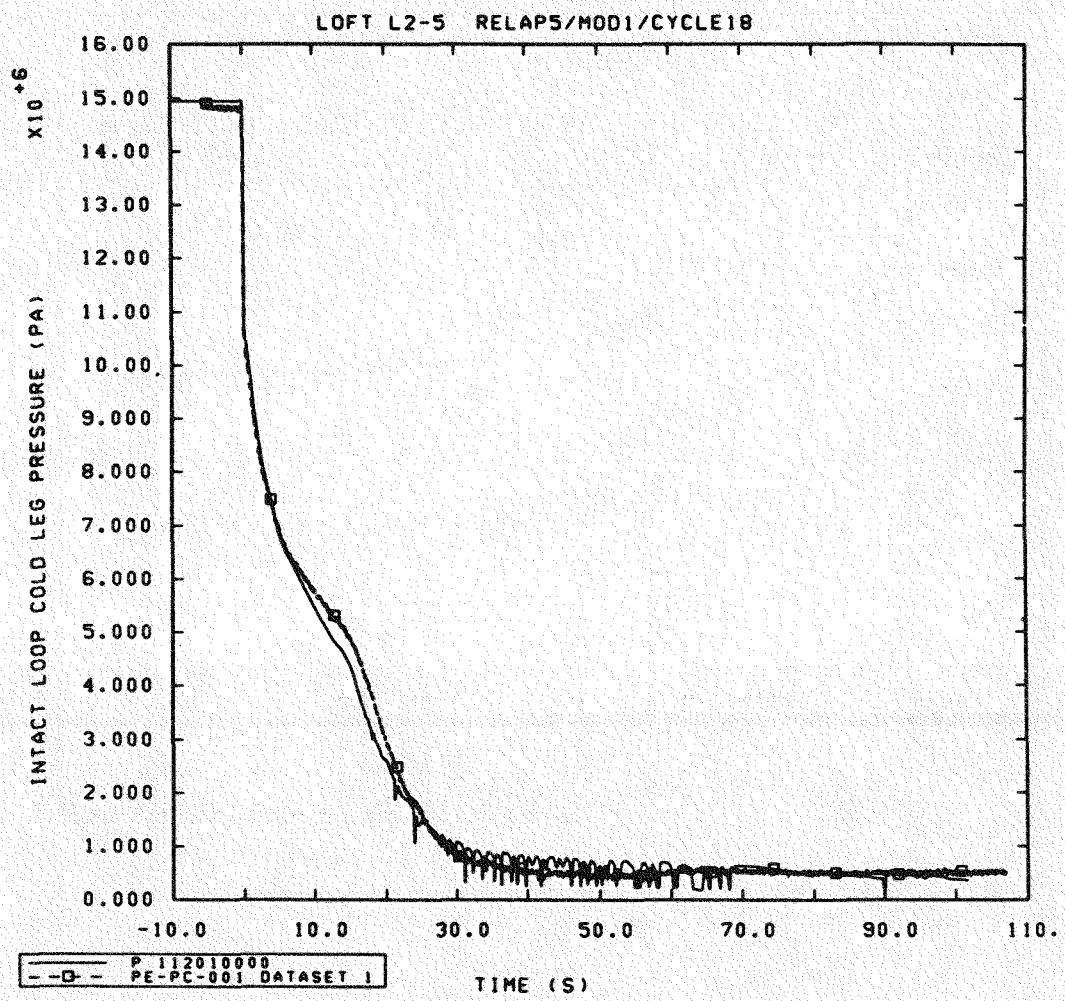


Figure 3.3.1 Calculated and Measured Intact Loop Cold Leg Pressures for LOFT L2-5

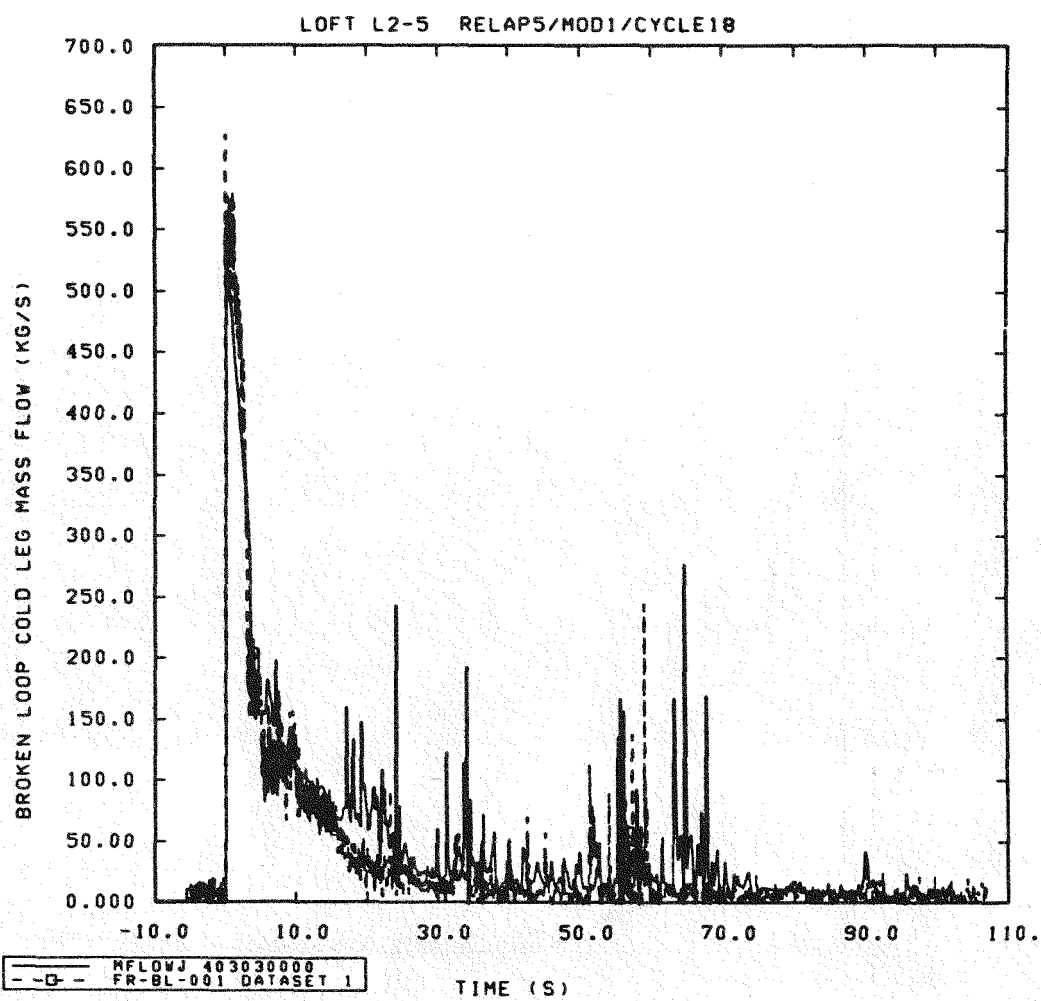


Figure 3.3.2 Calculated and Measured Pump-side (Hot Leg) Break Mass Flows for LOFT L2-5

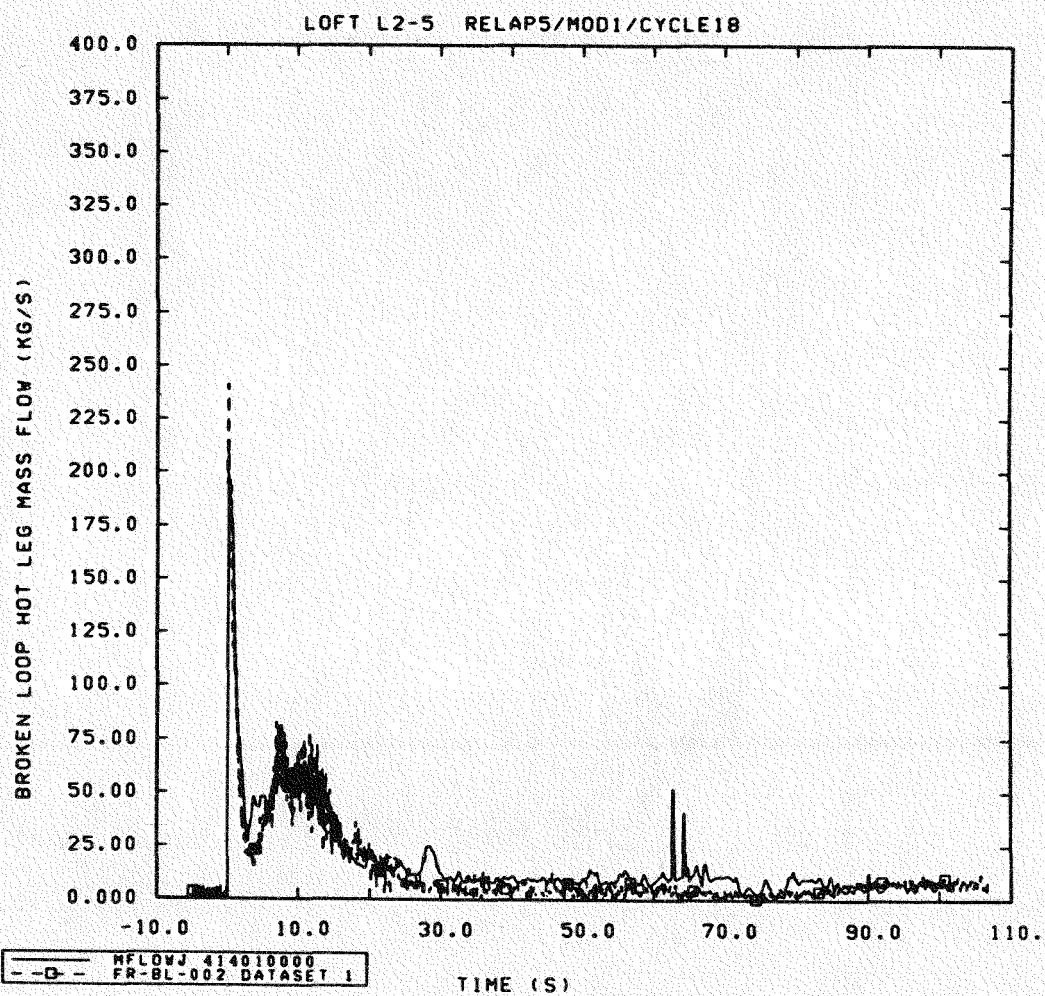


Figure 3.3.3 Calculated and Measured Vessel-side (Cold Leg) Break Mass Flows for LOFT L2-5

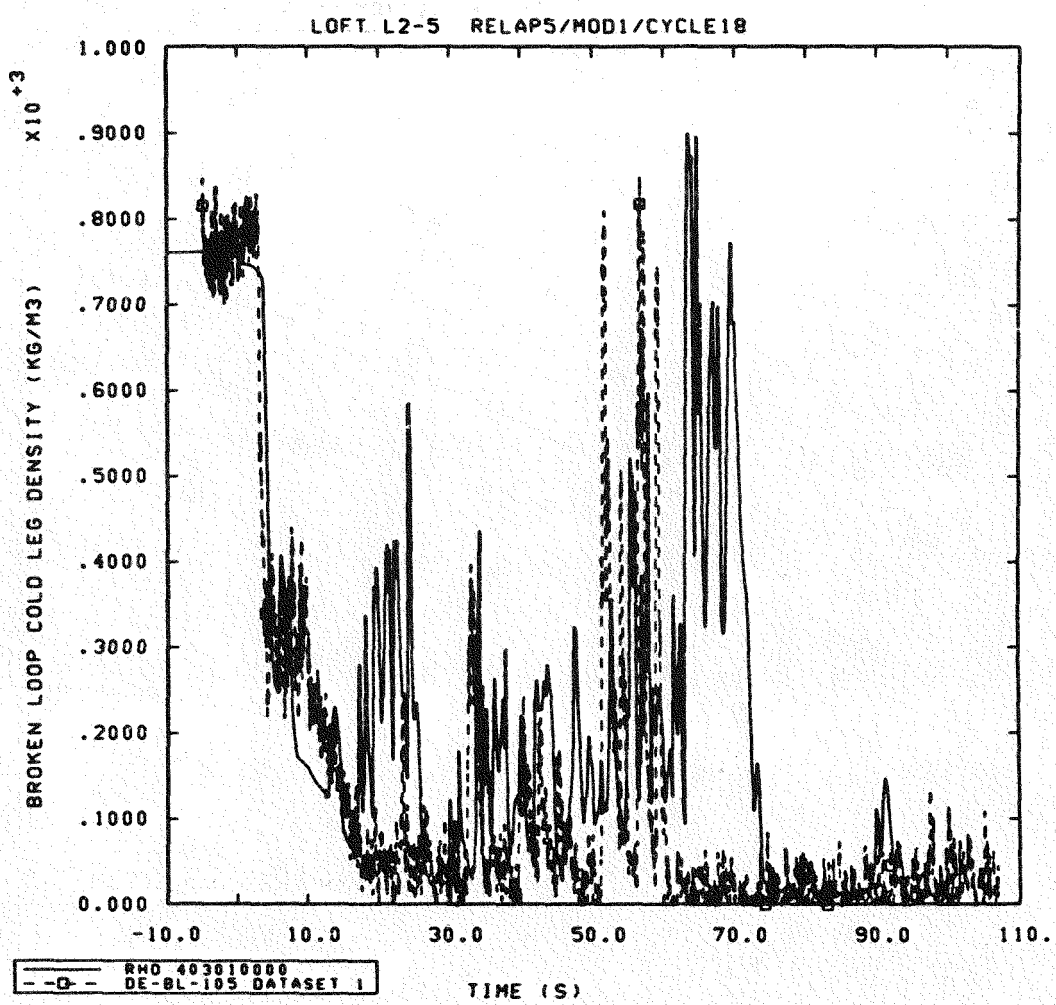


Figure 3.3.4 Calculated and Measured Broken Loop Cold Leg Densities for LOFT Test L2-5

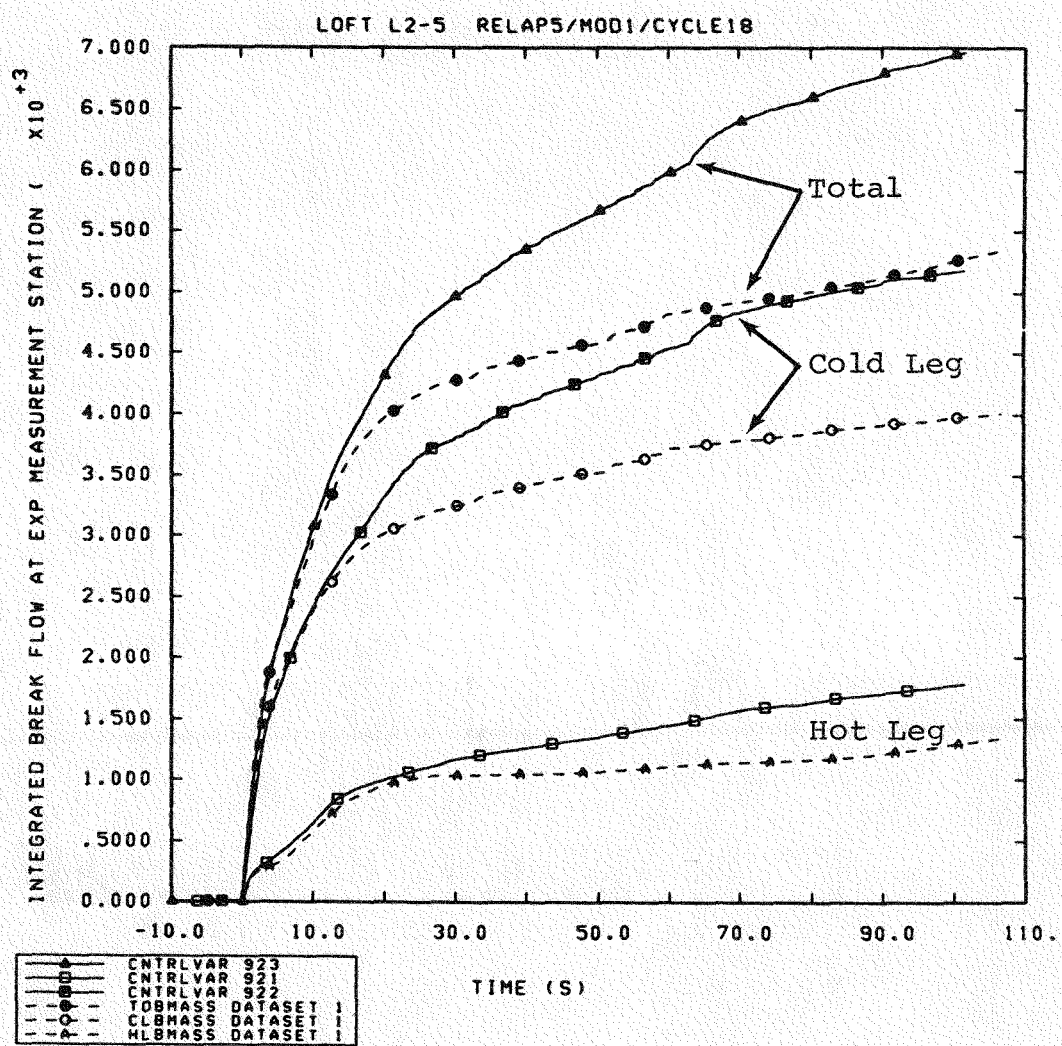


Figure 3.3.5 Calculated and Measured Integrated Break Mass Flows for LOFT Test L2-5

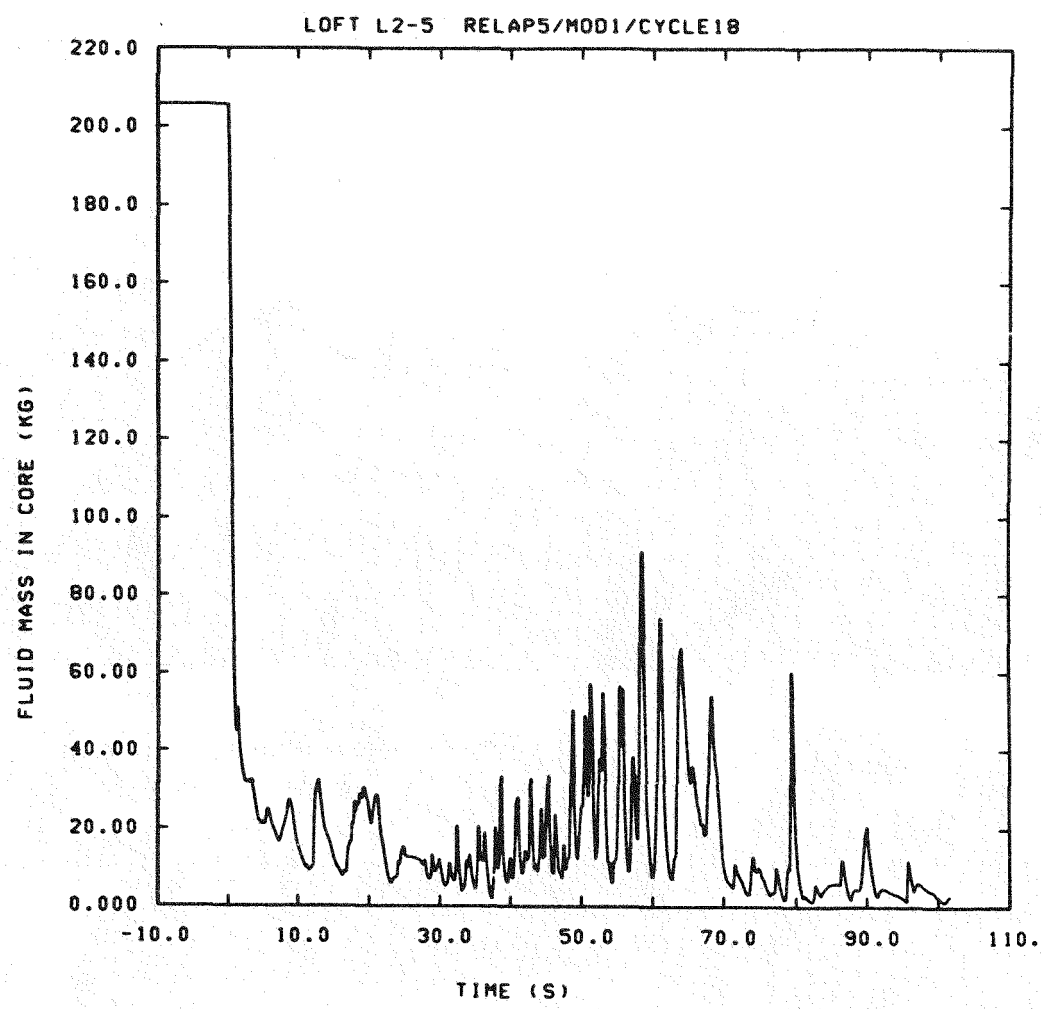


Figure 3.3.6 Calculated Fluid Mass in Core for  
LOFT L2-5

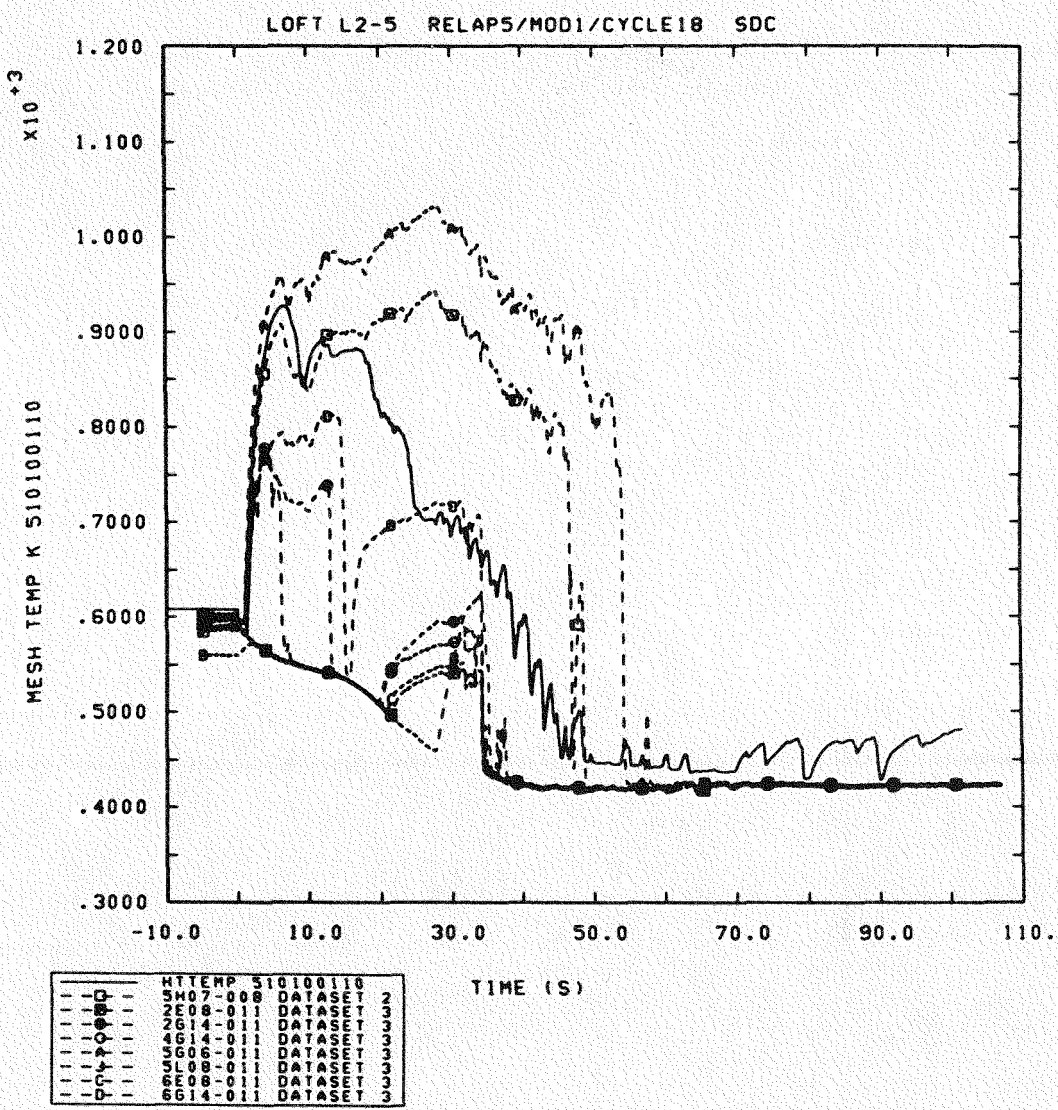


Figure 3.3.7 Calculated and Measured Core Clad Temperatures at 0.21 m Core Elevation for LOFT L2-5

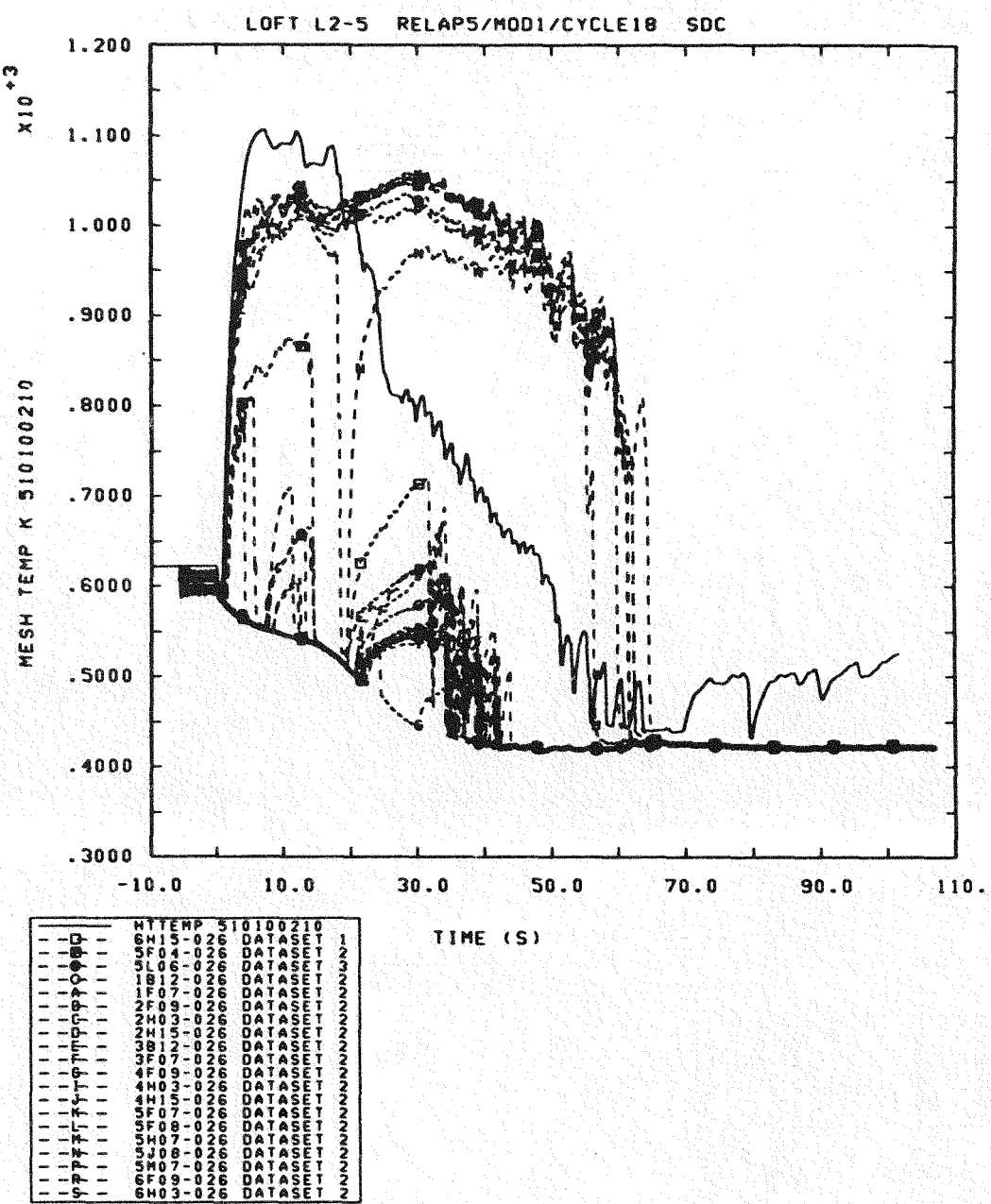


Figure 3.3.8 Calculated and Measured Core Clad Temperatures at 0.64 m Core Elevation for LOFT L2-5

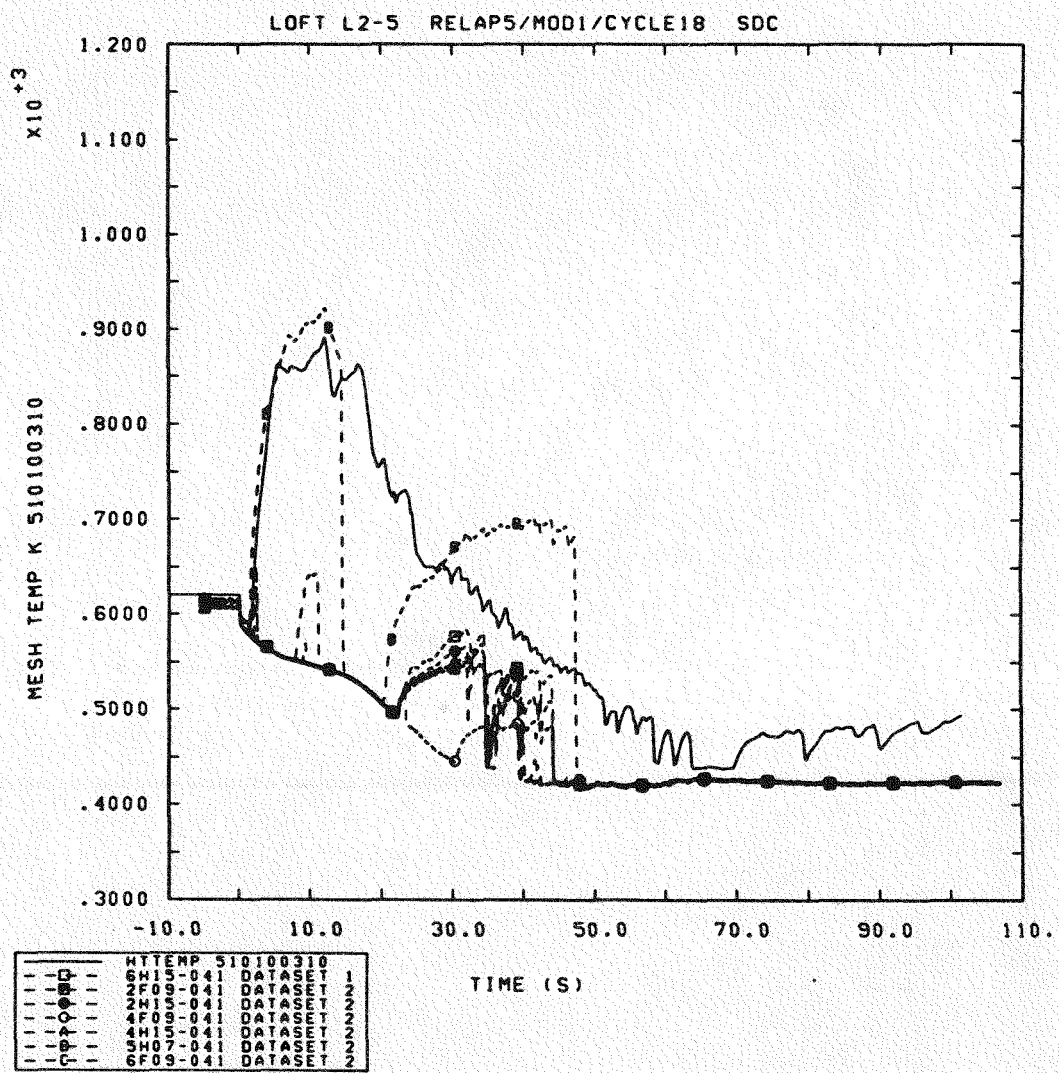


Figure 3.3.9 Calculated and Measured Core Clad Temperatures at 1.06 m Core Elevation for LOFT L2-5

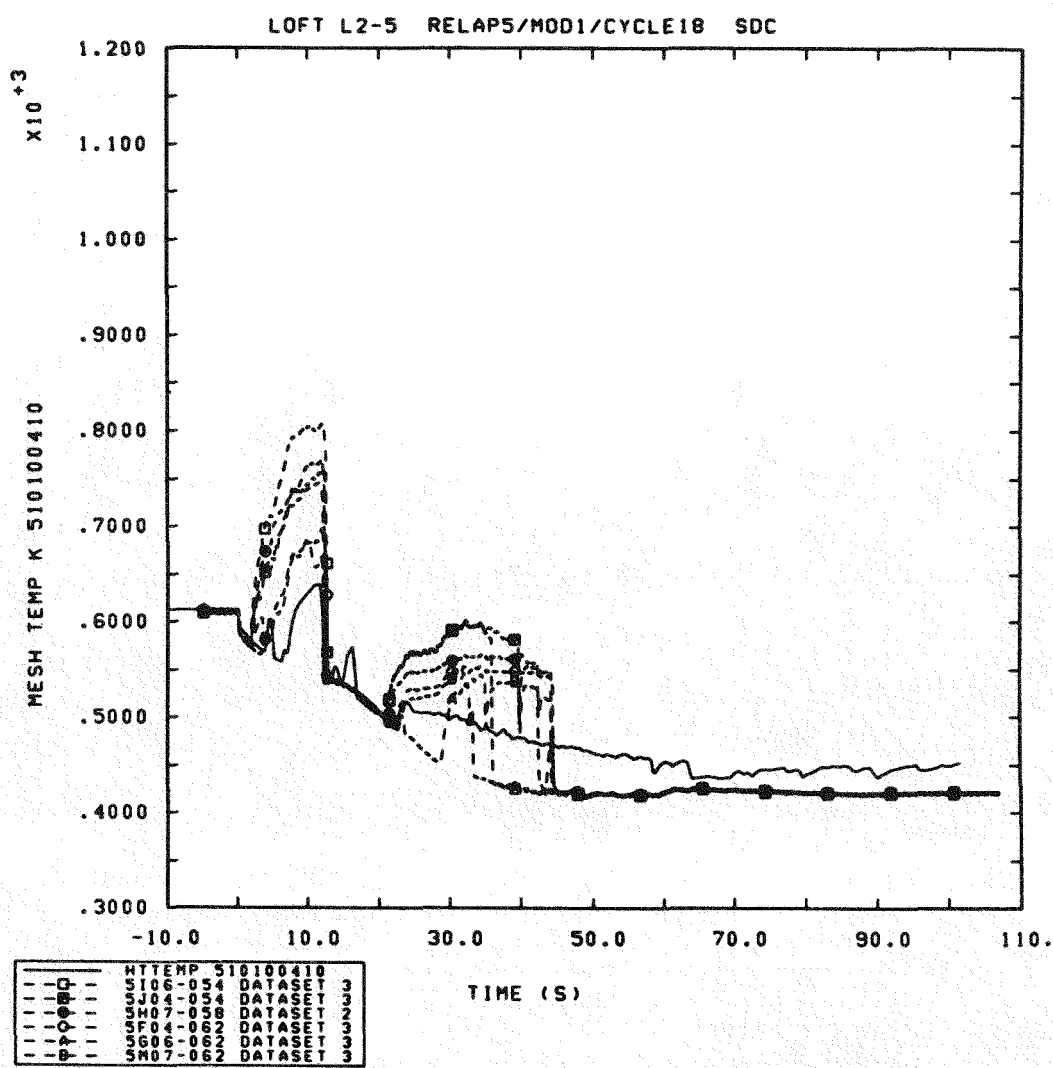


Figure 3.3.10 Calculated and Measured Core Clad Temperatures at 1.47 m Core Elevation for LOFT L2-5

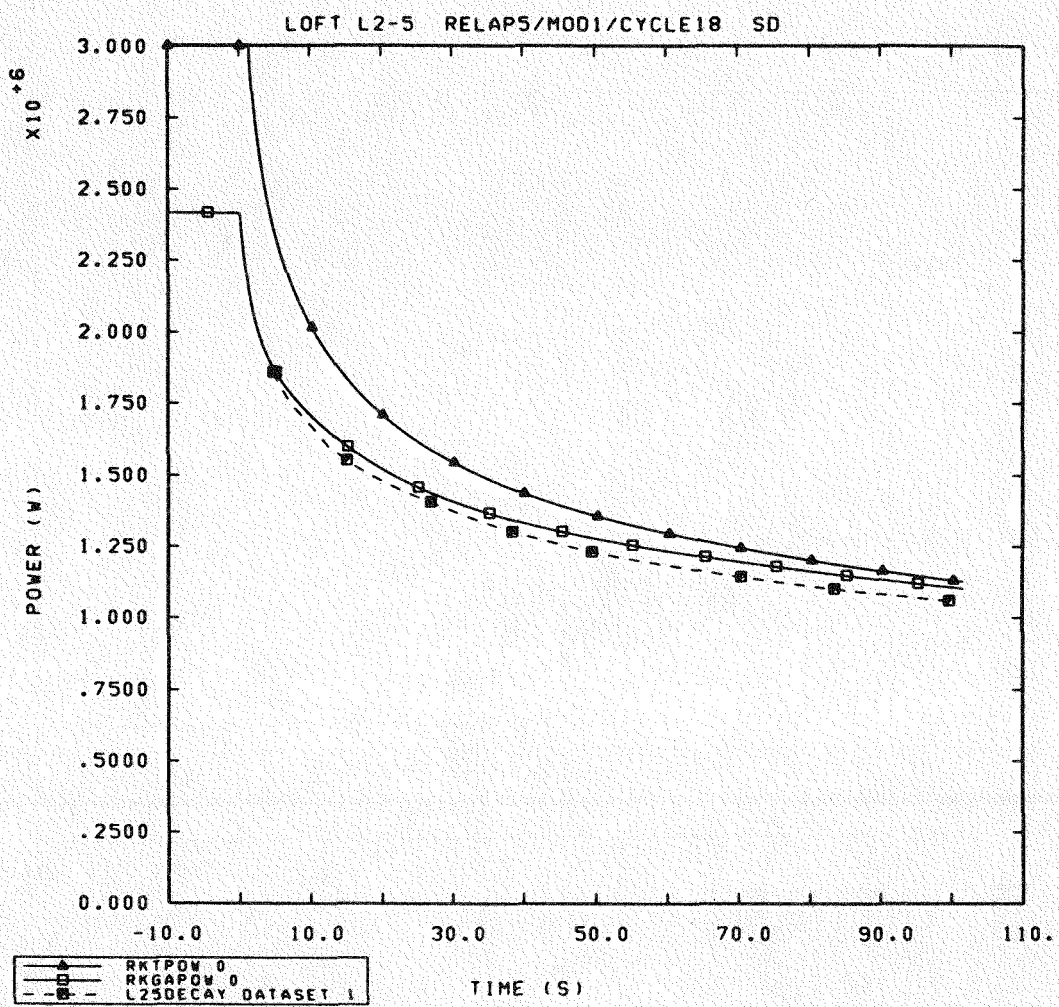


Figure 3.3.11 Calculated and Measured Core Decay Heats for LOFT L2-5

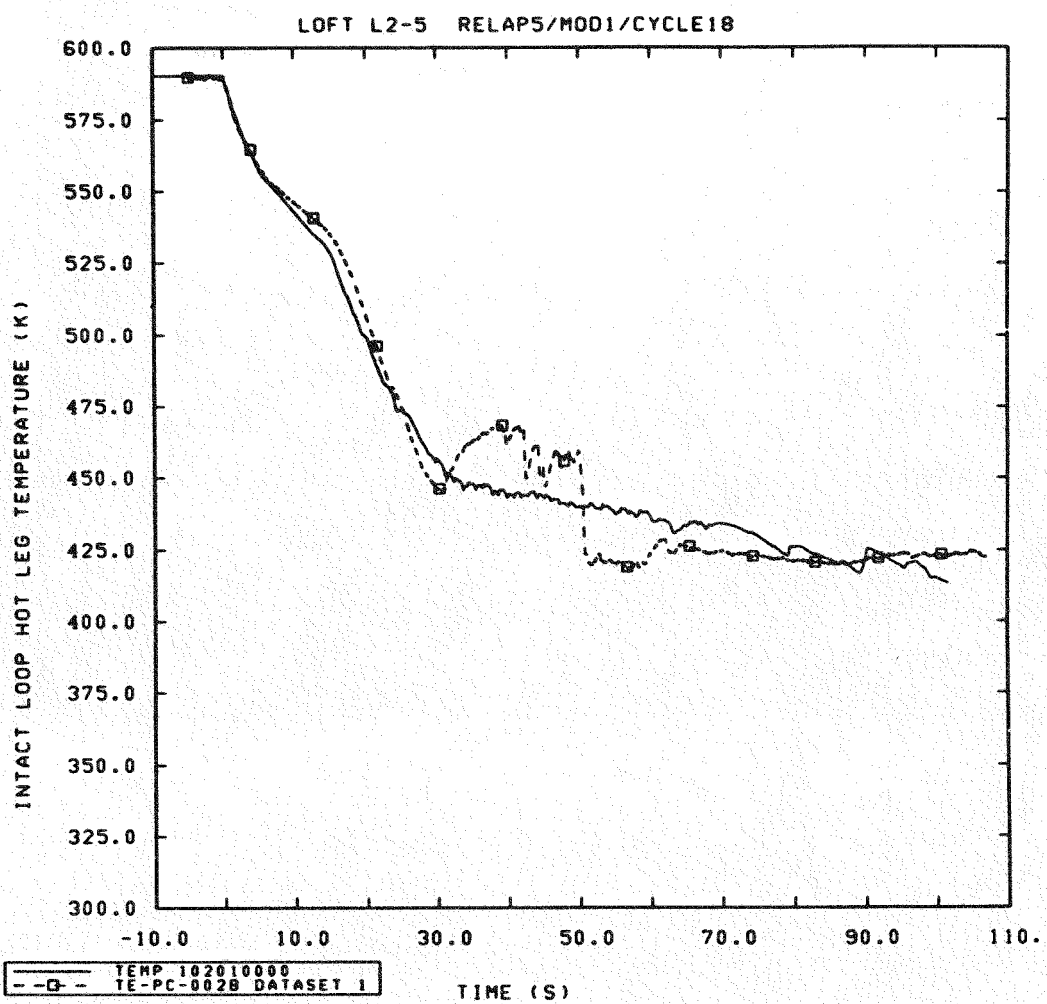


Figure 3.3.12 Calculated and Measured Intact Loop Hot Leg Temperatures for LOFT L2-5

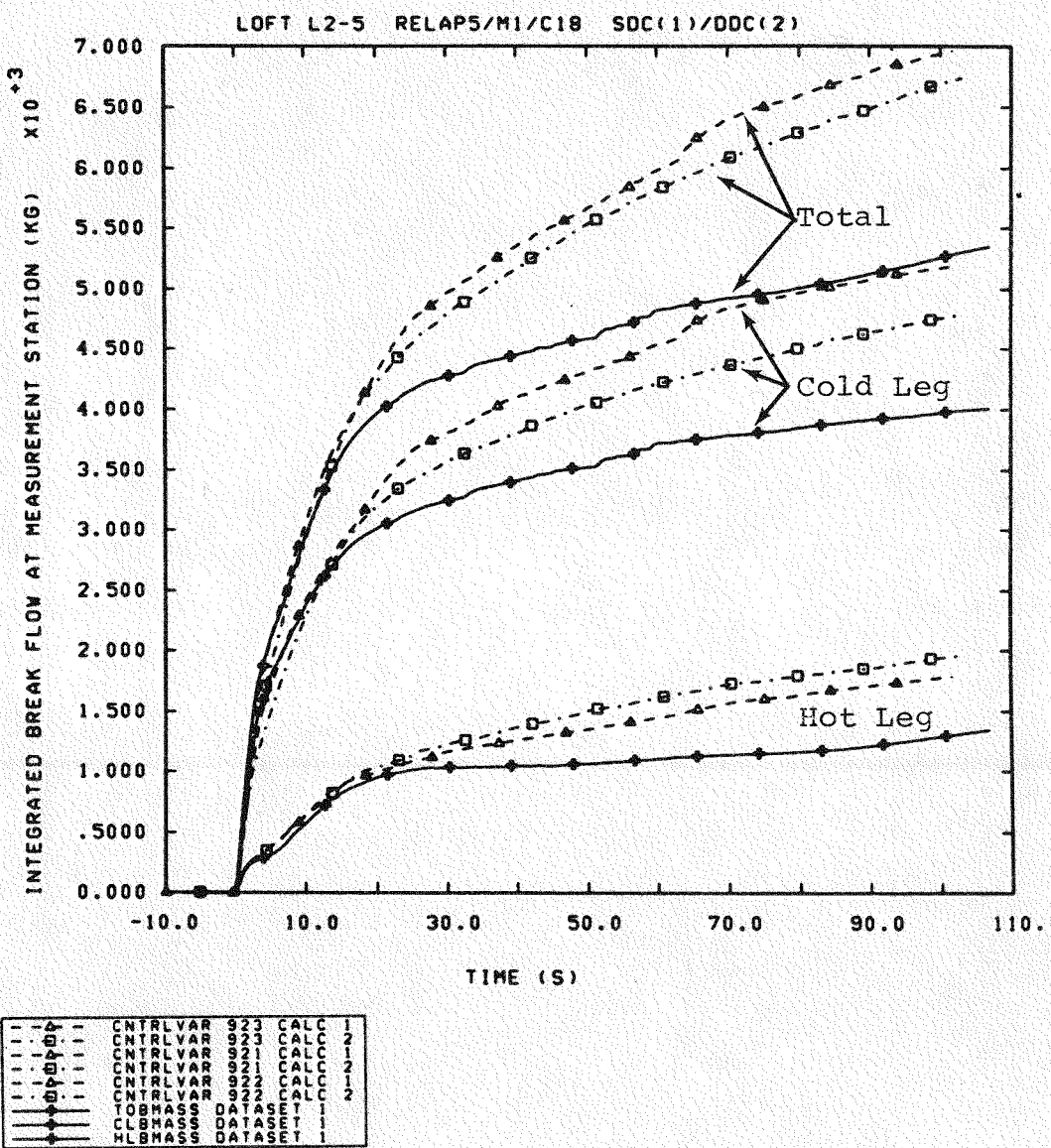


Figure 3.4.1 Calculated and Measured Integrated Break Flows using Original and Split- Downcomer Nodalizations for LOFT Test L2-5

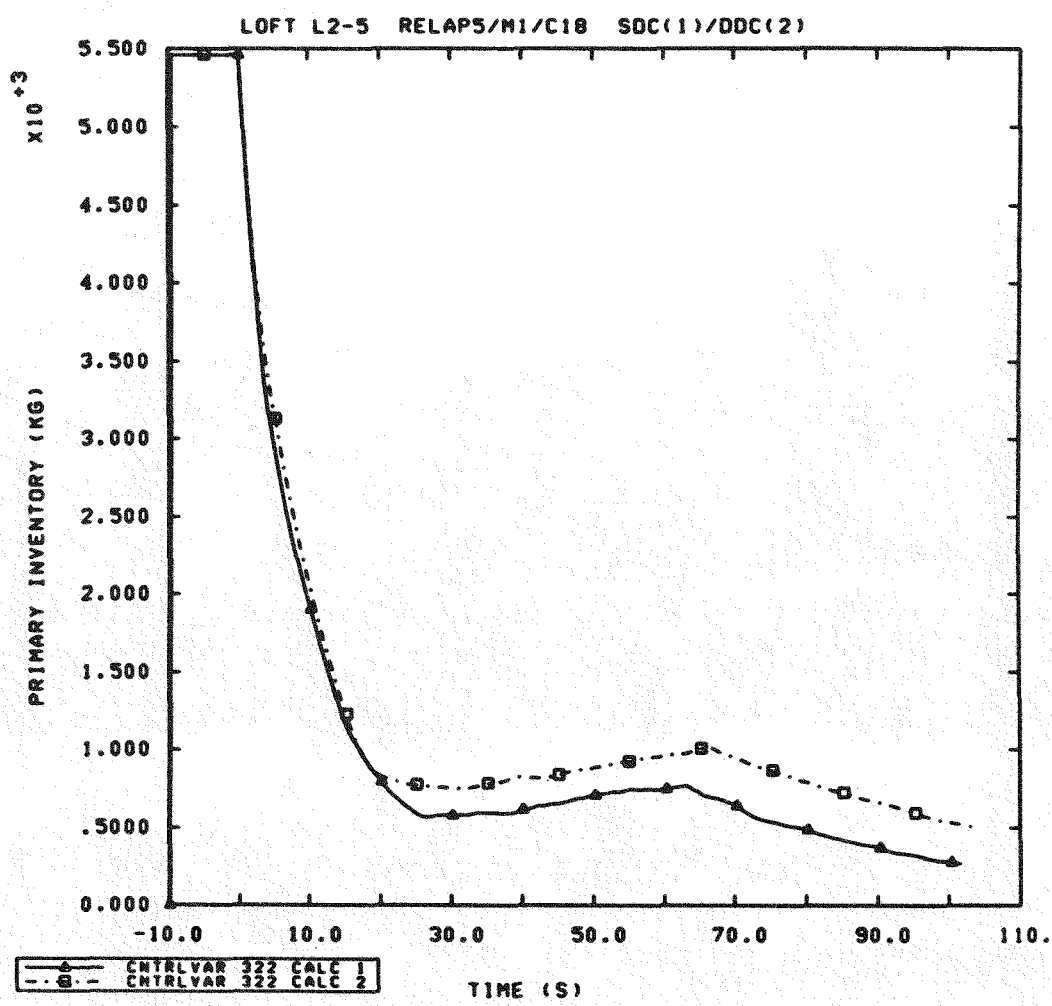


Figure 3.4.2 Calculated Primary Mass Inventories using Original and Split- Downcomer Nodalizations for LOFT Test L2-5

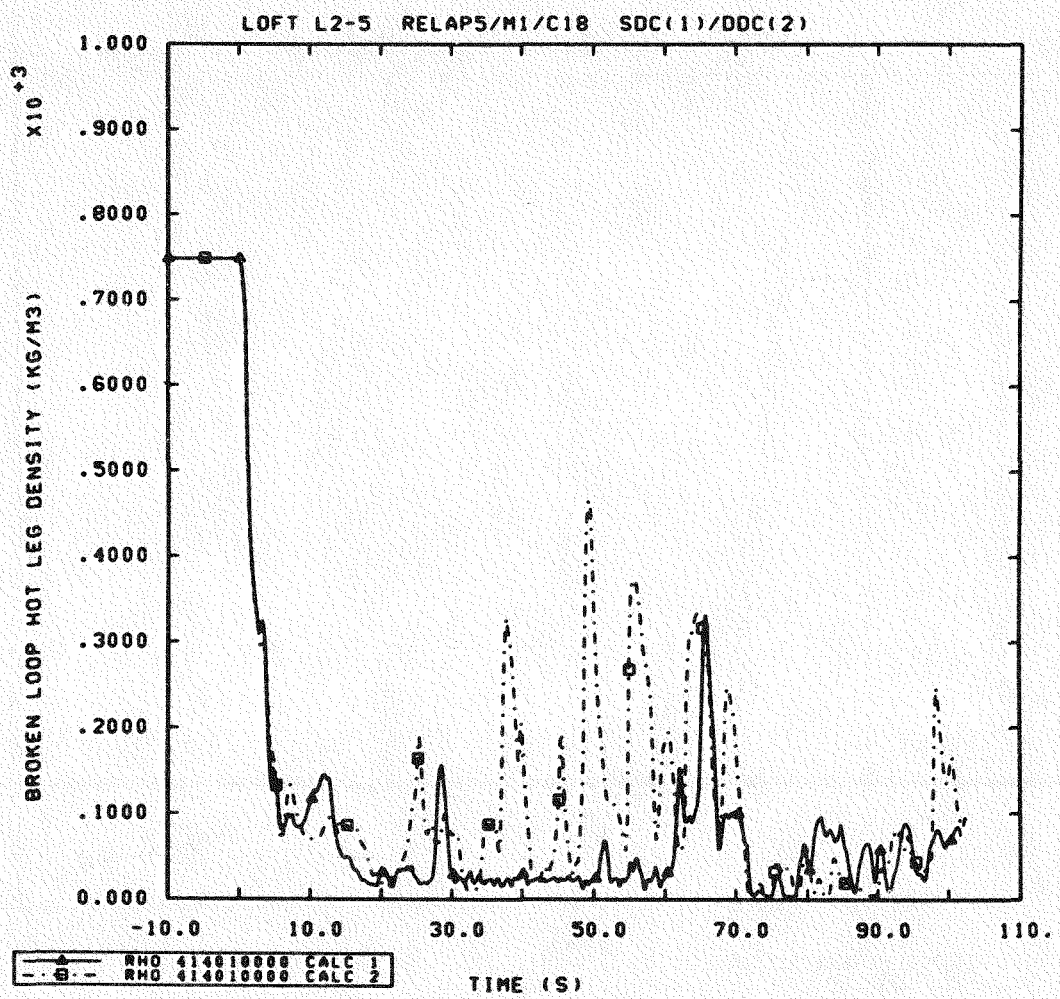


Figure 3.4.3 Calculated Broken Loop Hot Leg Densities using Original and Split- Downcomer Nodalizations for LOFT Test L2-5

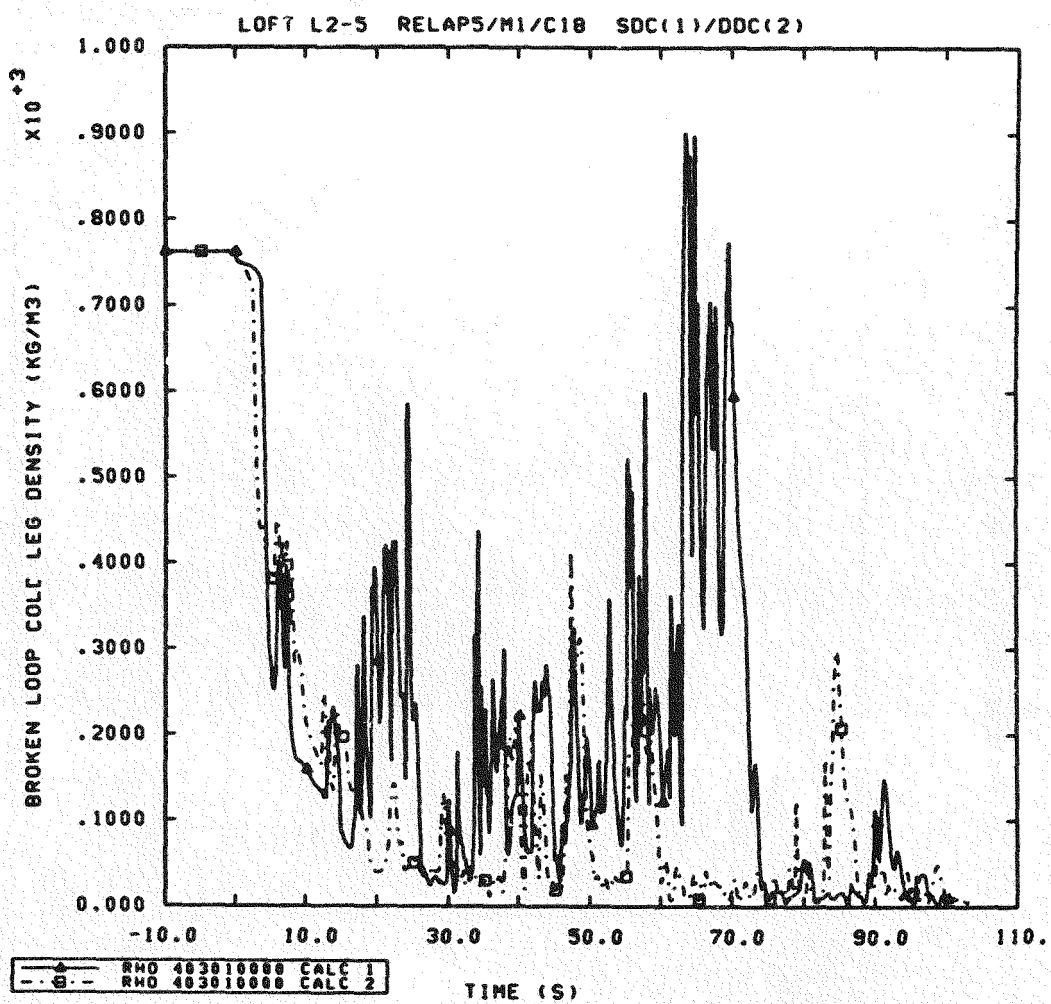


Figure 3.4.4 Calculated Broken Loop Cold Leg Densities using Original and Split- Downcomer Nodalizations for LOFT Test L2-5

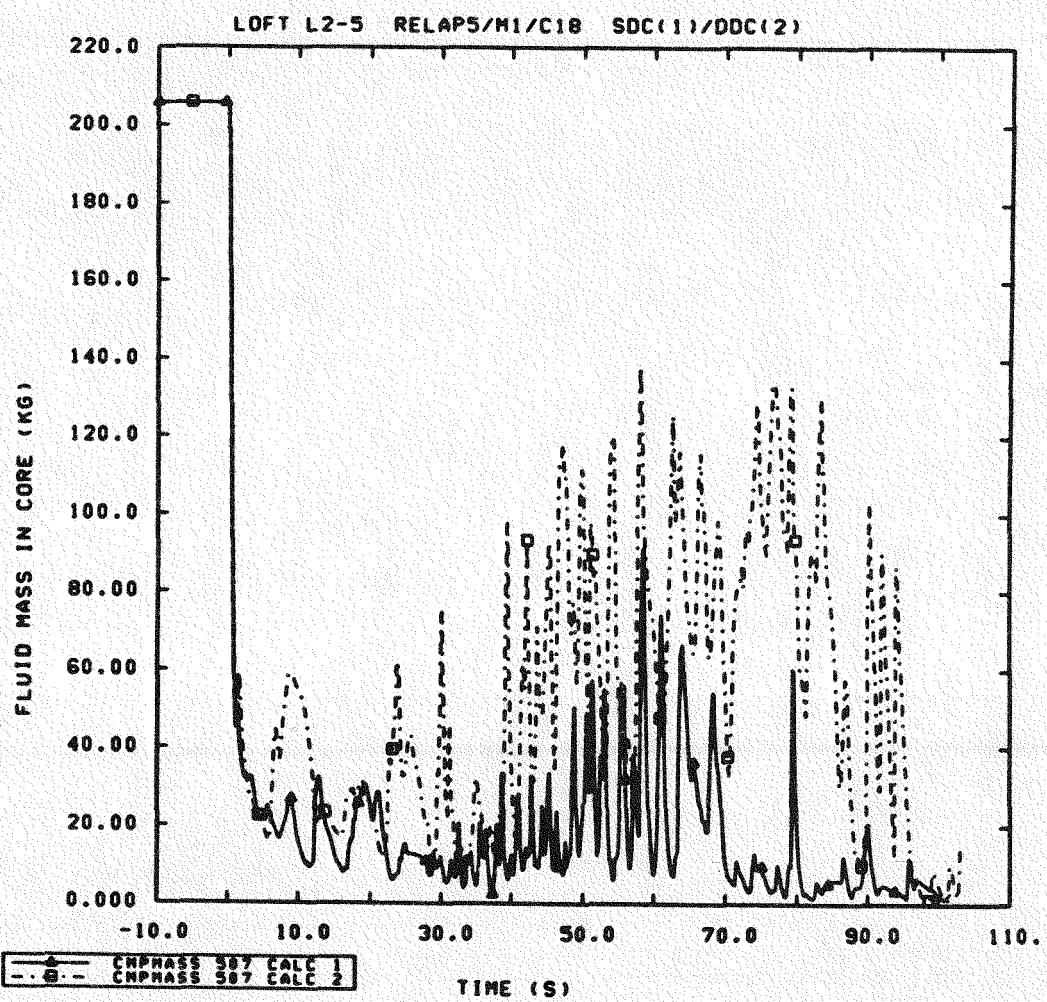


Figure 3.4.5 Calculated Fluid Mass in Core using Original and Split- Downcomer Nodalizations for LOFT Test L2-5

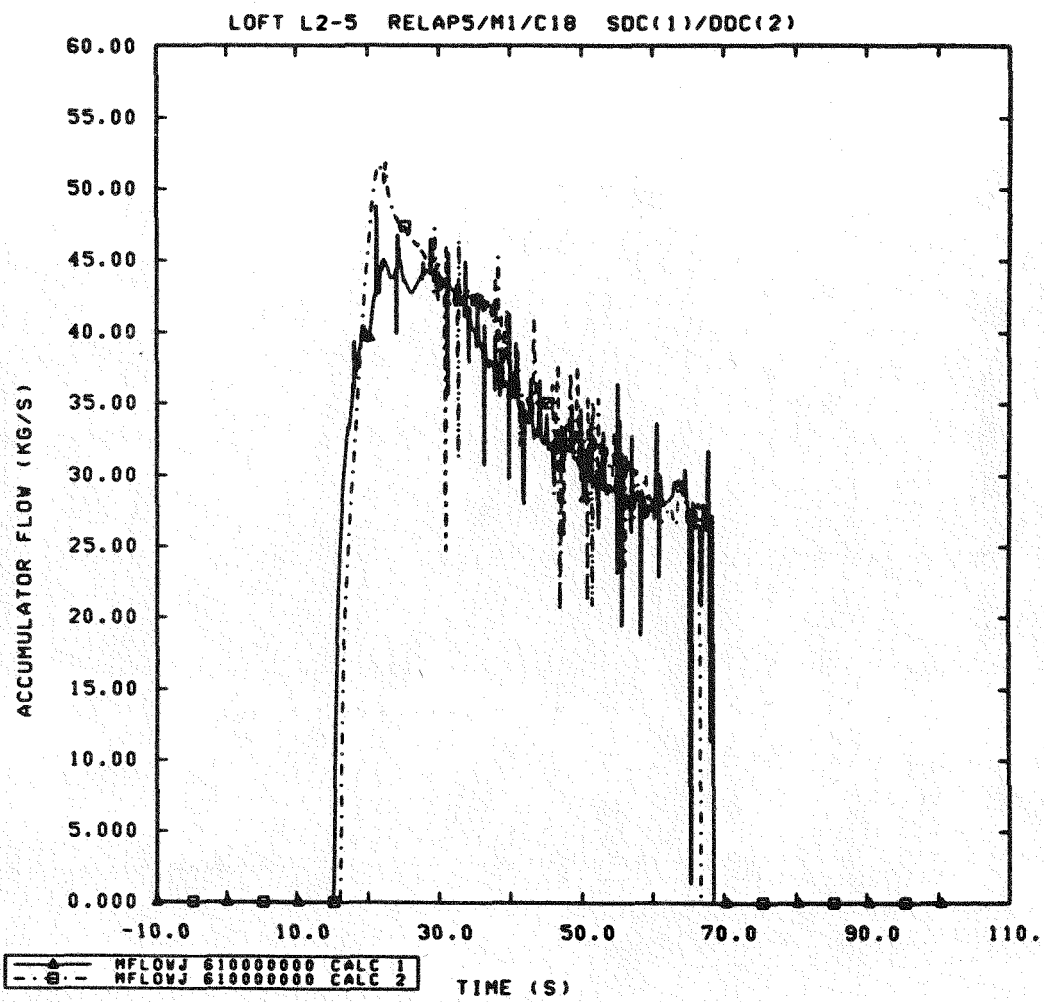


Figure 3.4.6 Calculated Accumulator Injection Flow Rates using Original and Split- Downcomer Nodalizations for LOFT Test L2-5

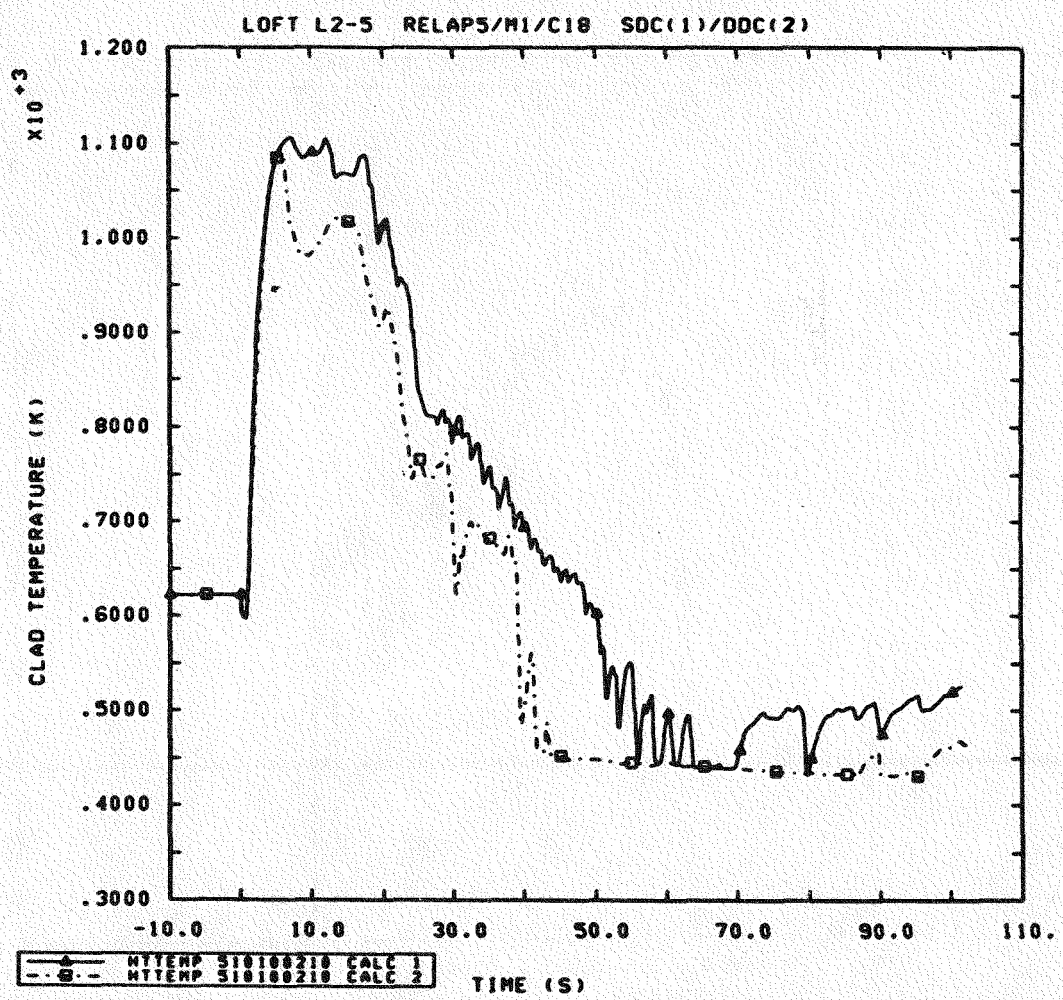


Figure 3.4.7 Calculated Rod Clad Temperatures at 0.64 m Core Elevation using Original and Split-Downcomer Nodalizations for LOFT Test L2-5

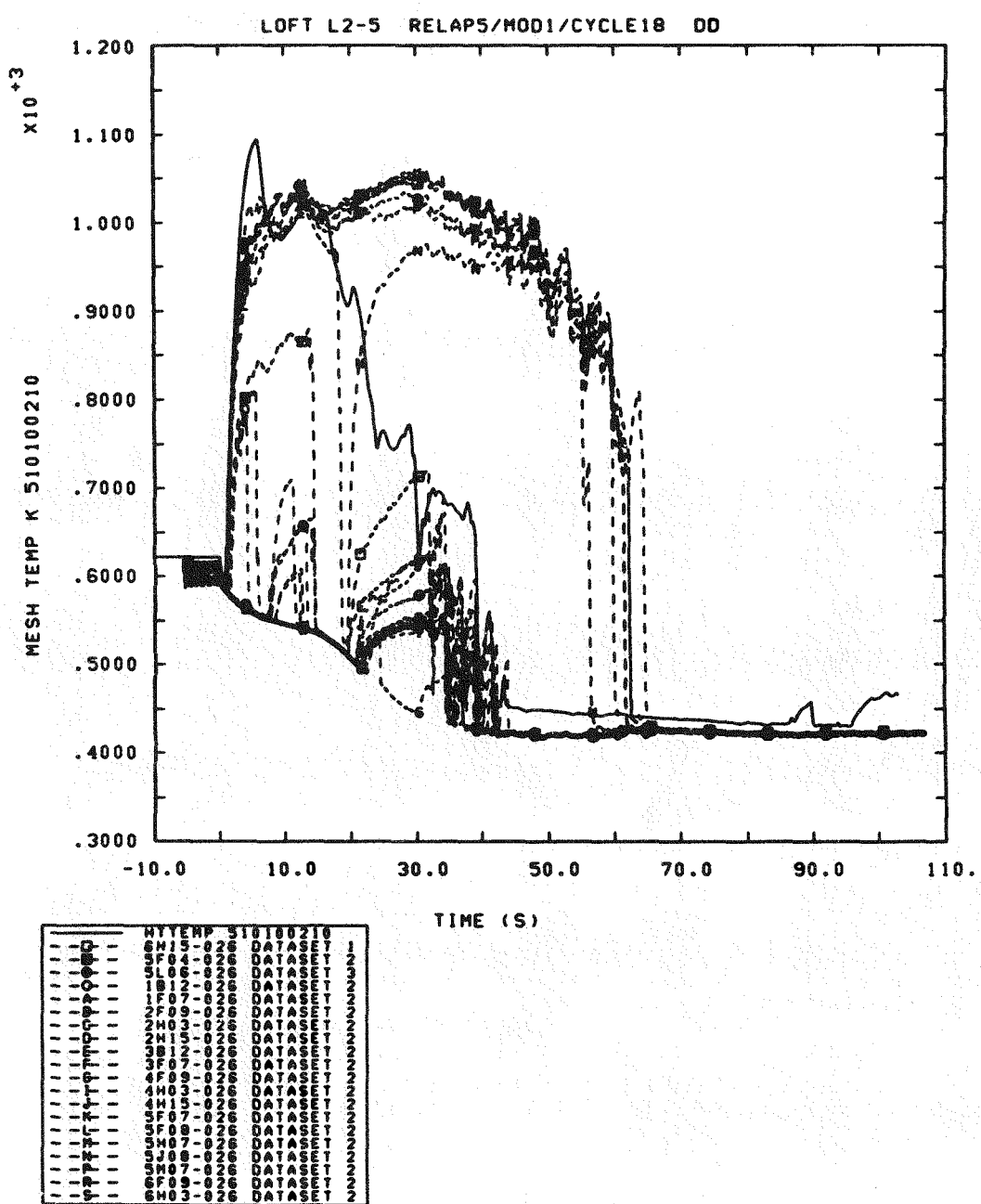


Figure 3.4.8 Calculated and Measured Rod Clad Temperatures at 0.64 m Core Elevation using Split- Downcomer Nodalization for LOFT Test L2-5

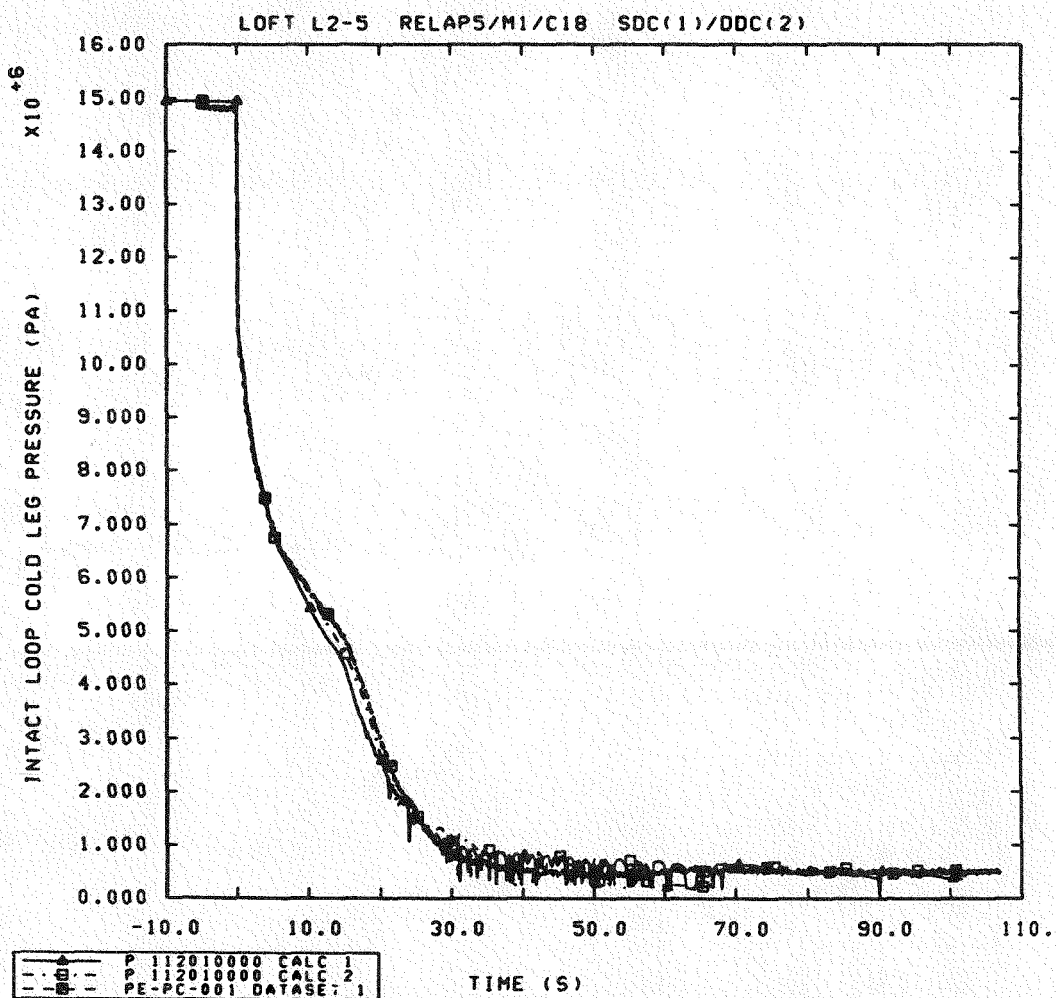


Figure 3.4.9 Calculated and Measured Primary System Pressures using Original and Split-Downcomer Nodalizations for LOFT Test L2-5

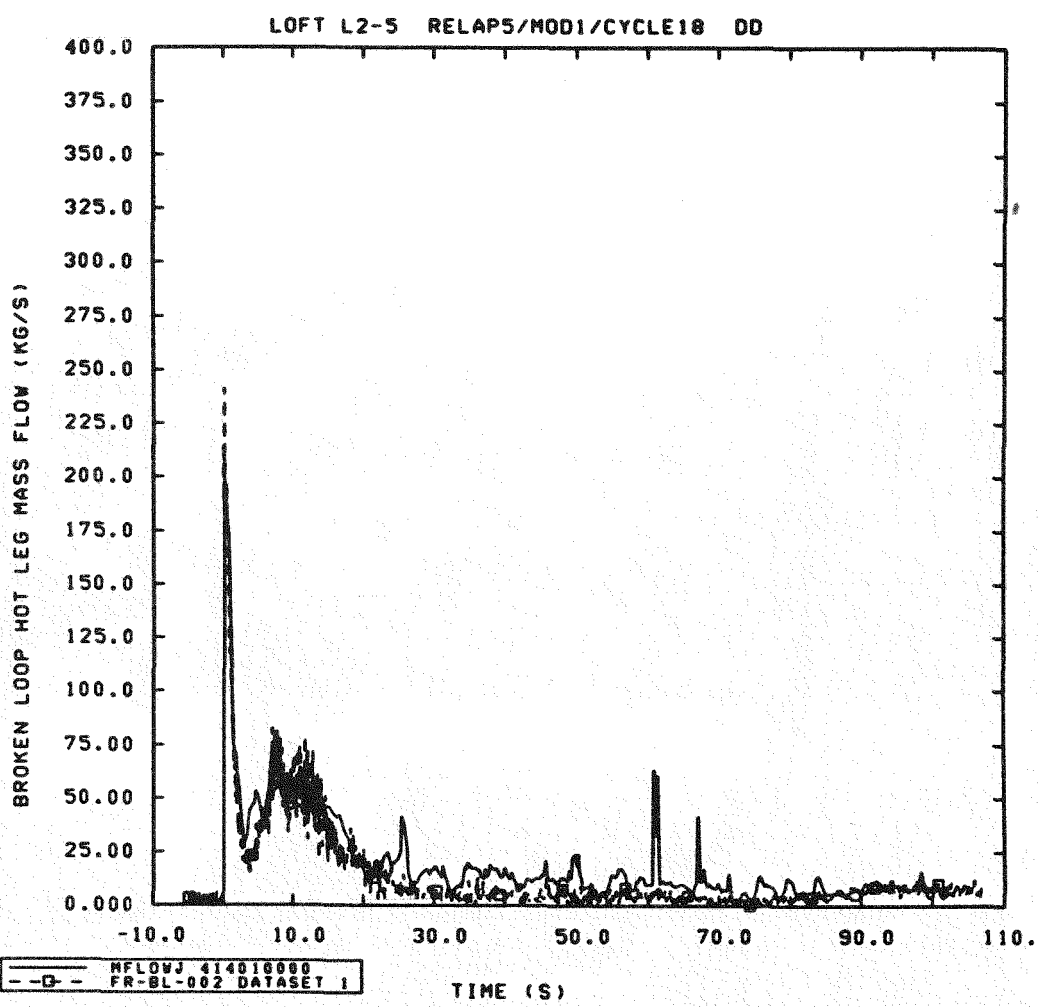


Figure 3.4.10 Calculated and Measured Broken Loop Hot Leg (Pump-side) Break Flows using Split- Downcomer Nodalization for LOFT Test L2-5

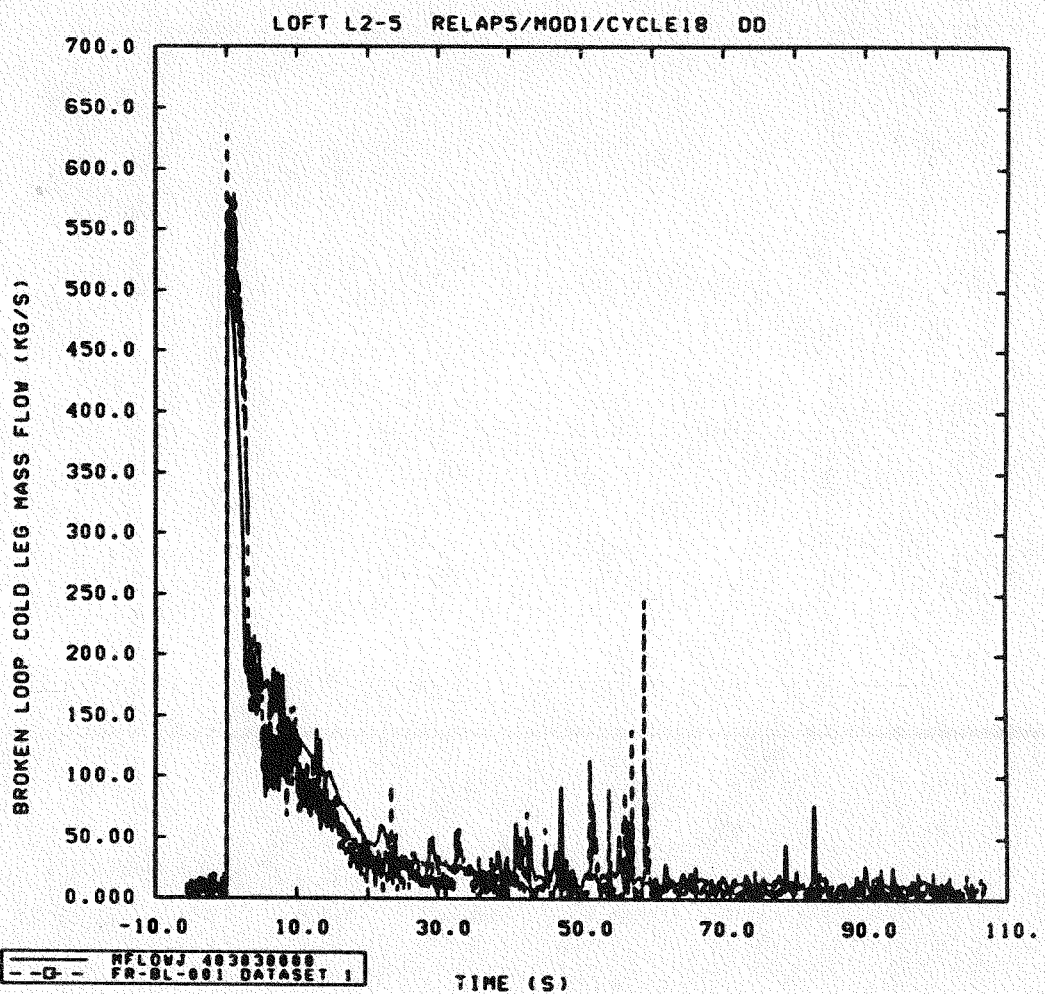


Figure 3.4.11 Calculated and Measured Broken Loop Cold Leg (Vessel-side) Break Flows using Split- Downcomer Nodalization for LOFT Test L2-5

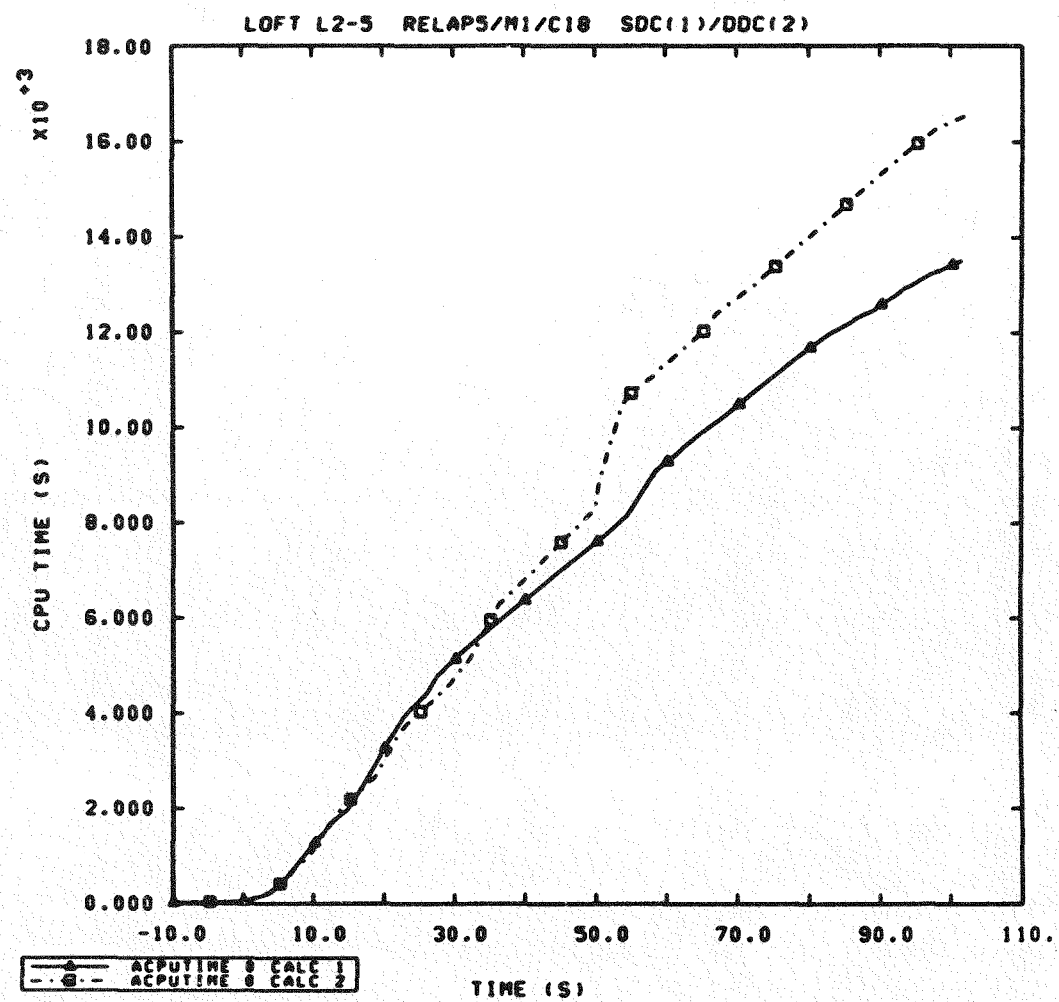
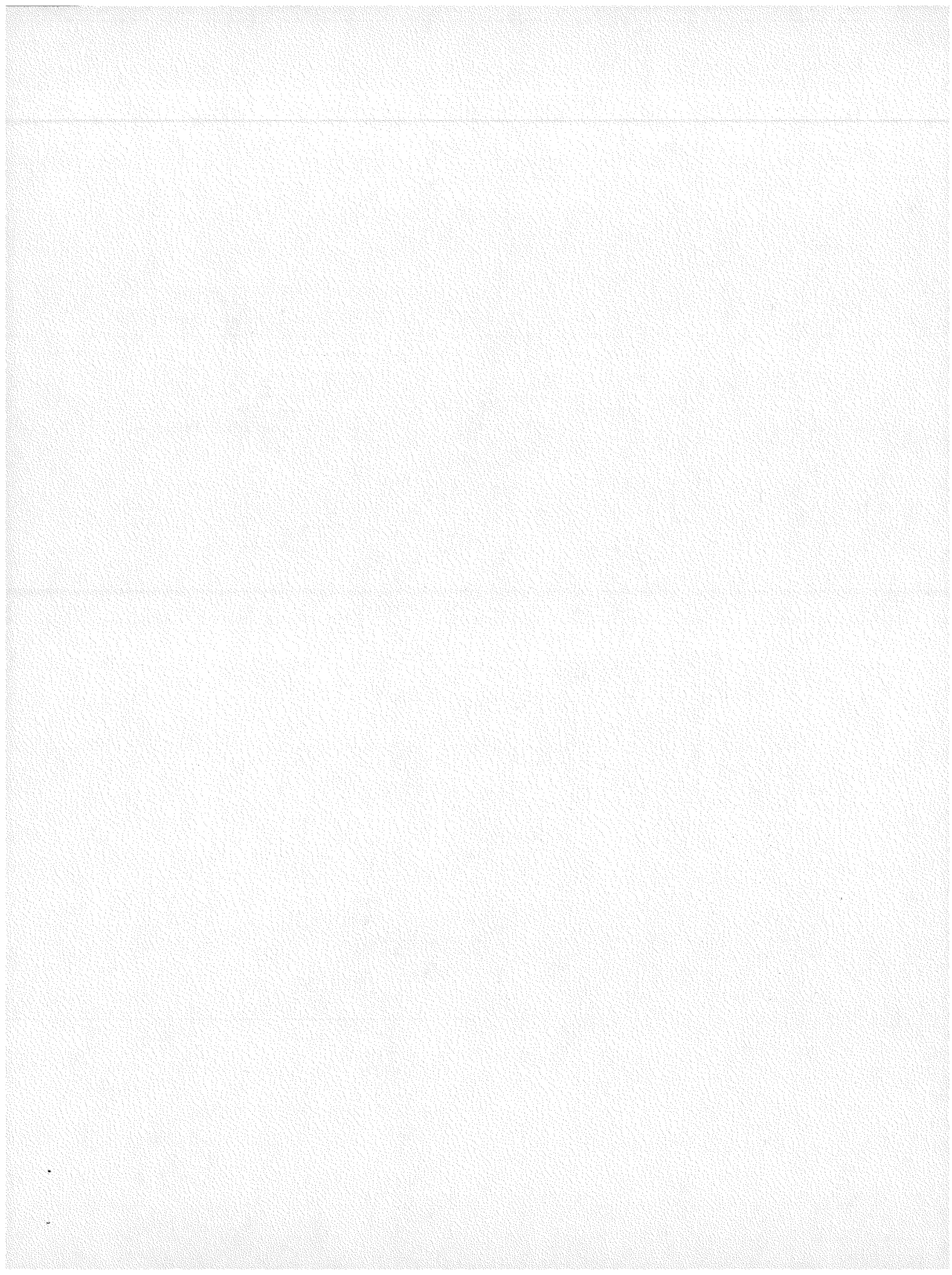


Figure 3.5.1 CPU Time using Original and Split-  
Downcomer Nodalizations for LOFT  
Test L2-5



#### 4.0 DISCUSSION AND CONCLUSIONS

Our LOFT L2-5 analyses show that RELAP5/MOD1 correctly calculates many of the major system variables in a large break LOCA, such as the primary system pressure and break flows, particularly during blowdown. The major problem encountered was the excess ECC bypass calculated throughout the later portions of the test, which resulted in too-large late-time break flows and high system pressure due to prolonged choked flow conditions. The excess ECC bypass also resulted in a second core heatup being calculated after the accumulator emptied, since water was not being retained in the vessel. Otherwise-identical transient calculations with a split-downcomer nodalization delivered more ECC water to the lower plenum, but that water was then swept up the core and upper plenum and out the other (pump-side) break; no other significant differences in overall behavior were evident between the calculations.

The early fuel rod heatup is generally calculated to be in good agreement with experimental data; the code, however, predicts early PCT during blowdown at ~10 s while the data shows PCT occurring at ~30 s, a time corresponding to the start of reflood. (The data does show an almost flat plateau in the higher-powered regions during this time.) The calculated PCT of 1105 K is in good agreement with data (1077 K), but one should be careful of comparing an average calculated PCT (with no radial peaking modelled) with an absolute PCT determined from a single (hottest) thermocouple measurement in a facility with significant radial peaking; the calculated PCT is high compared to the average data. Part of the reason for this is thought to be that cycle 18 of RELAP5/MOD1 overpredicts the decay heat throughout most of the transient, which results in higher calculated clad temperatures.

In general, the calculated clad temperatures agree better with measured data in the lower half of the core and fall progressively below data with increasing core elevation, and at later times. We believe that this occurs because MOD1 is not calculating a core fluid mixture of superheated steam and entrained saturated droplets (with the heat transfer occurring from the rods primarily to the hot steam and only indirectly to the entrained liquid present); the calculation is vaporizing all the liquid present before superheating any steam. We expect such a mixture of superheated steam and entrained saturated droplets to be generated in the lower portions of the core as the ECC water comes in and begins quenching the rods.

The primary coolant pump response (after pump trip at the start of the transient) has not been correctly predicted. Efforts to calculate correct pump coastdown and subsequent speedup involved replacing parts of the pump homologous curves with new

pump curves developed by LOFT based on the L3-6 (pumps-off small break test) experimental data [12], and using the one-velocity formalism in the loop seal junctions to force clearing at the correct time. These two changes resulted in better calculated early-time pump behavior, but had no significant effect on the overall system behavior, and did not correct the excess pump speedup calculated later in the transient.

This excessive pump speedup corresponds to the time during which the accumulator is injecting a large amount of subcooled ECC water into the intact loop cold leg, so that the most probable cause of the excess speedup being calculated is that the condensation-induced pressure drop at the ECC injection point, which creates a suction effect pulling more flow through the intact loop, is being overestimated and that too much flow is being pulled through the hot leg piping, steam generator and pump. Whether the higher mass flows are caused by too large an ECC condensation pressure drop (as suggested by the timing), or are simply due to the code calculating too high a two-phase natural circulation flow rate (as indicated by other assessment calculations [13,14]), the higher mass flow calculated accounts for the large pump speedup.

Another problem encountered during the L2-5 analyses was the code failure when the accumulator emptied and was to start injecting nitrogen. Discussions with the code developers revealed that this is a known (but undocumented) problem in both MOD1 and MOD1.5.

## 5.0 REFERENCES

1. V. H. Ransom, et al., RELAP5/MOD1 Code Manual Volume 1: System Model and Numerical Methods; Volume 2: Users Guide and Input Requirements, NUREG/CR-1826, EGG-2070, Idaho National Engineering Laboratory, March 1982.
2. V. H. Ransom, private communication, June 16, 1982.
3. D. L. Reeder, LOFT System and Test Description (5.5-ft Nuclear Core 1 LOCEs), NUREG/CR-0247, TREE-1208, Idaho National Engineering Laboratory, July 1978.
4. J. P. Adams, Quick-Look Report on LOFT Nuclear Experiment L2-5, EGG-LOFT-5912, Idaho National Engineering Laboratory, June 1982.
5. P. B. Bayless and J. M. Divine, Experiment Data Report for LOFT Large Break Loss-of-Coolant Experiment L2-5, NUREG/CR-2826, EGG-2210, Idaho National Engineering Laboratory, August 1982.
6. J. D. Burtt and S. A. Crowton, International Standard Problem 13 (LOFT Experiment L2-5) Preliminary Comparison Report, EGG-NTAP-6276, Idaho National Engineering Laboratory, April 1983.
7. S. L. Thompson and L. N. Kmetyk, RELAP5 Assessment: LOFT Turbine Trip L6-7/L9-2, NUREG/CR-3257, SAND83-0832, Sandia National Laboratory, July 1983.
8. Handout at Joint LOFT/Semiscale Modelling Workshop, August 18-19, 1981, at Idaho Falls, ID.
9. W. H. Giedt, Principles of Engineering Heat Transfer, Van Nostrand, Princeton NJ, 1957.
10. R. K. Byers and L. N. Kmetyk, RELAP5 Assessment: LOFT L9-1/L3-3 Anticipated Transient with Multiple Failures, NUREG/CR-3337, SAND83-1245, Sandia National Laboratory, August 1983.
11. R. M. Summers, RELAP5 Assessment: Semiscale Mod-3 Small Break Tests, NUREG/CR-3277, SAND83-1038, Sandia National Laboratories, July 1983.
12. T. H. Chen, Primary Coolant Pump Performance During LOFT L3-6 Experiment, EGG-LOFT-5414, Idaho National Engineering Laboratory, March 2, 1981.

13. S. L. Thompson and L. N. Kmetyk, RELAP5 Assessment: PKL Natural Circulation Tests, NUREG/CR-3100, SAND82-2902, Sandia National Laboratories, January 1983.
14. J. M. McGlaun and L. N. Kmetyk, RELAP5 Assessment: Semiscale Natural Circulation Tests S-NC-2 and S-NC-7, NUREG/CR-3258, SAND83-0833, Sandia National Laboratories, May 1983.
15. L. N. Kmetyk, RELAP5 Assessment: LOFT Small Break L3-6/L8-1, NUREG/CR-3163, SAND83-0245, Sandia National Laboratories, March 1983.
16. J. L. Orman and L. N. Kmetyk, RELAP5 Assessment: LOFT Intermediate Break Tests L5-1 and L8-2, NUREG/CR-3406, SAND83-1575, Sandia National Laboratories, August 1983.
17. L. N. Kmetyk, RELAP5 Assessment: LOBI Large Break Transients, NUREG/CR-3075, SAND82-2525, Sandia National Laboratories, March 1983.
18. S. L. Thompson et al., Thermal/Hydraulic Analysis Research Program Quarterly Report, January-March 1983, NUREG/CR-3329, SAND83-1171, Vol. 1 of 4, Sandia National Laboratories, June 1983.
19. P. N. Demmie, T.-H. Chen and S. R. Behling, Best Estimate Prediction for LOFT Nuclear Experiment L2-5, EGG-LOFT-5869, Idaho National Engineering Laboratory, May 1982.

## APPENDIX I FACILITY DESCRIPTION

The Loss-of-Fluid Test (LOFT) facility [2] is located at the Idaho National Engineering Laboratory and supported by the NRC. The facility is a 50 Mwt pressurized water reactor (PWR) with instrumentation to measure and provide data on the thermal/hydraulic conditions during a postulated accident. The experimental assembly includes five major subsystems: the reactor vessel, the intact loop (scaled to represent three operational loops), the broken loop, the blowdown suppression system and the emergency core cooling system (ECCS). The general philosophy in scaling coolant volumes and flow areas was to use the ratio of the LOFT core power (50 Mwt) to a typical PWR core (3000 Mwt). A summary of the LOFT primary volume distribution is given in Table AI.1. The LOFT configuration for test L2-5 is shown in Figure AI.1.

The intact loop, shown in Figure AI.2, simulates three loops of a commercial four-loop PWR and contains a steam generator, two primary coolant pumps in parallel, a pressurizer, a venturi flowmeter and connecting piping.

The coolant leaves the reactor vessel outlet nozzle through 14-in. Schedule 160 piping and proceeds to the steam generator inlet through a venturi flowmeter. The steam generator inlet is slightly higher than the reactor vessel outlet nozzle. The piping entering and leaving the steam generator is 16-in. Schedule 160. After dropping to the level of the reactor vessel nozzles, it proceeds into a 14-in. reducer and then down into a tee. At this point, the piping branches into two 10-in. Schedule 160 lines and proceeds to the pump inlets. A 10-in. Schedule 160 pipe connects the pump outlets to a tee, at which point the loop becomes 14-in. Schedule 160 piping joining the reactor vessel inlet. A brief summary of the intact loop piping is given in Figure AI.3 and Table AI.2.

The pressurizer includes a vertical cylindrical pressure vessel, immersion-type electrical heaters, a surge nozzle, pressure relief and spray nozzles. The surge line connects to the primary coolant loop between the flow venturi and the reactor vessel. The spray line connects to the primary coolant system downstream of the pump discharge. Pressure is increased by energizing the electric immersion heaters and decreased by spray flow of relatively cool primary coolant into the steam space. The pressurizer is described in Figure AI.4, while the surge line piping is summarized in Figure AI.5 and Table AI.3.

The steam generator is a vertical shell and U-tube recirculation-type heat exchanger with primary coolant flow in the tube side and secondary coolant in the shell side. The steam

generator, located between the reactor outlet and primary coolant pump suction, is elevated such that its entire primary volume will tend to drain into the reactor vessel. Orifices are installed in the inlet and outlet plena to scale primary flow through the intact loop for simulation of PWR response to a LOCA. Penetrations in the shell are provided for the steam outlet, feedwater inlet, top and bottom blowdown, level control, draining, and primary coolant inlet and outlet. The steam generator is shown in Figure AI.6 and some steam generator design parameters are given in Tables AI.4 and AI.5.

The broken loop, shown in Figure AI.7, consists of a hot leg and a cold leg that are connected to the reactor vessel and the blowdown suppression tank (BST) header. Each leg consists of a break plane orifice, a quick-opening blowdown valve, an isolation valve, and connecting piping. Recirculation lines (not shown) establish a small flow from the broken loop to the intact loop and are used to warm up the broken loop prior to experiment initiation. The broken loop hot leg also contains a simulated steam generator and a simulated pump; these simulators have hydraulic orifice plate assemblies which have similar (passive) resistances to flow as an active steam generator and pump. A brief summary of the broken loop piping is given in Figure AI.8 and Table AI.6.

The blowdown suppression system consists of the blowdown suppression tank (BST) itself, the BST header, the nitrogen pressurization system and the BST spray system. The blowdown header is connected to the suppression tank downcomers which extend inside the tank below the water level. The header is also directly connected to the BST vapor space to allow pressure equilibration. The nitrogen pressurization system is supplied by the LOFT inert gas system and uses a remote-controlled pressure regulator to establish and maintain the specified BST initial pressure. The spray system consists of a centrifugal pump that discharges through a heatup heat exchanger and any of three spray headers or a pump recirculation line that contains a cooldown heat exchanger. The spray pump suction can be aligned to either the BST or the borated water storage tank (BWST). The three spray headers have flow rate capacities of 1.3, 3.8 and 13.9 l/s, respectively, and are located in the BST along the upper centerline. The BST spray pump suction was connected to the BWST and the liquid was sprayed into the BST so that the BST pressure simulated the containment backpressure expected during a LOCA.

The LOFT ECCS simulates the ECCS of a commercial PWR. It consists of two accumulators, a high-pressure injection system and a low-pressure injection system. Each system is arranged to inject scaled-down flow rates of emergency core coolant directly into the primary coolant system. All ECC flow was directed to the

intact loop cold leg during experiment L2-5. The HPIS injection was delayed until  $23.90 \pm 0.02$  s, and the LPIS injection was delayed until  $37.32 \pm 0.02$  s. Both these injection systems drew suction from the BWST. (During the recovery, ECC was injected into the reactor vessel lower plenum.)

The LOFT reactor vessel, shown in Figure AI.9, has an annular downcomer, a lower plenum, upper and lower core support plates, a nuclear core and an upper plenum. The vessel volume distribution is given in Table AI.7, and the metal mass present is summarized in Table AI.8. The station numbers in Figure AI.10 are explained in Table AI.9.

The reactor vessel itself is a vertical stainless steel clad, low alloy steel cylinder with a semi-elliptical bottom head and a flanged, bolted two-piece top head. The vessel has two primary coolant inlet and outlet nozzles in the same plane above the core; they are diametrically opposite and provide the interface between the primary coolant and the reactor systems. The core support barrel, a single stainless steel structure, is a cylindrical barrel with a heavy top flange whose shoulder rests on the reactor vessel; the flange is also counterbored to accept the upper core support plate assembly. The cylindrical section of the core barrel has approximately a 0.76 m (30-in) ID, 4.6 m (15.1-ft) length and 0.04 m (1.5-in) wall thickness. Outlet nozzles in the core barrel are aligned with the reactor vessel outlet nozzles. An interior shoulder at the lower end of the barrel supports the lower core support structure. The core support barrel forms the inside of the annular downcomer, separates the inlet from the outlet coolant, and also serves as the outside of the cylindrical outlet plenum above the core.

The core support structure consists of three assemblies: the upper core support plate, the upper core support tubes and the lower core support structure. The upper core support plate is a 0.99 m (39-in) diameter, 0.18 m (7-in) thick plate made of Type 304 stainless steel, bolted to a ledge in the core support barrel. It has a 0.23 m (9-in) square hole in the center (which provides access for the replacement of the center fuel module) and four circular holes (for passage of control rod shafts). The lower core support structure, seated on the interior ledge of the core support barrel, is made of Type 304 stainless steel. It is basically a three-plate assembly surrounded by a cylindrical shell with an outside diameter approximately the same as the inside diameter of the core support barrel (the lower core support skirt). Support for the three plates is provided by the cylinder and inner structural columns. The upper (core mounting) plate is 38 mm (1-1/2-in) thick and has 24 round flow distribution holes. The intermediate (diffuser) plate acts as a diffuser to improve coolant distribution to the core; it is 0.025 m (1-in) thick and is supported only by the interior structure (columns).

The flow paths for the coolant are through 1543 holes in the diffuser plate and 154 holes through the lower core support skirt. The bottom core support plate has a 0.76 m (29.96-in) outside diameter and a 0.11 m (4.22-in) thickness; coolant flow through this plate is through five 0.15 m (6-in) square holes and four 0.1 m (3.9-in) circular holes.

The flow skirt and core filler assembly are considered as one assembly due to the similarity of purpose and design. The core filler is fabricated by bolting relatively small sections to the flow skirt. The flow skirt and core filler assemblies consist of three subassemblies which stack vertically to form a structure that lines the length of the core support barrel above the lower core support structure. Core filler subassemblies have the same length as the flow skirt sections and are permanently attached to them. The fillers occupy the volume between the flow skirt and the fuel assembly envelope. Coolant bypass channels (discussed below) are provided through and around the flow skirt core filler to limit the temperature rise in this assembly due to nuclear heating.

The purpose of the reactor vessel fillers is to displace excess coolant in the inlet and downcomer regions to maintain a ratio of water in the inlet and downcomer to that in the core and primary system similar to the ratio found in a full-size PWR; the fillers also serve to distribute inlet coolant and ECC downcomer flow. The filler assemblies form the outer edge of the annular downcomer regions. A 0.05 m (2-in) thick annulus is formed with the core support barrel except in the nozzle region where a 0.089 m (3.5-in) thick by 0.69 m (27-in) high annulus is formed. This larger annulus links the two inlet nozzles and acts as a main flow distribution channel. A thin [6.4 mm (0.25-in)] secondary annular downcomer is formed by the clearance between the filler assembly and the reactor vessel.

The flow has several paths available when it enters the reactor vessel. The main flow path is around the distributor annulus, down the downcomer, through the core, and out the outlet nozzles. There are several alternate paths available which do not direct the coolant through the core; these are termed core bypass paths. Figure AI.10 shows the reactor flow paths schematically. There are five possible core bypass flow paths (paths 1 through 5) and one path (path 6) which allows communication between the core and a bypass path. These are shown and numbered in Figure AI.9 and detailed in Figure AI.11. Path 1 allows coolant to flow between the lip at the bottom of the core support barrel and the lower core support plate. From there it travels between the lower core support structure and the core barrel upwards to the bottom of the flow skirt, then travels in the annulus between the core barrel and support skirt to the top of the support skirt and into

the hot leg nozzle region. Path 2 allows coolant which has gone through the lower core support structure to flow underneath the core filler blocks and in the gap between the filler blocks and the flow skirt or in the gaps between the filler blocks. This path has the opportunity to communicate with the core at station 173.236. The coolant entering path 2 will either flow in the flow skirt-filler block gaps to the top of the upper flow skirt or communicate with the core flow at the lower to intermediate flow skirt mating or the intermediate to upper flow skirt mating. Path 3 allows coolant to flow from the downcomer directly into the core support barrel-flow skirt annulus. After the coolant enters the core support barrel-flow skirt annulus, it flows upward to the top of the flow skirt and into the hot leg nozzle region. Path 4 allows coolant to flow from the cold leg nozzle region directly to the hot leg nozzle region. The coolant flows in the gap between the reactor vessel filler blocks and the reactor vessel and then through the gap between the core support barrel hot leg nozzle and the reactor vessel into the hot leg nozzle area. Path 5 allows coolant to flow from the cold leg nozzle region into the upper plenum. The controlling flow areas and their equivalent diameters, as well as the nominal flow rates in each bypass, are given in Table AI.10.

The 1.68 m (5.5-ft) core used in LOFT is designed to have the same physical, chemical and metallurgical properties as those in commercial PWRs. It is also designed to provide thermal/hydraulic relationships, mechanical response, and fission product release behavior during the LOCEs and ECC recovery which are representative of PWRs during a LOCA. The core contains 1300 nuclear fuel rods arranged in five square (15 x 15) assemblies and four triangular (corner) assemblies, shown in Figure AI.12. The center assembly is highly instrumented, and its fuel rods were prepressurized to 2.4 MPa; the fuel rods in the peripheral assemblies are unpressurized. Two of the corner and one of the square assemblies are not instrumented. The fuel rods have an active length of 1.67 m and an outside diameter of 10.72 mm. The fuel consists of UO<sub>2</sub> sintered pellets with an average enrichment of 4.0 wt% fissile uranium (U-235) and with a density that is 93% of theoretical density. The fuel pellet diameter and length are 9.29 and 15.24 mm, respectively. Both ends of the pellets are dished with the total dish volume equal to 2% of the pellet volume. The cladding material is Zircaloy-4. The cladding inside and outside diameters are 9.48 and 10.72 mm, respectively.

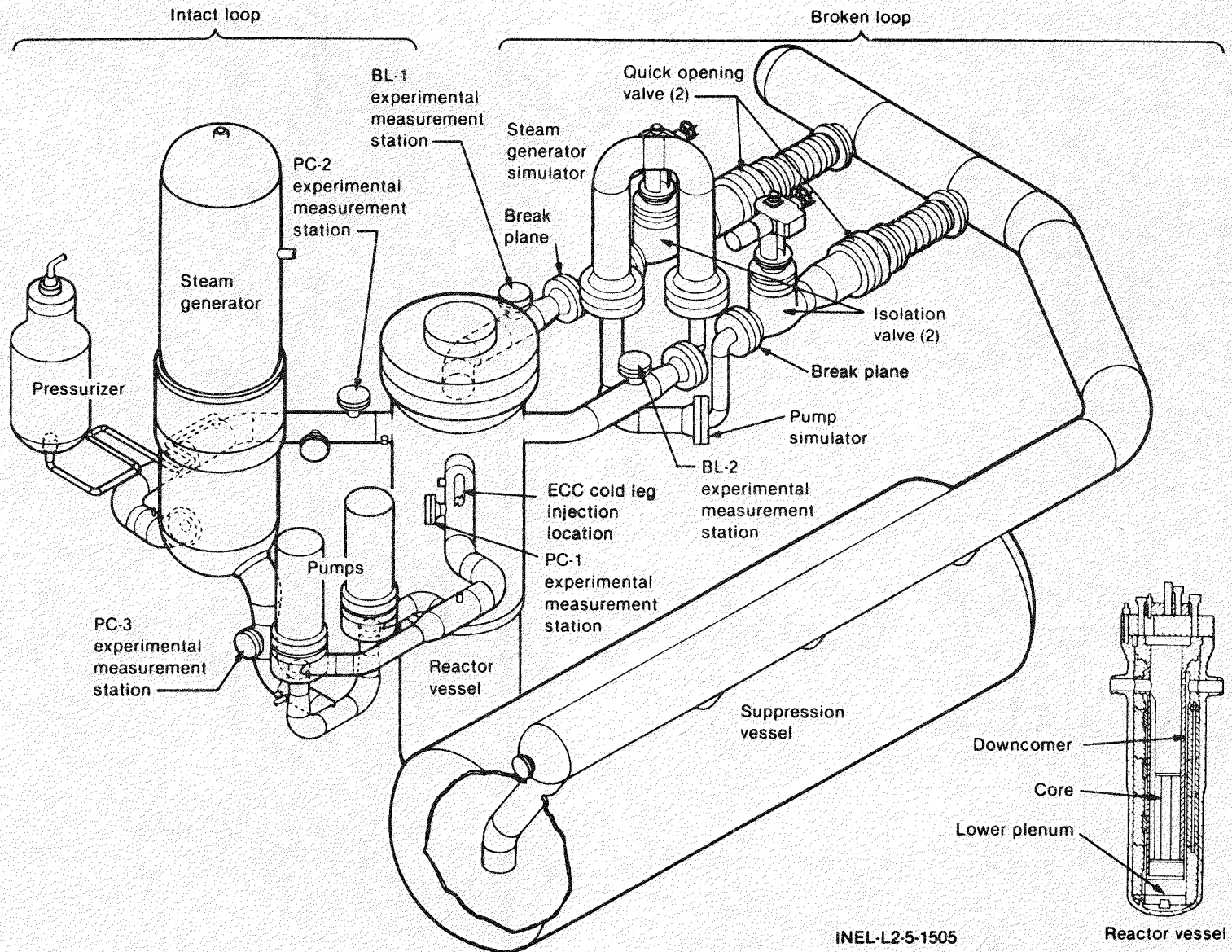


Figure AI.1 LOFT Configuration for L2-5

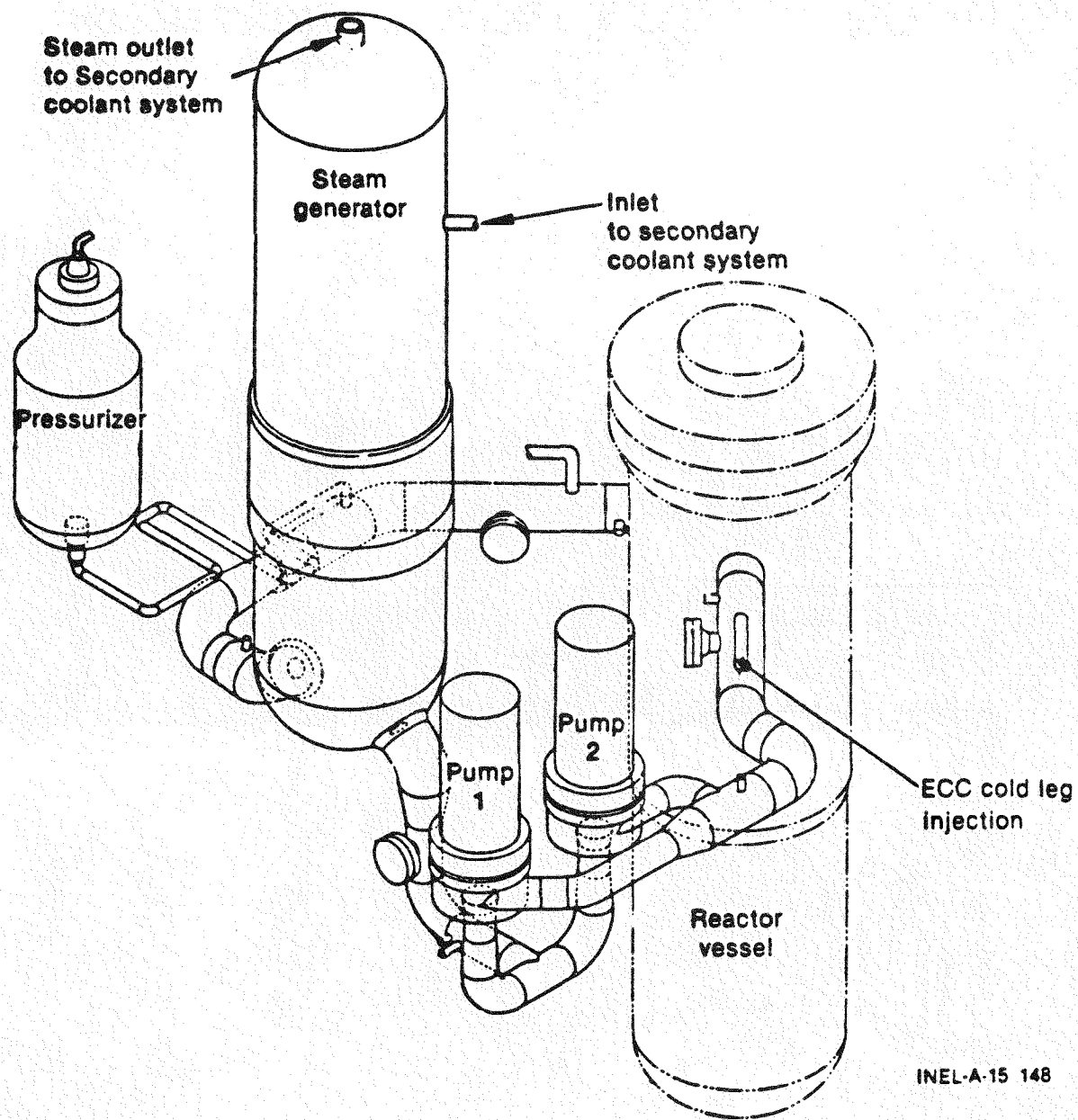
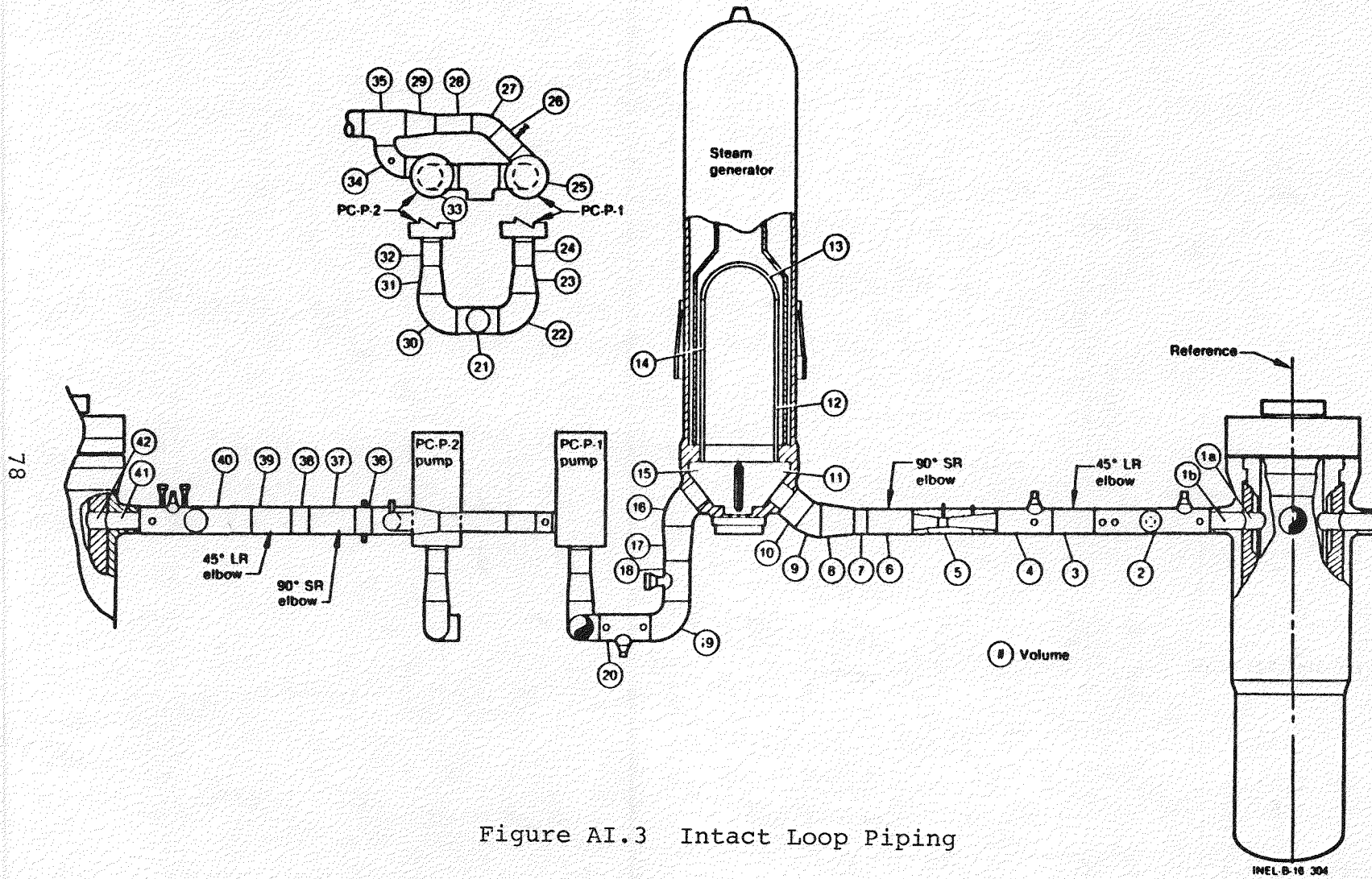
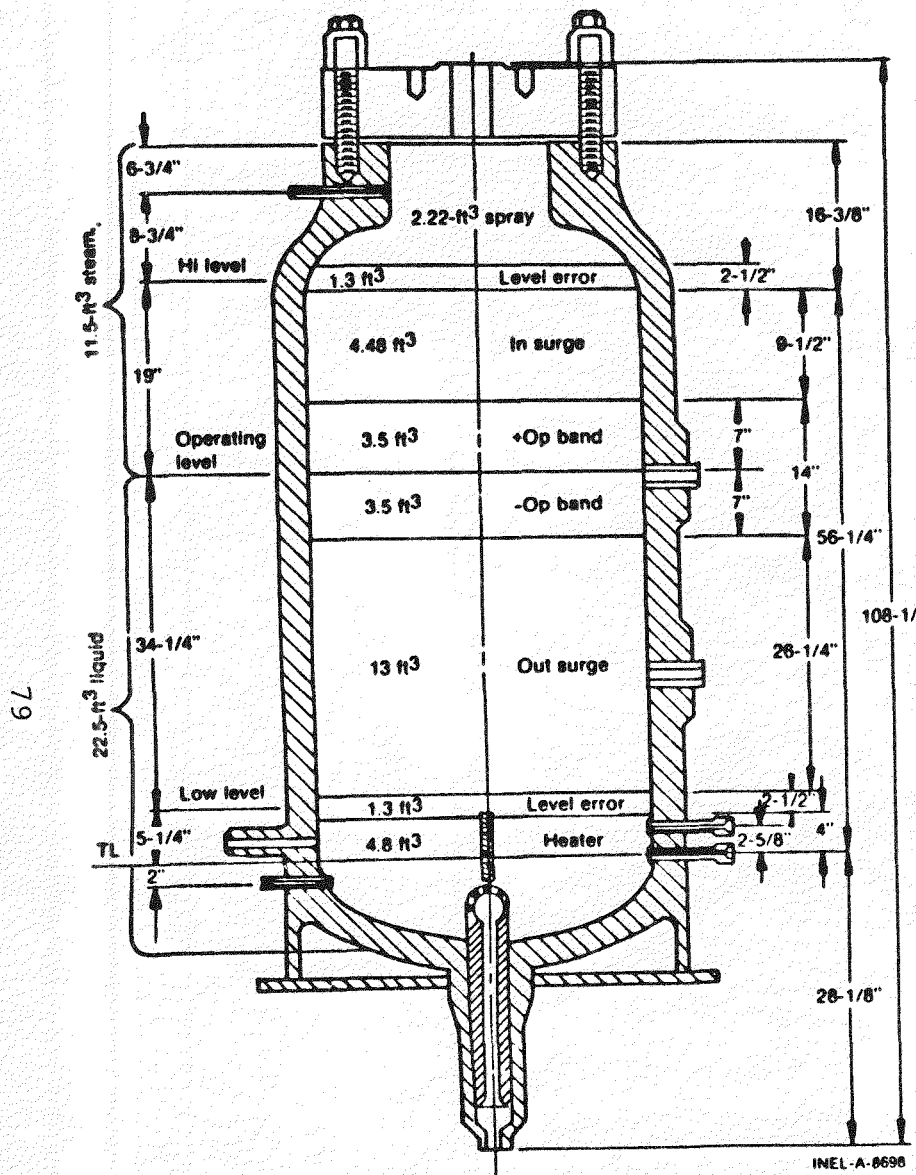


Figure AI.2 LOFT System -- Intact Loop



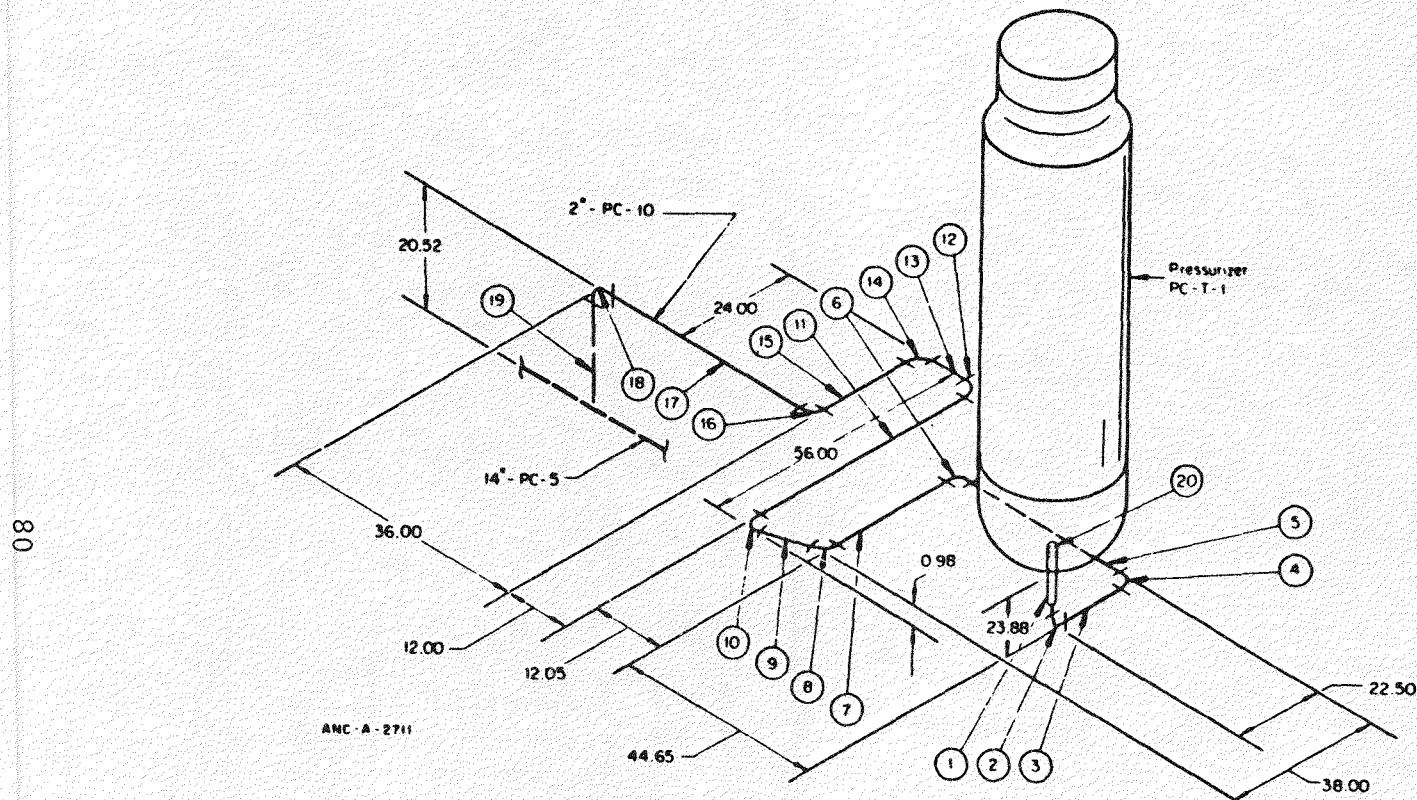


#### THERMAL-HYDRAULIC DATA -- PRESSURIZER

Parameter	Value
Normal operating pressure	15.51 MPa (2250 psig)
Normal operating temperature	617 K (650°F)
Normal variation in pressure	
Operating <sup>[a]</sup>	±0.10 MPa (+15 psia)
Accuracy <sup>[a]</sup>	±0.31 MPa (+45 psia)
Pressurizer volume	0.96 m <sup>3</sup> (34 ft <sup>3</sup> )
Steam volume	0.33 m <sup>3</sup> (11.5 ft <sup>3</sup> )
Liquid volume	0.64 m <sup>3</sup> (22.5 ft <sup>3</sup> )
Volume/MW(t)	0.0175 m <sup>3</sup> /MW(t) [0.618 ft <sup>3</sup> /MW(t)]
Maximum heater input by heaters	48 kW
Continuous spray flow	0.03 l/s (0.5 gpm)
Spray rate (maximum)	1.26 l/s (20 gpm)
Spray nozzle differential pressure at maximum spray rate and 555 K (540°F)	0.13 MPa (20 psid)

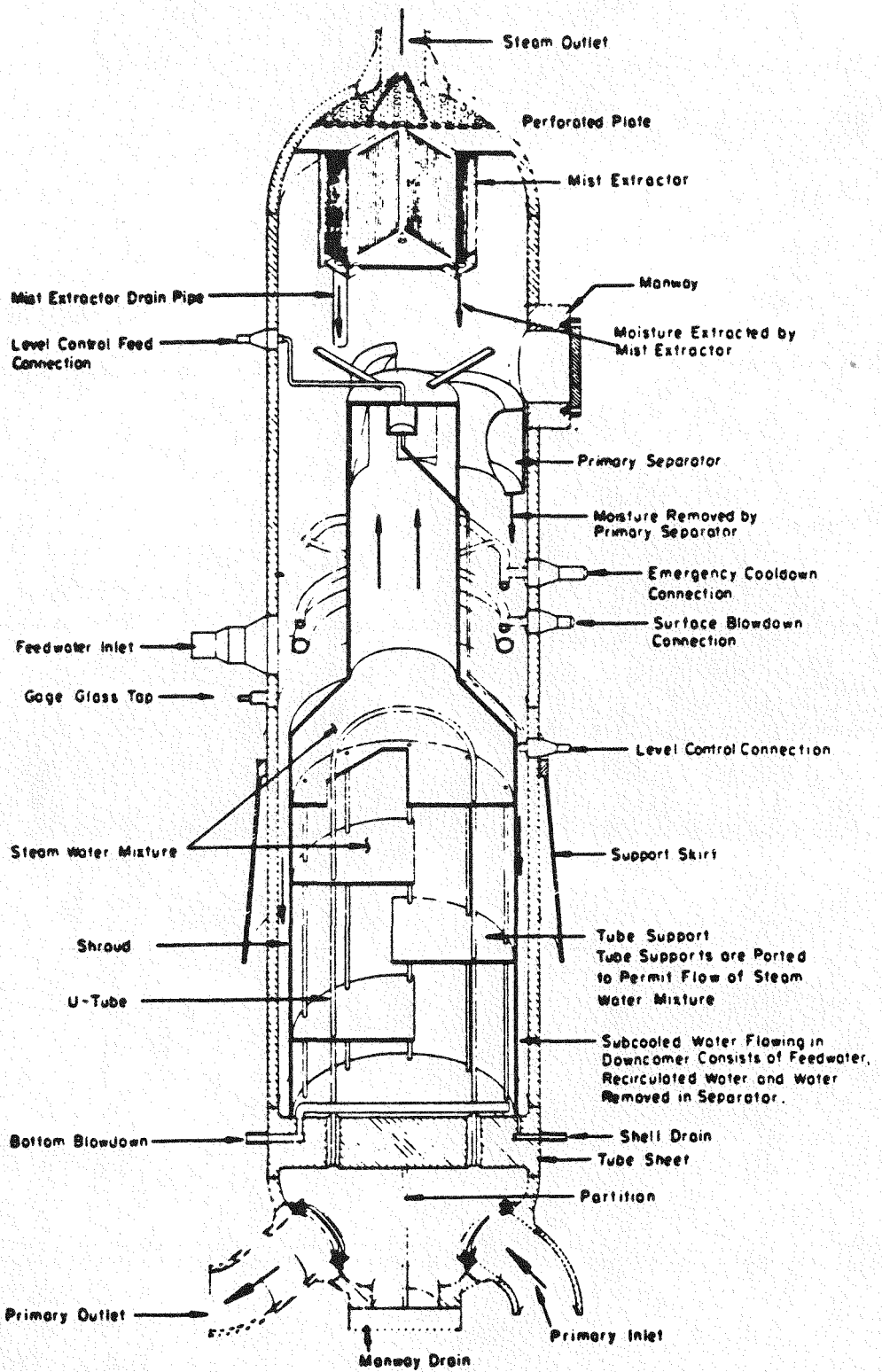
[a] The error band of the pressure transducers is ±0.310 MPa (+45 psia); however, the transducers are repeatable within 0.103 MPa (+15 psia).

Figure AI.4 Pressurizer Geometry



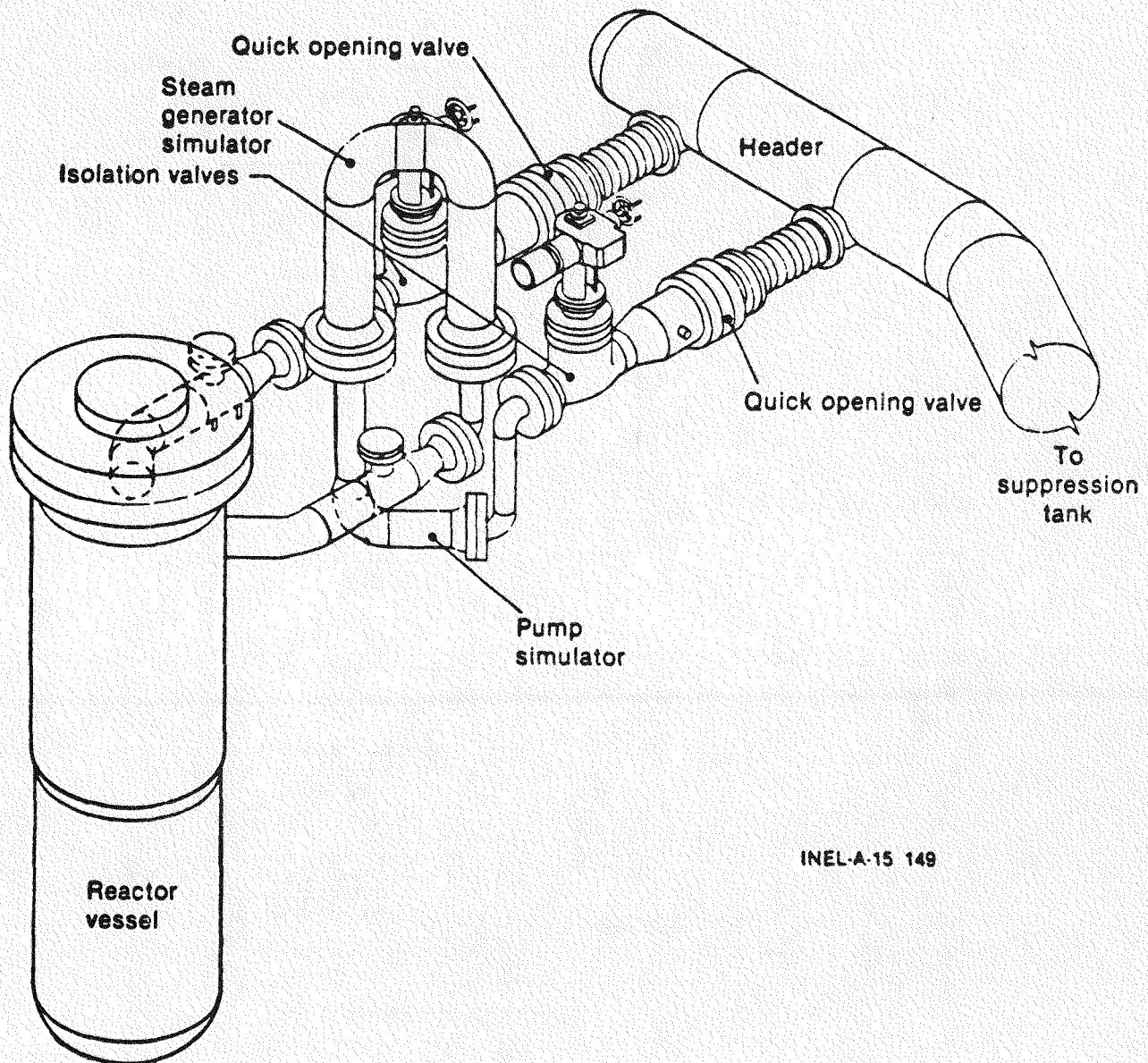
Pressurizer surge line routing.

Figure AI.5 Pressurizer Surge Line Routing



ANL-4-9722

Figure AI.6 Steam Generator Schematic



INEL-A-15 149

Figure AI.7 LOFT System -- Broken Loop

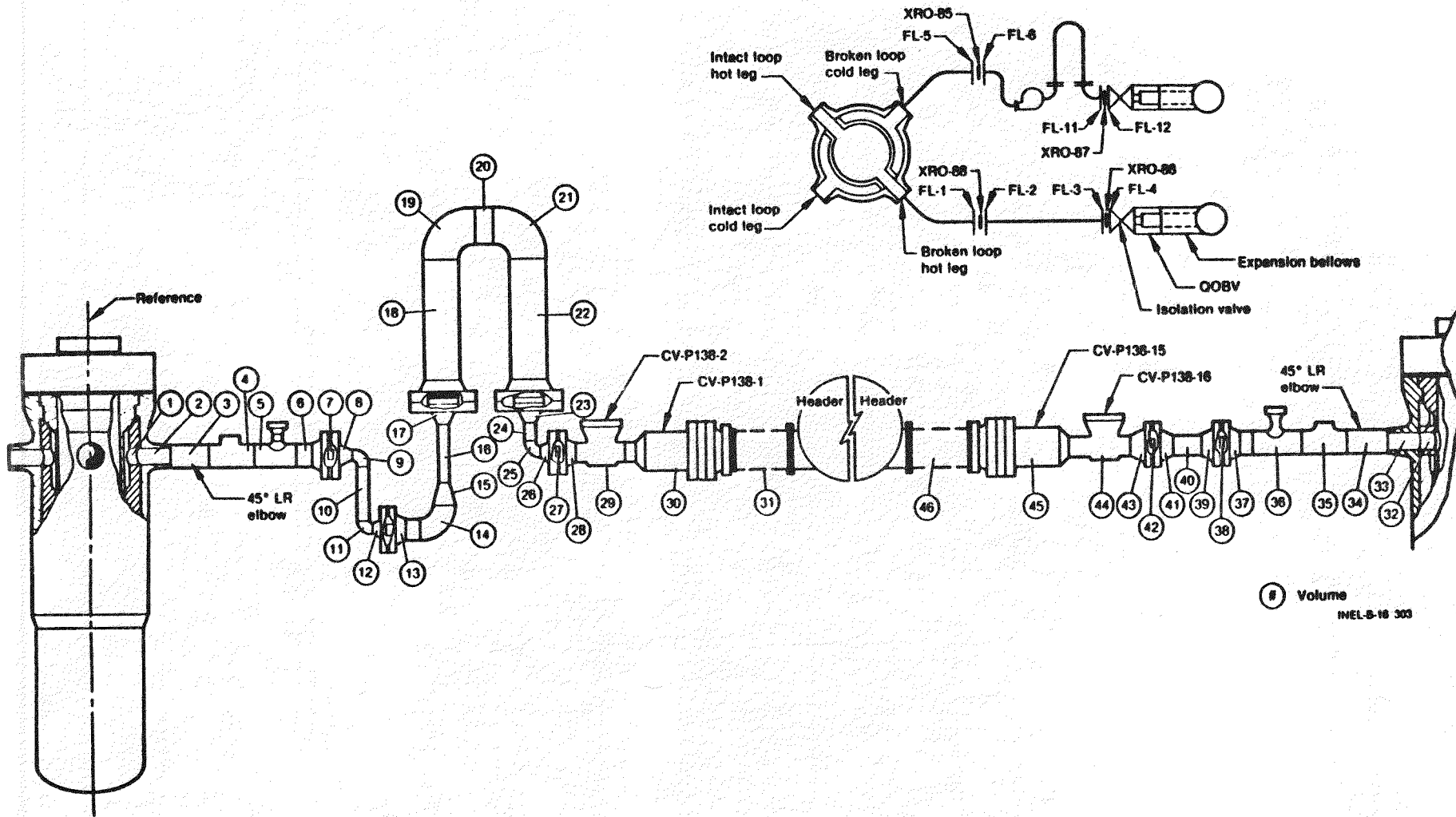


Figure AI.8 Broken Loop Piping

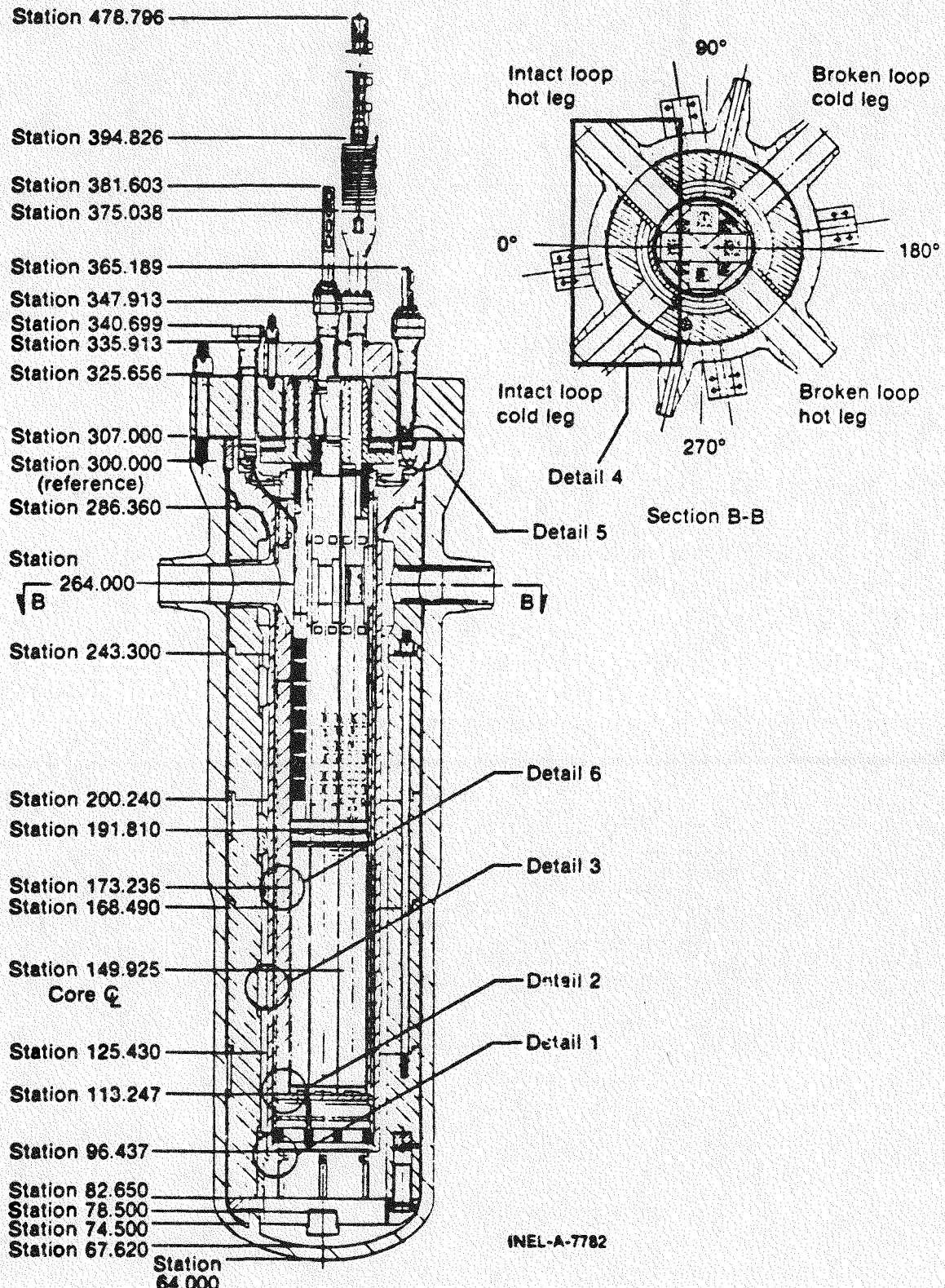


Figure AI.9 Reactor Vessel Showing Core Bypass Paths

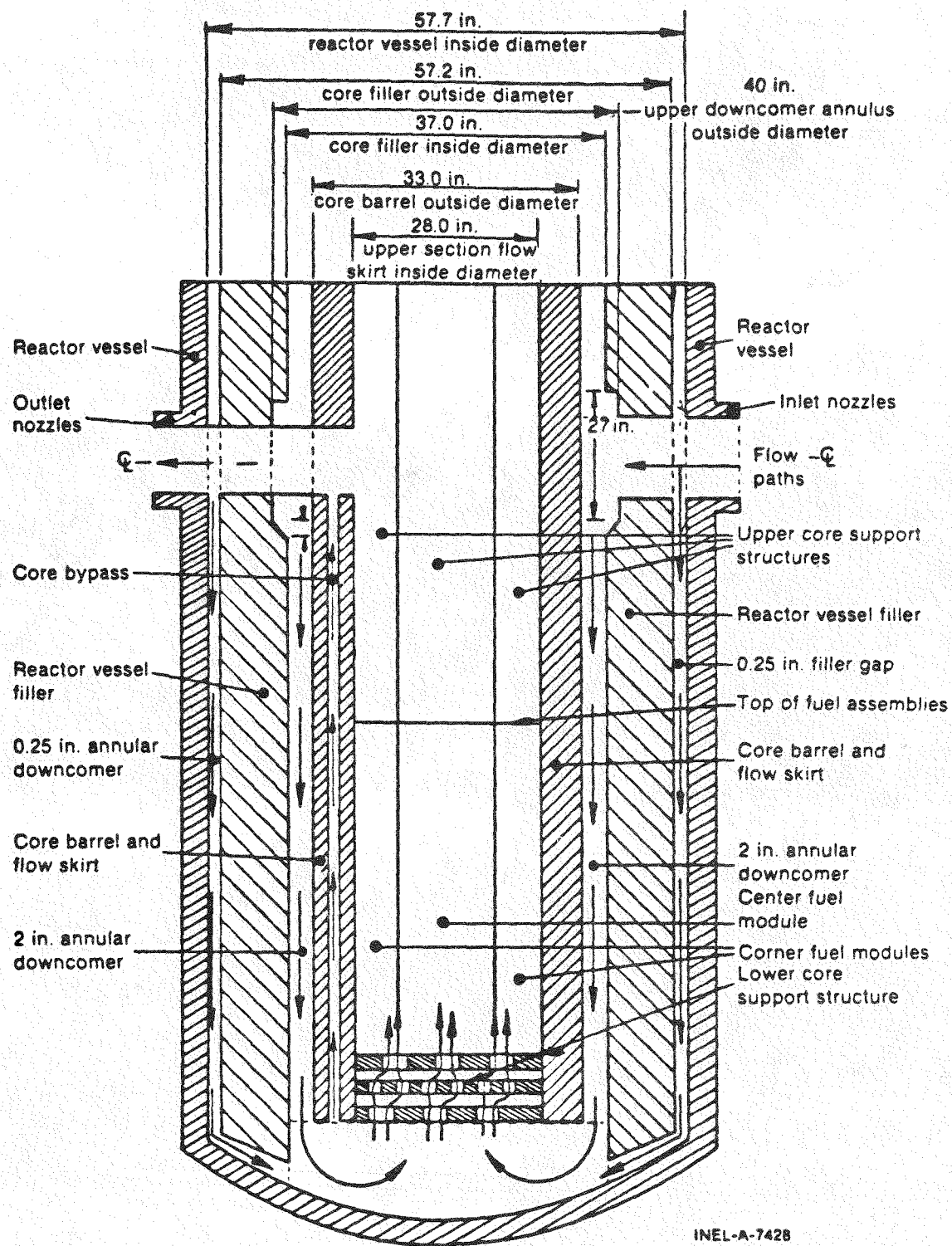


Figure AI.10 Reactor Vessel Schematic With Flow Paths

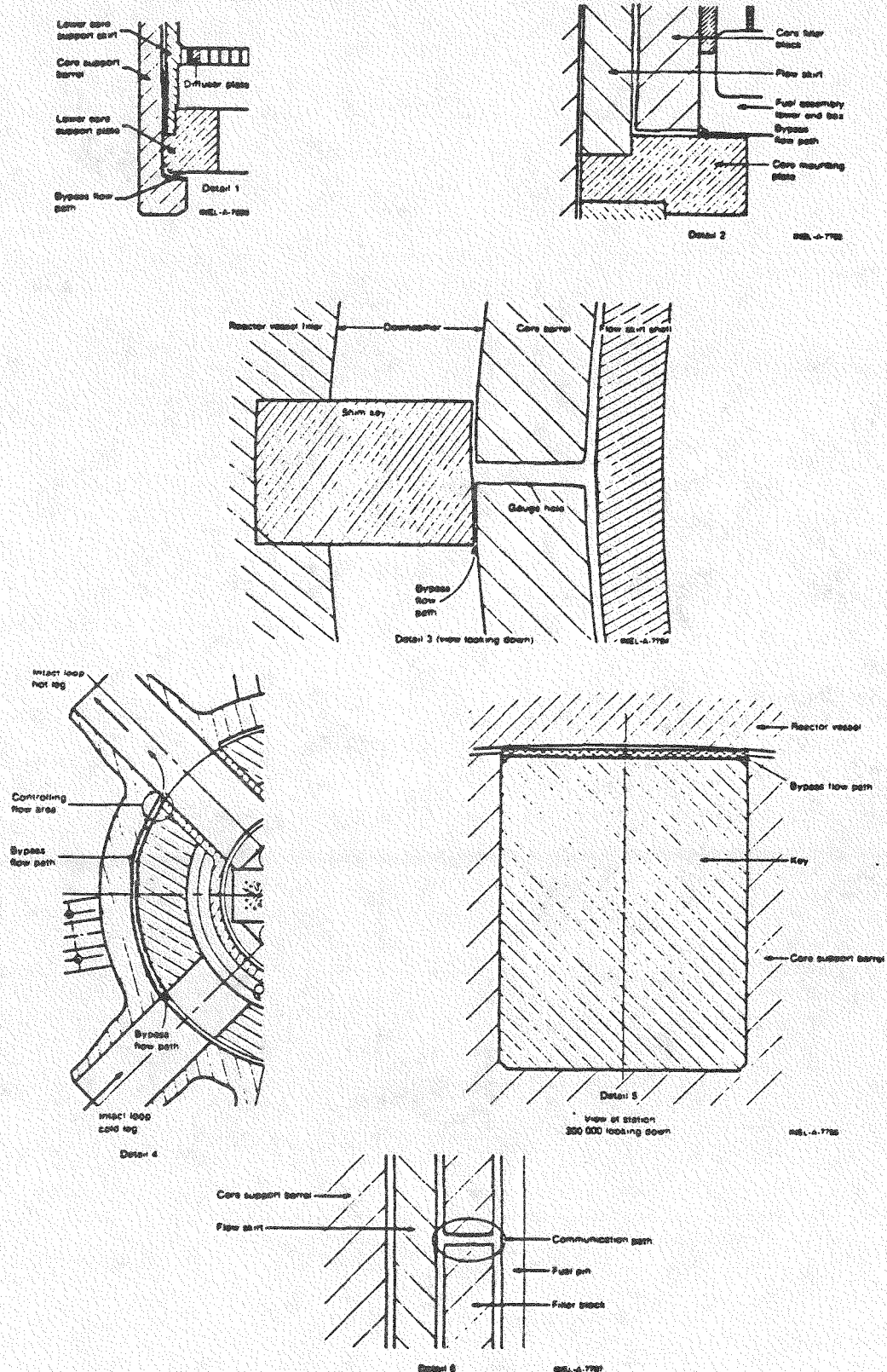


Figure AI.11 Core Bypass Details

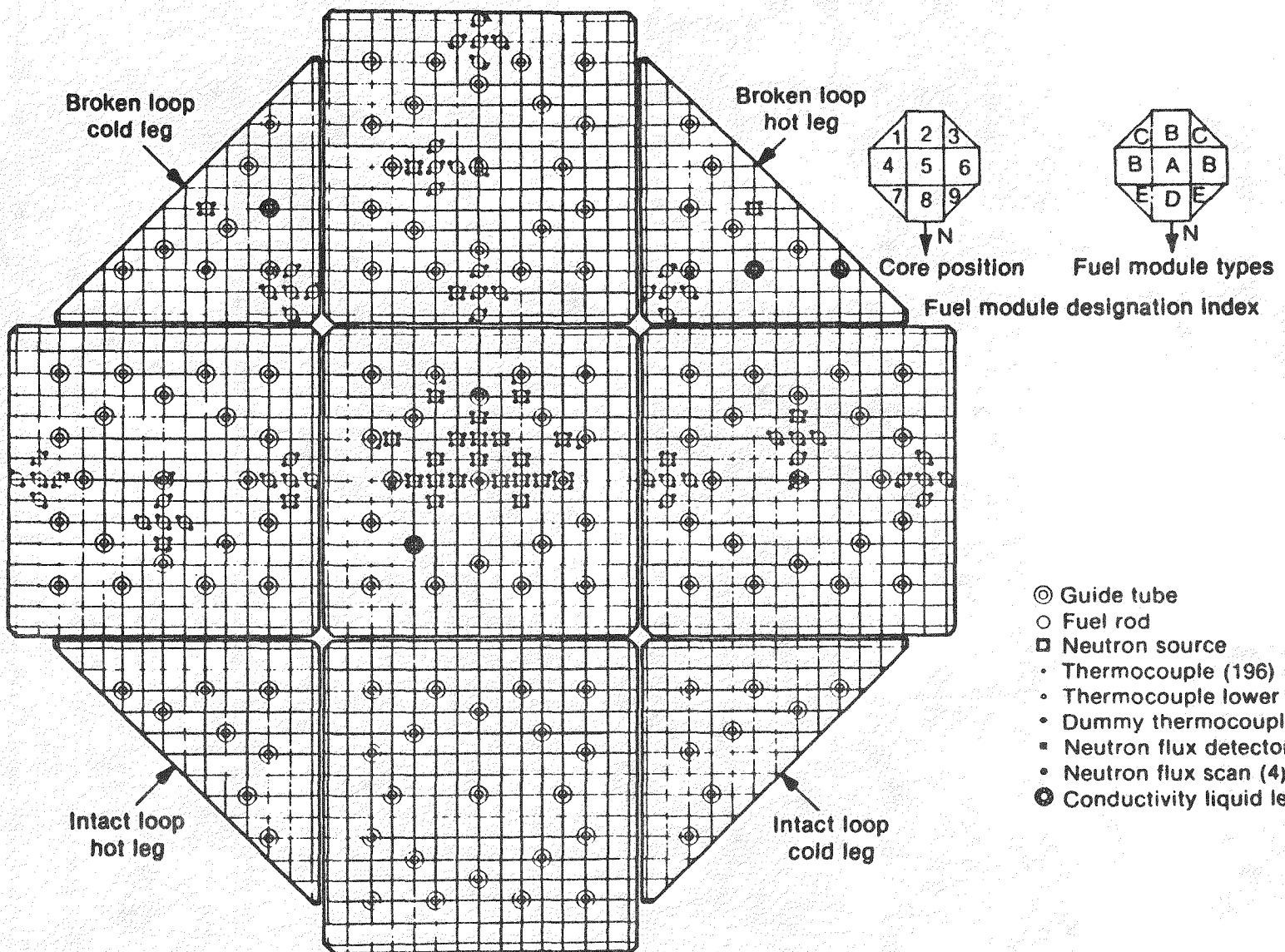


Figure AI.12 LOFT Core Configuration and Instrumentation

Table AI.1

## LOFT VOLUME DISTRIBUTION [a]

Parameter	Value [ $m^3$ ( $ft^3$ )]			
<b>Reactor Vessel</b>				
<b>Downcomer region</b>				
Vessel to filler gap	0.285	(10.05)		
<b>Distribution annulus</b>				
Above bottom of nozzles	0.104	(3.67)		
Below bottom of nozzles	0.068	(2.41)		
Downcomer annulus	0.564	(19.91)		
<b>Lower plenum</b>				
Below core support structure	0.564	(19.92)		
Within lower core support	0.096	(3.39)		
Above lower core support to active core	0.020	(0.71)		
Core	0.293	(10.36)		
Core bypass	0.053	(1.89)		
Upper plenum	<u>0.896</u>	<u>(31.63)</u>		
Reactor vessel total	2.943	(103.94)		
<b>Intact loop</b>				
Hot leg from reactor vessel to steam generator inlet	0.384	(13.56)		
Steam generator plenums and tubes	1.452	(51.27)		
Pump suction piping	0.337	(11.89)		
Pumps	0.198	(7.00)		
Cold leg from pump outlet to reactor vessel	0.333	(11.75)		
Pressurizer	0.928	(32.88)		
Pressurizer surge line	<u>0.012</u>	<u>(0.44)</u>		
Intact loop total	3.647	(128.79)		

Table AI.1 (Continued)

Parameter	Value [ $m^3$ ( $ft^3$ )]	
Broken loop		
From reactor vessel to centerline of joint A including hot leg side of reflood assist bypass system	0.332	(11.74)
From reactor vessel to centerline of joint C including cold leg side of reflood assist bypass system	0.358	(12.64)
Spool piece	0.023	(0.80)
Simulator section	0.617	(21.77)
From joint F to isolation valve	0.013	(0.47)
From joint B to isolation valve	<u>0.014</u>	<u>(0.48)</u>
Broken loop total	1.356	(47.90)
Total system liquid volume [b]	7.566	(267.20)
Total system volume [c]	7.896	(278.86)
Suppression system		
Tank (w/downcomers)	85.23	(3010)
Header	19.40	(685)
Downcomers inside tank (4)	2.61 (0.65 each)	92 (23 each)
Downcomers between tank and headers (4)	0.99 (0.24 each)	34.8 (8.7 each)
Accumulator A line volumes		
Accumulator A to cold leg	0.36	(12.8)
Accumulator A to lower plenum	0.37	(12.9)
Accumulator A to downcomer	0.56	(19.7)
Borated water storage tank	102.22	(3610)

[a] These volumes represent the best knowledge of the system at this time (September 1980).

[b] The system is defined as the intact loop piping and components, the reactor vessel, and the broken loop piping and components up to the break planes.

[c] Includes pressurizer gas volume of  $0.33 m^3$  ( $11.7 ft^3$ ).

Table AI.2 Intact Loop Piping Geometry

Volume No. <sup>a</sup>	Description	Piece	Flow Length (m)	Elevation (Station)		Diameter (m)		Area (m <sup>2</sup> )		Volume (m <sup>3</sup> )
				Ref. to Exit	Entry	Exit	Entry	Exit	Entry	
1a	Core barrel nozzle	0.351	0.736	264.00	264.00	0.292	0.292	0.0670	0.0670	0.0239
1b	Vessel nozzle	0.526	1.262	264.00	264.00	0.284	0.284	0.0634	0.0634	0.0336
2	14-in. Sch 160	1.322	2.584	264.00	264.00	0.284	0.284	0.0634	0.0634	0.0869
3	14-in. Sch 160 45° LR elbow	0.419	3.003	264.00	264.00	0.284	0.284	0.0634	0.0634	0.0266
4	14-in. Sch 160	0.719	3.722	264.00	264.00	0.284	0.284	0.0634	0.0634	0.0461
5	Venturi	0.965	4.688	264.00	264.00	0.284	0.290	0.0634	0.0659	0.0490
	Throat	--	--	--	--	0.206	--	0.0333	--	--
6	14-in. Sch 160 90° SR elbow	0.559	5.246	264.00	264.00	0.284	0.284	0.0634	0.0634	0.0354
7	14-in. Sch 160	0.195	5.441	264.00	264.00	0.284	0.284	0.0634	0.0634	0.0124
8	16 x 14-in. Sch 160 reducer	0.356	5.797	264.00	264.00	0.284	0.325	0.0634	0.0832	0.0260
9	16-in. Sch 160 38° elbow	0.270	6.066	264.00	267.39	0.325	0.325	0.0832	0.0832	0.0224
10	16-in. Sch 160	0.260	6.327	267.39	273.70	0.325	0.325	0.0832	0.0832	0.0217
11	SG <sup>c</sup> inlet plenum	0.630	6.956	273.70	293.89	0.325	0.439	0.0832	0.1512	0.3353
12	SG straight tube	2.135	9.091	293.89	377.93	0.439	0.439	0.1512	0.1512	0.3226
13	SG curved tube	0.899	9.990	377.93	377.93	0.439	0.439	0.1512	0.1512	0.1359
14	SG straight tube	2.135	12.125	377.93	293.89	0.439	0.439	0.1512	0.1512	0.3226
15	SG outlet plenum	0.630	12.754	293.89	273.70	0.439	0.325	0.1512	0.0832	0.3353
16	16-in. Sch 160 52° elbow	0.369	13.123	273.70	261.09	0.325	0.325	0.0832	0.0832	0.0307
17	16 x 14-in. Sch 160 reducer	0.356	13.479	261.09	247.09	0.325	0.284	0.0832	0.0634	0.0260
18	14-in. Sch 160	0.511	13.990	247.09	226.98	0.284	0.284	0.0634	0.0634	0.0332
19	14-in. Sch 160 90° SR elbow	0.559	14.548	226.98	212.98	0.284	0.284	0.0634	0.0634	0.0354
20	14-in. Sch 160	0.622	15.171	212.98	212.98	0.284	0.284	0.0634	0.0634	0.0401
21	14-in. Sch 160 tee Main run (pump 1)	0.439	15.609	212.98	212.98	0.284	0.284	0.0634	0.0634	0.0464
	Branch run (pump 2)	0.439	0.439	212.98	212.98	0.284	0.284	0.0634	0.0634	
22	14-in. Sch 160 90° SR elbow	0.559	16.168	212.98	226.98	0.284	0.284	0.0634	0.0634	0.0354

Table AI.2 (continued)

Volume No. <sup>a</sup>	Description	Flow Length (m)		Elevation (Station)		Diameter (m)		Area (m) <sup>2</sup>		Volume (m <sup>3</sup> )
		Ref. <sup>b</sup>	Piece to Exit	Entry	Exit	Entry	Exit	Entry	Exit	
23	14 x 10-in. Sch 160 reducer	0.330	16.498	226.98	239.98	0.284	0.216	0.0634	0.0366	0.0163
24	10-in. Sch 160	0.292	16.790	239.98	251.48	0.216	0.216	0.0366	0.0366	0.0107
25	Pump 1	0.457	17.247	251.48	264.00	0.216	0.216	0.0366	0.0366	0.0991
26	10-in. Sch 160	0.203	17.450	264.00	264.00	0.216	0.216	0.0366	0.0366	0.0074
27	10-in. Sch 160 45 <sup>o</sup> LR elbow	0.299	17.750	264.00	264.00	0.216	0.216	0.0366	0.0366	0.0110
28	10-in. Sch 160	0.799	18.549	264.00	264.00	0.216	0.216	0.0366	0.0366	0.0292
29	10 x 14-in. Sch 160 reducer	0.330	18.879	264.00	264.00	0.216	0.284	0.0366	0.0634	0.0163
30	14-in. Sch 160 90 <sup>o</sup> SR elbow	0.559	0.997	212.98	226.98	0.284	0.284	0.0634	0.0634	0.0354
31	14 x 10-in. Sch 160 reducer	0.330	1.328	226.98	239.98	0.284	0.216	0.0634	0.0366	0.0163
32	10-in. Sch 160	0.292	1.620	239.98	251.48	0.216	0.216	0.0366	0.0366	0.0107
33	Pump 2	0.457	2.077	251.48	264.00	0.216	0.216	0.0366	0.0366	0.0991
34	10-in. Sch 160 90 <sup>o</sup> SR elbow	0.399	2.476	264.00	264.00	0.216	0.216	0.0366	0.0366	0.0146
35	14 x 10-in. Sch 160 tee Main run (pump 1)	0.559	19.438	264.00	264.00	0.284	0.284	0.0634	0.0634	0.0408
	Branch run (pump 2)	0.424	2.900	264.00	264.00	0.216	0.284	0.0366	0.0634	
36	14-in. Sch 160	0.217	19.655	264.00	264.00	0.284	0.284	0.0634	0.0634	0.0138
37	14-in. Sch 160 90 <sup>o</sup> SR elbow	0.559	20.213	264.00	264.00	0.284	0.284	0.0634	0.0634	0.0354
38	14-in. Sch 160	0.194	20.408	264.00	264.00	0.284	0.284	0.0634	0.0634	0.0123
39	14-in. Sch 160 45 <sup>o</sup> LR elbow	0.419	20.827	264.00	264.00	0.284	0.284	0.0634	0.0634	0.0266
40	14-in. Sch 160	1.412	22.239	264.00	264.00	0.284	0.284	0.0634	0.0634	0.0917
41	Vessel nozzle	0.526	22.765	264.00	264.00	0.284	0.284	0.0634	0.0634	0.0336
42	Vessel filler	0.224	22.988	264.00	264.00	0.286	0.286	0.0641	0.0641	0.0143

a. The volume numbers correspond to the circled numbers in Figure AI.3.

b. Ref. - Reference at centerline of reactor vessel, see Figure AI.3.

c. SG - steam generator.

Table AI.3 Pressurizer Surge Line Component Identification

Location <sup>[a]</sup>	Description	Centerline Length [m (ft)]	Metal Weight [kg (lb)]	Cross-Section Flow Area <sup>2</sup> [m <sup>2</sup> (ft <sup>2</sup> )]	Fluid Volume [m <sup>3</sup> (ft <sup>3</sup> )]	ID Surface Area <sup>2</sup> [m <sup>2</sup> (ft <sup>2</sup> )]	Equivalent Length [m (ft)]	L/D
1	4-in. pressurizer stub	0.581 (1.9062)	0.835 (1.84)	0.006 (0.0167)	0.003 (0.1176)	0.157 (1.686)	0.581 (1.906)	6.6
2	2-in. Sch 160 LR EL <sup>[b]</sup>	0.120 (0.3932)	1.361 (3.0)	0.001 (0.0156)	0.0002 (0.0061)	0.016 (0.174)	0.858 (2.815)	20.0
3	2-in. Sch 160 pipe	0.419 (1.3750)	4.627 (10.2)	0.001 (0.0156)	0.001 (0.0214)	0.056 (0.608)	0.419 (1.375)	9.8
4	2-in. Sch 160 LR EL	0.120 (0.3932)	1.361 (3.0)	0.001 (0.0156)	0.0002 (0.0061)	0.016 (0.174)	0.858 (2.815)	20.0
5	2-in. Sch 160 pipe	0.982 (3.2214)	10.886 (24.0)	0.001 (0.0156)	0.001 (0.0503)	0.132 (1.425)	0.982 (3.221)	22.9
6	2-in. Sch 160 LR EL	0.120 (0.3932)	1.361 (3.0)	0.001 (0.0156)	0.0002 (0.0061)	0.016 (0.174)	0.858 (2.815)	20.0
7	2-in. Sch 160 pipe	0.838 (2.7500)	9.299 (20.5)	0.001 (0.0156)	0.001 (0.0382)	0.113 (1.215)	0.838 (2.750)	19.5
8	2-in. Sch 160 SR EL	0.080 (0.2617)	0.907 (2.0)	0.001 (0.0156)	0.0001 (0.0041)	0.011 (0.115)	1.287 (4.221)	30.0
9	2-in. Sch 160 pipe	0.204 (0.6706)	2.268 (5.0)	0.001 (0.0156)	0.0003 (0.0105)	0.027 (0.296)	0.205 (0.671)	4.8
10	2-in. Sch 160 SR EL	0.080 (0.2617)	0.907 (2.0)	0.001 (0.0156)	0.0001 (0.0041)	0.011 (0.115)	1.287 (4.221)	30.0
11	2-in. Sch 160 pipe	1.321 (4.333)	14.606 (32.2)	0.001 (0.0156)	0.0002 (0.0676)	0.178 (1.915)	1.321 (4.333)	30.8
12	2-in. Sch 160 SR EL	0.080 (0.2617)	0.907 (2.0)	0.001 (0.0156)	0.0001 (0.0041)	0.011 (0.115)	1.287 (4.221)	30.0
13	2-in. Sch 160 pipe	0.203 (0.6667)	2.268 (5.0)	0.001 (0.0156)	0.0003 (0.0104)	0.027 (0.295)	0.203 (0.667)	4.7
14	2-in. Sch 160 SR EL	0.080 (0.2617)	0.907 (2.0)	0.001 (0.0156)	0.0001 (0.0041)	0.011 (0.115)	1.287 (4.221)	30.0
15	2-in. Sch 160 pipe	0.483 (1.5833)	5.352 (11.8)	0.001 (0.0156)	0.001 (0.0247)	0.065 (0.700)	0.483 (1.584)	11.2
16	2-in. Sch 160 LR EL	0.0120 (0.3932)	1.361 (3.0)	0.001 (0.0156)	0.0002 (0.0061)	0.016 (0.174)	0.858 (2.815)	20.0
17	2-in. Sch 160 pipe	0.762 (2.5000)	8.437 (18.6)	0.001 (0.0156)	0.001 (0.039)	0.103 (1.104)	0.762 (2.500)	17.8
18	2-in. Sch 160 LR EL	0.120 (0.3932)	1.361 (3.0)	0.001 (0.0156)	0.0002 (0.0061)	0.016 (0.174)	0.858 (2.815)	20.0
19	2-in. Sch 160 pipe	0.303 (0.9935)	3.357 (7.4)	0.001 (0.0156)	0.0004 (0.0155)	0.041 (0.439)	0.303 (0.994)	7.1
20	Screen	-----	-----	-----	-----	-----	-----	24.7

[a] Location numbers correspond to circled numbers on Figure AI.5.

[b] Equivalent length is the length of pipe that will give the same pressure drop as the piping section described.

[c] EL - elbow.

Table AI.4 Steam Generator Design Parameters

Parameter	Value
<b>Tubes</b>	
Minimum length including tube sheet	4.27 m (14.0 ft)
Maximum length including tube sheet	6.19 m (20.3 ft)
Average length including tube sheet	5.17 m (16.95 ft)
External surface area of tubes less tube sheet	335 m <sup>2</sup> (3610 ft <sup>2</sup> )
Surface area of tubes inside tube sheet	43 m <sup>2</sup> (463 ft <sup>2</sup> )
Internal cross-sectional area of tubes	82 mm <sup>2</sup> (0.127 in. <sup>2</sup> )
Outside diameter of tubes	12.7 mm (0.50 in.)
Average wall thickness	1.24 mm (0.049 in.)
Number of tubes	1845
Thickness of tube sheet	0.292 m (11.5 in.)
Tube arrangement	Equilateral triangular pitch on 19-mm (0.75-in.) centers
Material	Inconel-600
Maximum height from bottom of tube sheet	2.73 m (107.5 in.)
Minimum height from bottom of tube sheet	2.15 m (84.5 in.)
Tube bundle diameter	1.22 m (48 in.)
Internal volume of tubes including tube sheet	0.781 m <sup>3</sup> (27.6 ft <sup>3</sup> )
Internal volume of tubes inside tube sheet	0.088 m <sup>3</sup> (3.12 ft <sup>3</sup> )
<b>Primary plenums</b>	
Inlet plenum volume	0.223 m <sup>3</sup> (7.887 ft <sup>3</sup> )
Outlet plenum volume	0.223 m <sup>3</sup> (7.887 ft <sup>3</sup> )
<b>Secondary side</b>	
Secondary shell volume	6.654 m <sup>3</sup> (235 ft <sup>3</sup> )
Secondary shell material	Carbon steel MIL-QQ-S691a, Grade C
Normal operating pressure	15.51 MPa (2250 psig)

Table AI.5 Steam Generator Data

## STEAM GENERATOR INFORMATION

NUMBER OF TUBES	1845
TUBE INSIDE DIAMETER	0.402 IN.
TUBE OUTSIDE DIAMETER	0.500 IN.
AVERAGE TUBE LENGTH INCLUDING TUBE SHEET	16.957 FT
TUBE SHEET THICKNESS	11.5 IN.
DOWNCOMER OUTSIDE DIAMETER	56.00 IN.
DOWNCOMER INSIDE DIAMETER	51.75 IN.
SHROUD INSIDE DIAMETER	50.75 IN.
BAFFLES	
NUMBER	4
SPACING	17.375 IN.
AREA OF 3 LOWER BAFFLES	4.867 SQ FT
AREA OF TOP BAFFLES	4.314 SQ FT
COOLANT MASS	
50 MW OPERATION	4130 LBM
37 MW OPERATION	4505 LBM

## STEAM GENERATOR ELEVATIONS ABOVE TUBE SHEET

	ELEVATION <sup>*</sup> INCHES
TUBE BEND LINE	72.50
LOW TUBE SPILLOVER	73.00
BOTTOM OF FRUSTRUM	88.125
HIGH TUBE SPILLOVER	96.00
TOP OF FRUSTRUM	101.22
NORMAL WATER LEVEL	126.00 <sup>**</sup>
BOTTOM OF SEPARATOR	144.63
TOP OF RISER	161.75

<sup>\*</sup> TUBE SHEET TOP IS 41.39 INCHES ABOVE THE COLD LEG CENTERLINE

<sup>\*\*</sup> OPERATING LEVEL IS 116 + 1 INCH FOR EVERY 10% POWER

Table AI.6 Broken Loop Piping Geometry

Volume No. <sup>a</sup>	Description	Flow Length (m)		Elevation (Station)		Diameter (m)		Area (m <sup>2</sup> )		Volume (m <sup>3</sup> )
		Piece	Ref. <sup>b</sup> to Exit	Entry	Exit	Entry	Exit	Entry	Exit	
1	Vessel filler	0.224	0.736	264.00	264.00	0.286	0.286	0.0641	0.0641	0.0143
2	Vessel nozzle	0.526	1.262	264.00	264.00	0.284	0.284	0.0634	0.0634	0.0336
3	14-in. Sch 160 45° LR elbow	0.419	1.681	264.00	264.00	0.284	0.284	0.0634	0.0634	0.0266
4	14 x 14 x 10-in. Sch 160 tee	0.559	2.240	264.00	264.00	0.284	0.284	0.0634	0.0634	0.0403
	10-in. branch	—	—	—	—	—	0.216	—	0.0366	—
5	14-in. Sch 160	0.695	2.935	264.00	264.00	0.284	0.284	0.0634	0.0634	0.0449
6	Flange	0.450	3.385	264.00	264.00	0.284	0.103	0.0634	0.0084	0.0050
7	Orifice plate	0.076	3.461	264.00	264.00	0.103	0.103	0.0084	0.0084	0.0006
8	Flange	0.168	3.629	264.00	264.00	0.103	0.103	0.0084	0.0084	0.0014
9	5-in. Sch XX 90° LR elbow	0.299	3.928	264.00	256.50	0.103	0.103	0.0084	0.0084	0.0025
10	6-in. Sch 160	0.832	4.760	256.50	223.75	0.132	0.132	0.0136	0.0136	0.0114
11	5-in. Sch XX 90° LR elbow	0.299	5.059	223.75	216.25	0.103	0.103	0.0084	0.0084	0.0025
12	Flange	0.168	5.228	216.25	216.25	0.103	0.103	0.0084	0.0084	0.0014
13	Pump simulator	0.473	5.701	216.25	216.25	0.103	0.287	0.0084	0.0645	0.0102
	Orifice plate	—	—	—	—	—	0.008	—	0.0101	—
	Support plate	—	—	—	—	—	0.152	—	—	—
14	14-in. Sch 160 90° SR elbow	0.559	6.259	216.25	230.25	0.284	0.284	0.0634	0.0634	0.0354
15	14 x 5-in. Sch 160 reducer	0.330	6.590	230.25	243.25	0.284	0.110	0.0634	0.0094	0.0107
16	5-in. Sch 160	0.937	7.526	243.25	280.12	0.110	0.110	0.0094	0.0094	0.0088
17	Flange	0.206	7.732	280.12	288.24	0.103	0.103	0.0084	0.0084	0.0008
18	SG simulator	2.051	9.784	288.24	369.00	0.103	0.371	0.0084	0.1079	0.1725
	Support plate	—	—	—	—	—	0.119	—	0.0112	—
	Orifice plate	—	—	—	—	—	0.124	—	0.0326	—
19	18-in. Sch 160 90° SR elbow	0.718	10.502	369.00	387.00	0.367	0.367	0.1056	0.1056	0.0759
20	18-in. Sch 160	0.263	10.765	387.00	387.00	0.367	0.367	0.1056	0.1056	0.0278
21	18-in. Sch 160 90° SR elbow	0.718	11.483	387.00	369.00	0.367	0.367	0.1056	0.1056	0.0759
22	SG simulator	2.051	13.535	369.00	288.24	0.371	0.103	0.1079	0.0084	0.1725
	Support plate	—	—	—	—	0.119	—	0.0112	—	—
	Orifice plate	—	—	—	—	—	0.123	—	0.0326	—
23	Flange	0.206	13.741	288.24	280.12	0.103	0.103	0.0084	0.0084	0.0008

Table AI.6 (continued)

Volume No. <sup>a</sup>	Description	Flow Length (m)		Elevation (Station)		Diameter (m)		Area (m <sup>2</sup> )		Volume (m <sup>3</sup> )
		Piece	Ref. <sup>b</sup> to Exit	Entry	Exit	Entry	Exit	Entry	Exit	
24	5-in. Sch XX	0.282	14.023	280.12	269.00	0.103	0.103	0.0084	0.0084	0.0024
25	5-in. oversize 90° elbow	0.199	14.223	269.00	264.00	0.103	0.103	0.0084	0.0084	0.0017
26	Flange	0.168	14.391	264.00	264.00	0.103	0.103	0.0084	0.0084	0.0014
27	Orifice	0.076	14.467	264.00	264.00	0.077	0.114	0.0046	0.0108	0.0005
28	Flange	0.244	14.712	264.00	264.00	0.257	0.257	0.0520	0.0520	0.0127
29	Isolation valve	0.762	15.474	264.00	264.00	0.257	0.257	0.0519	0.0519	0.0838
30	Q08VC	1.651	17.125	264.00	264.00	0.257	0.273	0.0520	0.0520	0.1050
31	Expansion joint	0.991	18.115	264.00	264.00	0.273	0.298	0.0586	0.0700	0.0972
32	Core barrel nozzle	0.351	0.736	264.00	264.00	0.292	0.292	0.0670	0.0670	0.0239
33	Vessel nozzle	0.526	1.262	264.00	264.00	0.284	0.284	0.0634	0.0634	0.0336
34	14-in. Sch 160 45° LR elbow	0.419	1.681	264.00	264.00	0.284	0.284	0.0634	0.0634	0.0266
35	14 x 14 x 10-in. Sch 160 tee	0.559	2.240	264.00	264.00	0.284	0.284	0.0634	0.0634	0.0403
	Branch	—	—	—	—	—	0.216	—	0.0366	—
36	14-in. Sch 160	0.695	2.935	264.00	264.00	0.284	0.284	0.0634	0.0634	0.0449
37	Flange	0.450	3.385	264.00	264.00	0.284	0.110	0.0634	0.0309	0.0054
38	Orifice plate	0.076	3.461	264.00	264.00	0.114	0.077	0.0102	0.0046	0.0005
39	Flange	0.206	3.667	264.00	264.00	0.173	0.173	0.0235	0.0235	0.0049
40	8-in. Sch 160	0.494	4.161	264.00	264.00	0.173	0.173	0.0235	0.0235	0.0116
41	Flange	0.206	4.368	264.00	264.00	0.173	0.173	0.0235	0.0235	0.0049
42	Orifice plate	0.076	4.444	264.00	264.00	0.173	0.173	0.0235	0.0235	0.0018
43	Flange	0.244	4.688	264.00	264.00	0.257	0.257	0.0520	0.0520	0.0127
44	Isolation valve	0.762	5.450	264.00	264.00	0.257	0.257	0.0519	0.0519	0.0838
45	Q08V	1.651	7.101	264.00	264.00	0.257	0.273	0.0520	0.0520	0.1050
46	Expansion joint	0.991	8.092	264.00	264.00	0.273	0.298	0.0586	0.0700	0.0972

a. The volume numbers correspond to the circled numbers in Figure AI.8

b. Ref. - Reference at centerline of reactor vessel, see Figure AI.8

c. Q08V - quick-opening blowdown valve.

Table AI.7

LOFT REACTOR VESSEL VOLUME DISTRIBUTION <sup>a</sup>

Parameter	Value [ $\text{m}^3$ ( $\text{ft}^3$ )]	
Downcomer region		
Vessel to filler gap	0.285	(10.05)
Distribution annulus		
Above bottom of nozzles	0.104	(3.67)
Below bottom of nozzles	0.068	(2.41)
Downcomer annulus	0.564	(19.91)
lower plenum		
Below core support structure	0.564	(19.92)
Within lower core support	0.096	(3.39)
Above lower core support to active core	0.020	(0.71)
Core	0.293	(10.36)
Core bypass	0.053	(1.89)
Upper plenum	<u>0.896</u>	<u>(31.63)</u>
Total	2.943	(103.94)

[a] These volumes represent the best knowledge of the system at this time (September 1980).

Table AI.8

## REACTOR VESSEL MATERIAL

Component	Estimate Weight [kg (lb)]	Material
<b>Reactor vessel closure heads</b>		
Instrumentation head	11 000 (24,000)	ASME SA 336, modified to Code Case 1332-1, clad with Type 308L SS
Closure plate	2300 (5000)	ASME SB 166 (Inconel-600)
Pressure vessel	34 000 (75,000)	ASME SA 336, modified to Code Case 1332-1, clad with Type 308L SS
Core support barrel	10 000 (22,200)	Type 304L SS
Upper core support plate	800 (1800)	Type 304 SS
Upper reactor vessel filler	6600 (14,600)	Type 304L SS
Lower reactor vessel filler	25 000 (55,200)	Type 304L SS
Flow skirt	640 (1400)	Type 304L SS
Lower core support structure	550 (1200)	Type 304L SS
Upper core support structure	2100 (4706)	Type 304L SS
Fuel assembly end boxes	200 (430)	Type 304L SS
Fuel pins (cladding only)	155 (340)	Zr-4
Fuel pellets	1470 (3240)	$UO_2$

Table AI.9

## DIMENSIONAL DATA--REACTOR VESSEL

Elevation Points	Station [a]	Height Above Reactor Vessel Bottom [m (in.)]
Bottom (inside) of reactor vessel	67.80	0.00 (0.0) [b]
Bottom of downcomer annulus	96.44	0.727 (28.64)
Top of lower core support structure	113.25	1.154 (45.45)
Top of lower grid plate	116.24	1.230 (48.44)
Bottom of uninstrumented fuel	116.93	1.248 (49.13)
Bottom of instrumented fuel pins	117.24	1.256 (49.44)
Bottom of spacer grid 1	117.74	1.268 (49.94)
Bottom of instrumented fuel	117.93	1.273 (50.13)
Bottom of spacer grid 2	134.34	1.690 (66.54)
Bottom of spacer grid 3	150.94	2.112 (83.14)
Bottom of spacer grid 4	167.44	2.531 (99.64)
Top of uninstrumented fuel	182.93	2.924 (115.13)
Top of instrumented fuel	183.93	2.950 (116.13)
Bottom of spacer grid 5	184.04	2.953 (116.24)
Top of uninstrumented fuel pins	186.62	3.018 (118.82)
Bottom of upper grid plate	187.62	3.043 (119.82)
Top of fuel module	191.82	3.150 (124.02)
Top of downcomer annulus	247.33	4.560 (179.53)
Vessel nozzle centerline	264.00	4.983 (196.20)
Top of distributor annulus	277.05	5.315 (209.25)
Internals support ledge in vessel	300.00 [b]	5.898 (232.20)
Inside surface of vessel flange	307.0	6.076 (239.20)

[a] The station numbers shown in this table are elevations in inches, with reference station 300.0 at the internals support ledge of the pressure vessel.

[b] Reference point.

Table AI.10

## CORE BYPASS CHANNELS

Core Bypass Path [a]	Controlling Flow Area [mm <sup>2</sup> (in. <sup>2</sup> )]	Equivalent Diameter [mm (in.)]
1	874 (1.356)	3.13 (0.123)
2	3703 (5.740)	3.48 (0.137)
3	65 (0.100)	0.64 (0.025)
4	309 (0.479)	0.30 (0.012)
5	286 (0.443)	2.76 (0.109)
6	4162 (6.452)	3.91 (0.154)

[a] Numbers correspond to "Detail" numbers on Figure AI.9.

## CORE BYPASS

PATH*	% LOOP FLOW
1	1.31 - 1.34
2	1.02 - 1.04
3	0.96 - 1.01
** 4	4.38 - 6.58
** 5	0.04
6	0.27 - 0.28
**RABV	1.42 - 1.43
	9.40 - 11.72
	10.56 ± 1.16

\* NUMBERS REFER TO DETAILS ON FIGURE AI.9

\*\* STEAM VENTING PATHS

## **APPENDIX II**

### **INPUT LISTING**

**An input listing for the L6-7/L9-2 transient calculation run is given on attached microfiche.**

### APPENDIX III

#### ADDITIONAL UPDATES USED FOR CYCLE 18+

In June 1982, updates to bring RELAP5/MOD1 to the cycle 18 level were received from INEL. Also added to our version of cycle 18 were some other recommended updates from INEL. The recommended updates which were added are listed below by their identifier names for reference.

KERR015: This update adds a subroutine to check elevation changes around piping loops. The check is done during input processing.

DEBUGJ: Adds diagnostic printout during computation of junction properties.

DMKTIM: Adds mass error debug printout during computation of equation of state variables.

BRFIX: Attempts to fix a branching problem by multiplying viscous terms in momentum equation by the square of the ratio of the junction area to the volume flow area.

Also included in INEL's recommended updates was a new inter-phase drag model (identifier HXCRXXX). This update was not implemented in our version of RELAP5/MOD1/CYCLE18.

DISTRIBUTION: RELAP5 Assessment: LOFT Large Break L2-5

U. S. NRC Distribution Contractor (CDSI) (300)  
7300 Pearl Street  
Bethesda, MD 20014  
300 copies for R4

U. S. Nuclear Regulatory Commission (4)  
Analytical Models Branch  
Division of Accident Evaluation  
Office of Nuclear Regulatory Research  
7915 Eastern Avenue  
Silver Spring, MD 20910  
Attn: Louis M. Shotkin  
Fuat Odar  
R. Landry  
H. S. Tovmassian

EG&G Idaho (6)  
Idaho National Engineering Laboratory  
P. O. Box 1625  
Idaho Falls, ID 83415  
Attn: T. R. Charlton  
G. W. Johnsen  
Edna Johnson  
J. C. Lin  
V. H. Ransom  
R. J. Wagner

Thad D. Knight  
Dennis R. Liles  
Los Alamos National Laboratory (2)  
K553 Q-9  
Los Alamos, NM 87545

P. Saha, 130  
Department of Nuclear Energy  
Brookhaven National Laboratory  
Associated Universities, Inc.  
Upton, New York 11973

N. H. Shah  
Babcock & Wilcox Co. (NPGD)  
P. O. Box 1260  
Lynchburg, VA 24505

Jesse Fell (5)  
Deputy Director  
Water Reactor Programs  
Atomic Energy Establishment  
Winfrith  
Dorchester, Dorset  
DT28DH  
ENGLAND

6400 A. W. Snyder  
6410 J. W. Hickman  
6417 D. D. Carlson  
6420 J. V. Walker  
6421 T. R. Schmidt  
6422 D. A. Powers  
6423 P. S. Pickard  
6425 W. J. Camp  
6427 M. Berman  
6427 C. C. Wong  
6440 D. A. Dahlgren  
6442 W. A. von Riesemann  
6444 S. L. Thompson (16)  
6444 L. D. Buxton  
6444 R. K. Byers  
6444 R. K. Cole, Jr.  
6444 P. N. Demmie  
6444 D. Dobranich  
6444 M. G. Elrick  
6444 L. N. Kmetyk  
6444 R. Knight  
6444 J. M. McGlaun  
6444 J. Orman  
6444 A. C. Peterson  
6444 W. R. Schmidt  
6444 R. M. Summers  
6444 G. G. Weigand  
6449 K. D. Bergeron  
8424 M. A. Pound  
3141 C. M. Ostrander (5)  
3151 W. L. Garner

**BIBLIOGRAPHIC DATA SHEET**

3 TITLE AND SUBTITLE

RELAP5 Assessment: LOFT Large Break L2-5

6. AUTHOR(S)

S. L. Thompson and L. N. Kmetyk

8 PERFORMING ORGANIZATION NAME AND MAILING ADDRESS (Include Zip Code)

Sandia National Laboratories  
Albuquerque, New Mexico 87185

11 SPONSORING ORGANIZATION NAME AND MAILING ADDRESS (Include Zip Code)

Reactor Systems Research Branch  
Division of Accident Evaluation  
Office of Nuclear Regulatory Research  
U. S. Nuclear Regulatory Commission  
Washington, DC 20555

### 13. SUPPLEMENTARY NOTES

**14 ABSTRACT (200 words or less)**

The RELAP5 independent assessment project at Sandia National Laboratories is part of an overall effort funded by the NRC to determine the ability of various systems codes to predict the detailed thermal/hydraulic response of LWRs during accident and off-normal conditions. The RELAP5 code is being assessed at SNLA against test data from various integral and separate effects test facilities. As part of this assessment matrix, a large break transient performed at the LOFT facility has been analyzed.

The results show that RELAP5/MOD1 correctly calculates many of the major system variables (i.e., pressure, break flows, peak clad temperature) early in a large break LOCA. The major problems encountered in the analyses were incorrect pump coastdown and loop seal clearing early in the calculation, excessive pump speedup later in the transient (probably due to too much condensation-induced pressure drop at the ECC injection point), and excess ECC bypass calculated throughout the later portions of the test; only the latter problem significantly affected the overall results. This excess ECC bypass through the downcomer and vessel-side break resulted in too-large late-time break flows and high system pressure due to prolonged choked flow conditions. It also resulted in a second core heatup being calculated after the accumulator emptied, since water was not being retained in the vessel. Analogous calculations with a split-downcomer nodalization delivered some ECC water to the lower plenum, which was then swept up the core and upper plenum and out the other (pump-side) break; thus no significant differences in long-term overall behavior were evident.

**15a. KEY WORDS AND DOCUMENT ANALYSIS**

**15b. DESCRIPTORS**

**16. AVAILABILITY STATEMENT**

17 SECURITY CLASSIFICATION  
*(This report)*

**18. NUMBER OF PAGES**

Unc1  
19 SECURITY CLASSIFICATION

卷之三